GEORGES BANK BASIN STRATIGRAPHY: CRETACEOUS GAMMA LOG SEQUENCES CORRELATED WITH SEISMIC DATA

by

STEPHEN JACKSON GRAHAM

A thesis submitted to the

School of Graduate Studies

Rutgers, The State University of New Jersey

In partial fulfillment of the requirements

For the degree of

Master of Science

Graduate Program in Geological Sciences

Written under the direction of

Kenneth G. Miller

And approved by

_____

_____

_____

_____

New Brunswick, New Jersey

January, 2019

ABSTRACT OF THE THESIS

Georges Bank Basin Stratigraphy: Cretaceous Gamma Log Sequences

Correlated with Multichannel Seismic Profiles

by STEPHEN JACKSON GRAHAM

Thesis Director:

Kenneth G. Miller

This report is a contribution to the Mid-Atlantic Offshore Carbon Storage Resource Assessment Program (MAOCSRAP), a Department of Energy funded multi-institutional effort to evaluate several rift basins located offshore of the East Coast of North America for carbon capture and storage (CCS) potential. Previous studies have noted the presence of Cretaceous sands in the Eastern half of the Georges Bank Basin (GBB) have reservoirs that have a high potential for storage of supercritical CO_2, but most of the research in this basin was conducted between 1976 - 1982 and focused on potential petroleum. No additional research or data have been acquired since a drilling embargo was placed on the surrounding area in 1988 by both the Canadian and US governments. My task has been to compile and analyze the data available from exploratory surveys and drilling of 10 wells over 30 years ago through the use of a modern analysis software platform, and reevaluate it using modern tools and modern sequence stratigraphic methods to construct a better understanding of the development of the GBB through time and its potential as a CCS target.

There are six different 2D seismic surveys covering different areas of the GBB. These surveys were conducted at different times, by different exploratory companies, with different targets and goals. I have combined these six different data sets into one data set and added available well log data from the ten exploratory wells drilled in the basin in order to correlate two Cretaceous sand units from the Baltimore Canyon Trough to the GBB.

I identified the Logan Canyon Formation and the Missisauga Formation by their Gamma Ray (GR) character in several well logs, and constructed a preliminary well cross section of the basin. I then projected the GR logs onto the nearest 2D seismic profile, used my formation tops from the GR cross section to identify their correlating seismic reflectors, and traced those reflectors around the GBBB using a majority of the available seismic data. Some surveys did not have sufficient resolution at my target depths to provide useful results. The results of integrating these two different data types helped refine my interpretation. I then further refined my correlation of the two target formations by examining the stacking patterns of the parasequences visible on the GR logs. This allowed me to identify and correlate three sequences within the Logan Canyon Formation, and three sequences within the Missisauga Formations.

I determined that the Logan Canyon Formation is too shallow for CCS in the GBB, because the formation top lies above the minimum safe depth required to maintain supercritical pressure in liquid CO2 pumped into the seabed. The MAOCSRAP project stipulated 1000 meters below sea level (mbsl) for this cutoff depth, and over half of the Logan Canyon top lies above this depth. The Logan Canyon Formation also lacks a

sufficient seal to prevent any injected material from migrating upward past the formation top where the top is deeper than 1000 mbsl.

The Missisauga Formation has excellent potential for CCS in the GBB. It lies deep enough to maintain necessary storage pressure, and it is overlain by the Naskapi Formation, a basin-wide shale unit that acts as a confining bed for any injected materials. However, the heterolithic sands deposited in likely fluvial environments present a less desirable reservoir than the deltaic sands of the Logan Canyon Formation. I conclude that the GBB is a possible target for carbon storage, though less so than the Baltimore Canyon Trough.

Acknowledgements

Numerous people helped bring this project to fruition. Thanks goes to my committee for their guidance – to Ken Miller, for making me an "offer I couldn't refuse" to join the project and for his constant energetic positivity and encouragement; to Greg Mountain, for his kindness and generosity, which are truly inspiring; and to Don Monteverde, for his support of the project. Jim Browning has also been a constant and invaluable source of guidance and encouragement. To the folks at Battelle, who go to bat for scientific research and bring government and universities together – you guys drive the future. Jason Pappas deserves a medal for continually helping me update Petrel while battling the onslaught of externally mandated system updates and migrations, and for having extra monitors on hand when I need them. Jason, your patience is astounding. John Schmelz and Will Fortin provided invaluable background information for the thesis, and Bari, Chris J., and Aaron were collaborators with me in unraveling the mysteries of Petrel. My wife and children supported me throughout this journey, albeit reluctantly at times. Finally, I dedicate this thesis to the memory of Chris Lombardi, whom we lost in 2016. Chris was my closest collaborator in this project early on, helping me choose which software best fit the needs of the project, getting me up and running on the software, and catching me up on his own project to set me up for my own work. A more intellectually generous, kind, and fun-loving man may not come our way again. Chris, you are missed.

Table of Contents

List of Figures

List of Tables

Introduction

Carbon Capture and Storage (CCS) is a potentially valuable strategy for reducing anthropogenic emissions of carbon dioxide (CO_2; Metz et al. 2005; International Energy Agency 2014). Offshore storage in saline reservoirs may be implemented close to large point-sources of CO_2 while avoiding the land-based storage complications of NUMBY (not under my backyard; Kerr, 2010). The Mid-Atlantic U.S. passive continental margin has been suggested as a likely target for offshore storage, particularly the Baltimore Canyon Trough offshore of New Jersey-Delaware-Maryland (e.g., Monteverde et al., 2011; Miller et al., 2018; Schmelz et al., submitted). However, little to no consideration has been given to the offshore storage potential of the Georges Bank Basin (GBB), offshore Massachusetts.

My research is part of a high-level storage resource assessment of the East GBB, performed as part of the Mid-Atlantic U.S. Offshore Carbon Storage Resource Assessment Project (MAOCSRAP) managed by the Battelle Corporation under the U.S. Department of Energy's Carbon Storage Program. The GBB (Fig. 1A), ~67,000 km^2 in area, is ~160 km ESE of Cape Cod, MA, and contains sediments over 6.5 km thick, with an average water depth of ~80 m. The GBB sits between the Long Island Platform to the west, the LaHave Platform to the northeast, and the Gulf of Maine Platform to the north. The basin also borders the buried Yarmouth Arch (a Paleozoic basement high) to the northeast, and the East Coast Magnetic Anomaly (ECMA) and the Bear Seamount to the south. The GBB contains a collection of smaller Triassic rift basins formed when Pangea began to separate. Acoustic basement in the basin consists of metamorphic and igneous rocks in the north, sea floor basalts in the east between the Yarmouth Arch the East Coast

Magnetic Anomaly, and Paleozoic rocks and dipping rift sediments elsewhere, which are overlain by the Argo Salt and the Upper Triassic to Lower Jurassic Iroquois Formation (McIver, 1972; Poag, 1982; Amato and Bebout, 1980; Schlee and Klitgord, 1982).

Industry drilling and seismic profiles provide a baseline for evaluation of the GBB. Ten exploratory wells drilled in the GBB between 1976 and 1982 provide wireline log data used here to investigate the storage potential of two middle Cretaceous sand units: the Logan Canyon and the Missisauga Formations (McIver, 1972; Libby-French, 1982). The names of the lithologic units in the GBB were first proposed in 1972 by McIver (1972) in his characterization of the of stratigraphy of the Nova Scotia shelf, and then carried southward to the Baltimore Canyon Trough (Poag, 1978; Libby-French, 1981) before they were formally applied to the Georges Bank Basin (Scholle and Wenkham, 1982). The first two wells (G-1 and G-2) were drilled in the GBB in 1976 and 1977 as part of the Continental Offshore Stratigraphic Test (COST) program by energy consortia to acquire geologic data in the basin prior to the federal lease sale in 1979. Subsequently, eight additional exploration wells were drilled in the basin. I use gamma ray logs from these wells to show general lithologies and correlate formations. Neutron porosity and density porosity log data, coupled with published permeability and porosity data, enable evaluation of the suitability for storage, including potential capacity and identification of seals.

Until 2016 the only publicly available multichannel seismic profiles (MCS) across the GBB were USGS reconnaissance data collected in the 1970's (e.g., Schlee and Fritsch, J., 1983). Therefore, to conduct this study of CCS potential there was strong impetus to reprocess these data using modern techniques. Seismic data reprocessing was

completed under contract with Absolute Imaging (AI) Inc. of Calgary, Canada. Legacy processing was heavily limited by the computational capabilities available at the time of data collection; reprocessing by AI using a full suite of state-of-the-art techniques greatly improves seismic image quality and geologic interpretation potential. In particular, detailed velocity modeling and data migration are reprocessing steps responsible for improvements in imaging. Migration of seismic data properly locates reflected seismic energy when stratigraphic layers are dipping and is considered a standard and necessary procedure in modern data interpretation. Other significant improvements include: spike suppression, predictive deconvolution, and noise suppression. Removing noise and de-convolving the prestack seismic data with the predicted source wavelet produces sharper images, and ultimately better interpreted geology, with features that are properly located within complicated geologic settings.

Four lines comprising over 322 km (including data gaps) of the reprocessed seismic data from the larger MAOCSRAP project lie within the GBB (Fig. 1A). The reprocessing on these lines significantly improved imaging resolution at my target depths (2000 feeet below Kelly Bushing (ftkb) – 7500 ftkb). I ultimately used USGS Line 12 as the single unadjusted static 2D seismic survey for Petrel's (An advanced multi-channel seismic and well log analysis software package produced by Schlumberger) mis-tie analysis tool to adjust the amplitude, phase, and depth of all the industry seismic surveys to match (Table 4), and I used the four reprocessed USGS seismic lines as the model images to test the adjusted alignments.

During the reprocessing of the USGS reconnaissance data, BOEM and USGS jointly released numerous 2D seismic surveys (Triezenberg et. al., 2016). Six released

surveys include 799 tracklines comprising a total of 41,284 km of seismic profiles collected in the late 1970's to early 1980's (Table 2). While these data are not limited to the GBB (Fig 1B), they provide comprehensive coverage of the entire basin (Fig 1C). Some surveys in this set provide surprisingly good seismic data, such as B-03-75-AT, while others such as B-01-83 and B-02-79 were only marginally useful. I used 111 of these 2D surveys, covering more than ~4,100 km, in addition to the 4 reprocessed USGS profiles comprising 322 km, to trace seismic horizons corresponding to gamma ray zone tops and sequence boundaries.

This study uses industry wells and USGS and industry MCS data to evaluate the CO_2 storage potential of the GBB, focusing on the Logan Canyon and Missisauga Formation above 10,000 ft (3280 m), which is largely the Cretaceous section (Figs. 2A and B). Sand units in this target within both formations vary between 30 and 100 m thick, and have excellent porosity (average 25-35%) and permeability (over 1000 mD) (Amato and Bebout, 1980; Amato and Simonis, 1980). These target intervals are located deep enough to maintain the pressure required to store liquid CO_2, yet shallow enough to be cost-effective sequestration targets. Both potential reservoirs also underlie shale units that appear to be sufficiently thick and impermeable seals for containing injected CO_2. All these factors support GBB as a favorable storage location.

Methods

Guidance from Previous Studies

My evaluation of the GBB focuses on formations above 10,000 ft (3280 m) below Kelly bushing (ftkb), based on porosity and permeability in BOEM reports (Scholle and Wenkam, 1982; Amato and Bebout, 1980; Amato and Simonis, 1980). These reports show relatively low (<10% porosities) due to lithification/cementation.

Original raster well logs from all ten wells in the GBB are publicly available at the BOEM website (https://www.data.bsee.gov/Other/DiscMediaStore/WellData.aspx). All available logs and reports were ordered from BOEM, and delivered on DVD. Raster logs were then prioritized for digitization according to log type, scale, the percent of the well bore represented in the log, and image quality. Logs were digitized at the resolution of one data point every 0.5 feet using Neuralog and Petra software packages (table 3).

Data Compilation and Agreement

All relevant available digital log data were imported into Petrel. The importation process defines several characteristics of each well based on specifics obtained from published BOEM reports, including exact GPS location of the well head, Kelly Bushing elevation, sea floor depth, total drilled depth, and checkshot data. After importing log data, the quality and accuracy were evaluated against the caliper logs. Many porosity and permeability logs were deemed low quality and unreliable because they coincided with high caliper log readings. The common porosity logs and resistivity logs use pad devices which must contact the formation. In cases where the diameter of the wellbore was greater than the extension of the pad device full contact was not achieved, resulting in

invalid readings. Biostratigraphic data from published BOEM reports was incorporated where available (Amato and Bebout, 1980; Amato and Simonis, 1980, Edson et al, 2000a-i). Seismic survey data were also imported into Petrel.

After importing both well and seismic data, additional steps are required to integrate the two data types. Petrel requires the user to first create an "active time-depth relationship" (TDR) using checkshot data or a sonic log. After setting the TDR for each well, I displayed the gamma logs overlain onto the nearest 2D seismic line to see if the two data types matched up visually. I compared large changes in gamma log values to seismic reflectors that implied a high reflection coefficient to check the quality of the correlation between log and seismic data. Strong reflectors should generally match up with large changes in gamma ray values in a good correlation (Petrel geophysics manual, Miller et. al., 2018). I found that nine of the gamma ray logs projected into time using the TDR somewhat matched with the seismic profiles, but were often not consistent from well to well, or even within one gamma log. The tenth log, from Block 357, did not have checkshot data above 12,407 ft, causing the well projection into time to be uncertain. To correct the inconsistency, I created "integrated seismic well ties" through Petrel's seismic well tie tool. This process uses a sonic log, density log, checkshot data, gamma ray log, the nearest seismic survey, and a user-created synthetic wavelet to dynamically align the gamma ray log with the seismic data. I experimented with nine to twelve different synthetic wavelet calculation methods for each well tie, in order to find the synthetic wavelet that best matched the wave form of the CDP at the point where Petrel projected the well onto the 2D seismic line. Even after calibrating the log data to match the seismic data as closely as possible, some discrepancies are inevitable where the physical location

of the wireline log data is too far from the target depths within the well and/or the nearest seismic survey. The Tenneco 187 well was projected onto a line over 875 meters away because of the higher quality reprocessing on that line than two nearer options. In order to overcome the deficient checkshot data available for the Shell 357 well, I initially used the checkshot data from the nearest well (Mobil 312) above 12,000 ft., but then further refined that result by creating artificial checkshots that matched the projected gamma log zone tops to the same reflectors as seen in the Exxon 133 and Mobil 312 wells. The highly artificial nature of the resulting projection caused me to exclude the Shell 357 projection from consideration of inconsistencies and other conclusions.

Gamma Ray Log Interpretation

I created a preliminary cross section of the GBB by correlating the trends and patterns of the mid-Cretaceous sand units from Amato and Bebout (1980) on the GR logs from the COST G1 and COST G2 wells. I first correlated the largest trends and patterns from the COST wells across all ten wells in the basin, but found that this resulted in unreasonable variations of thickness and poor lateral continuity of lithologic units across the basin. I resolved these problems by separating the four westernmost wells into a separate cross section.

I applied sequence stratigraphic analysis techniques (e.g., Miller et al., 2018) to refine my preliminary gamma log cross section. These techniques include analyzing the stacking patterns of parasequences evident in the GR log (Fig. 3), and then considering the context of these stacking patterns within the log in order to identify depositional sequences on the GR log. The COST G-1 gamma log served as a template to correlate

published lithologic units (Amato and Bebout, 1980; Scholle and Wenkham, 1982; Poague, 1982) to the other nine wells in the basin. Gamma logs were shaded yellow (low values) to brown (high values; Fig. 3). This shading style simulates sand-colored layers at low gamma readings, to correlate with sand lithologic units, and mud-colored layers at high gamma readings, to correlate with mud or shale. I then used this color scheme to identify trends of fining and coarsening grain size. I identified potential depositional sequences by examining the stacking patterns of these fining and coarsening packages; three sequences in the Logan Canyon Formation, and three in the Missisauga Formation were identified and correlated to the GTS2012 using biostratigraphy. A typical sequence (Fig. 3) consists of a highstand systems tract (HST) at the top, a transgressive systems tract (TST) in the middle, which usually contains a maximum flooding surface (MSF) below the HST, and a lowstand systems tract (LST) below the TST. On a gamma log the HST pattern appears as a progradational sand, or group of sands, overlain by a sharp negative shift at the sequence boundary. Below the sandy HST, the TST can be retrogradational, but is often aggradational. The LST is similar to the HST in shape, as they are both progradational, but the LST has a smaller positive GR signature and is generally of a lesser magnitude than the HST. I used this difference in magnitude to distinguish between the HSTs of sequences, and the LSTs of the next sequence overlying them. The number and age of the sequences I found in the Logan Canyon Formation (LC3, LC2, and LC1 from older to younger) correlate with similarly named sequences in the Baltimore Canyon Trough (Miller et al., 2018).

Seismic Data Integration

I tested the compatibility of seven seismic surveys of the GBB by displaying the intersections of seismic lines from different surveys. In order to correct common misalignment between surveys, and often between lines within the same survey set, I used Petrel's mis-tie analysis tool to create variable and dynamic corrections for variations in vertical alignment, phase, and gain differences. Misalignment varied from 280 to -170 ft, but was generally within 30 feet in both positive and negative directions. This software tool kept the reprocessed USGS line 12 stationary, and adjusted all 471 other lines, including oil company surveys (Triezenberg et al., 2016), to match the five USGS lines at all 4038 intersections of all the 2D seismic lines within the basin. I then tested this automatically generated mis-tie set by choosing the seismic reflector which correlated with the top of the Logan Canyon sands (LC1/MK1; Libby French, 1982) on the COST G1 gamma ray log (Amato and Bebout, 1980), and loop-correlated it across the entire GBB through all 2D seismic survey sets, ultimately returning the correlation back to the first 2D seismic survey and the COST G1 Logan Canyon Top (Amato and Bebout, 1980). This loop correlation through the seismic grid confirms that the same reflection is faithfully traced and correlated to the wells.

I used the COST G1 well gamma ray (GR) log as the starting point to project GR-based log sequences across the 2-D seismic surveys in the GBB because it had the clearest delineation of sequences. I traced one seismic reflector across the entire basin for the tops of the Logan Canyon, Naskapi, and Missisauga Formations. I then compared the cross-section formation depths, at the other nine wells, to the traced seismic time horizons from the COST G1 sequences. Comparing lithologic tops against seismic time

horizons this way helped both further refine and confirm initial GR cross section and sequence interpretations. In some wells I lowered my interpreted Logan Canyon Top by 1-2 reflectors to exclude some sand packages I had previously included in the Logan Canyon Formation, while also more closely matching specific GR log features to refine my interpreted Naskapi Formation top.

Results

Overview

I correlated GR logs among the 10 wells using sequence stratigraphic procedures (e.g., Miller et. al, 2018) and projected them onto seismic data. My correlations resulted in a shallower top of the Logan Canyon sandstone than mapped in previous interpretations (Amato and Bebout, 1980; Poag, 1982). The Logan Canyon Formation top varies from 2230.8 feet to 2915 ftkb (600.84-785.77 meters below sea floor (mbsf); Figs. 3A and B), with ~55% of the formation top lying above 2500 ftKB (762 m), the minimum depth required to maintain super-critical pressure of CO_2. Supercritical CO_2 storage requires burial pressures >7.38 MPa at temperatures > 31.1°C (Bachu, 2000), which was computed for this region as 800 m assuming a typical geothermal gradient of 25°C/km, 12°C surface temperatures, and a lithostatic gradient of 27 MPa/km (Miller et al., 2018). The thickness of the Logan Canyon Formation ranges from 646.36 to 1415.15 ft (197.0 to 431.34 m) and average thickness is 1,036.0 feet (315.8 m; Table 1). The Logan Canyon Formation is comprised of three depositional sequences: the LC1, LC2, and LC3, from youngest to oldest (Figures 2A, B), similar to the BCT (Miller et al.,

2018). The lowermost sequence, the LC3, includes the entirety of the Naskapi Formation, which I've interpreted as the lowstand systems tract (LST) of the sequence.

The top of the Missisauga Formation has depth ranges from 2,635.12 feet to 4,603.26 feet below KB (994.48-1349.63 mbsf), with thicknesses from 804.22 to 2,167.37 feet (245.13 – 660.61 m), and an average thickness of 1,533 feet (467.26 m; Table 1). The Missisauga Formation also comprises three depositional sequences, the MS1, MS2, and MS3, from youngest to oldest (Figs. 2A, B).

Detailed descriptions of the parasequence stacking patterns of each of the ten wells in the GBB follow in the next ten subheadings of this paper. Figures 5A – 11B depict the results of my stacking pattern analysis and are meant to accompany the following descriptions.

COST G1

The sequence stratigraphic analysis of COST G1 extends from the top the first sand below the Turonian top (taken from Amato and Bebout (1980) at 1,878 ftKB (464.82 mbsf) down to the top of the Mohawk Formation at 5,891 ftbKB (1687.98 mbsf). There is a flooding surface at 2161 ftbKB (551.08 mbsf), and a fining upward (retrogradational) transgressive systems tract (TST) from 2161 to 2240 ft (551.08 to 712.62 mbsf; Fig. 5A). The maximum flooding surface (MFS; 2161 ftbKB; 551.08 mbsf) is thus just above the base of the Turonian (Fig. 5A) and globally correlates with Ocean Anoxic Event 2 (OAE2; Miller et al., 2018). A thin progradational package (2362-2408 ftbKB; 749.81 – 763.83 mbsf) is likely the LST of this Dawson Canyon unnamed

sequence ("DCx") that straddles the Cenomanian/Turonian boundary (Fig. 5A). The top of the Logan Canyon Formation is placed at the top of a sand (2408 ftbKB; 626.36 mbsf).

The Logan Canyon Formation top at 2408 ftbKB (626.36 mbsf) is also the sequence boundary at the top of the LC1 sequence (Fig. 6A). The LC1 sequence extends from 2408 ftbKB down to 2820.25 ftbKB (752.02 mbsf). The highstand systems tract (HST) consists of two progradational packages between 2408 ftbKB and 2781.5 ftbKB (740.21 mbsf) that are separated by a flooding surface at 2585 ftbKB (680.31 mbsf). The TST is a retrogradational package from the MFS at 2781.5 ftbKB (740.21 mbsf) to 2820.25 ftbKB (Fig. 5A; 752.02 mbsf). Below this retrogradational package lies the sequence boundary that defines the top of the LC2 sequence, at 2820.25 ftbKB (752.02 mbsf). The LST appears to be truncated or does not exist due to the relatively shallow top Albian biostratigraphic marker in this well.

The LC2 sequence at G-1 (Fig. 7A) extends from the upper sequence boundary at 2820.25 ftbKB (752.02 mbsf) down to 3086.2 ftbKB (833.079 mbsf). The upper part of this sequence (down to 2943 ftbKB) is the coarsening-upward highstand systems tract (HST) from the upper sequence boundary down to a retrogradational TST that extends from 2943 ftbKB down to 3033 ftbKB (789.43 – 816.86 mbsf). This retrogradational package is capped by the MFS indicated by the highest gamma ray log values (Fig. 7A). Below is a coarsening-upward LST package that extends down to the next sequence boundary at 3086.2 ftbKB (833.08 mbsf). The sequence is Albian to possibly lowermost Cenomanian based on correlation at Shell 357 (Fig. 6A).

The LC3 sequence extends from its upper sequence boundary at 3086.2 ftbKB (Fig. 8A; 833.08 mbsf) down to the base of the Naskapi Formation at 4013 ftbKB

(1115.57 mbsf). The HST at the top section of this sequence consists of two upward-coarsening packages from 3086.2 ftbKB down to 3377.14 ftbKB (833.08 – 921.76 mbsf). These two thick sand packages are the oldest sands of the Logan Canyon Formation, and the rest of the LC3 sequence below them is assigned to the Naskapi Shale. The Naskapi section of the LC3 sequence is primarily a retrogradational TST, and throughout it does not fine or coarsen significantly, but small-scale patterns can still be seen in the gamma log values. The majority of this section shows thin progradational parasequences, but there are retrogradational parasequences (indicated by blue arrows on Fig. 7A) from 3515 ftbKB to 3560.3 ftbKB (963.78 977.56 mbsf) and 3746 ftbKB to 3814.24 ftbKB (1034.19 – 1054.99 mbsf) and the overall section fines up to ~3750 ftbKB, where the MFS could be placed and generally remains fine grained to 3374, where the top of the TST and the MFS are tentatively placed . Both of these upward-fining packages are overlain by flooding surfaces, with the lower (3746 ftbKB; 1034.19 mbsf) the possible MFS based on the highest gamma log values. A progradational section below this with a thick sand~3925 ft) may mark a TS and the top of the LST. The base of the Naskapi Formation is also the top of the youngest sequence in the Missisauga Formation, the MS1.

The Missisauga Formation consists of 3 sequences, MS1, MS2, and MS3, from youngest to oldest. The MS1 sequence extends from the upper sequence boundary at 4014 ftbKB (1115.87 mbsf; Fig. 9A) down through three progradational parasequences in the HST, separated by flooding surfaces at 4101.4 and 4262.25 ftbKB (1142.51 and 1191.54 mbsf), down to MFS at 4353.12 ftbKB (1219.24 mbsf) indicated by the stacking pattern and the highest gamma log values. The TST sits below the MFS, and consists of

two retrogradational packages from 4431.27 ftbKB (1243.06 mbsf) up to the MFS, separated by a flooding surface at 4396.48 ftbKB (1232.45 mbsf). The LST at the base of the MS1 sequence on the GR log is a progradational pattern from 4431.27 to 4483.45 ftbKB (1243.06 – 1258.96 mbsf). Below this lies the sequence boundary denoting the top of the MS2.

The HST of the MS2 sequence (Fig. 10A) is made up of a series of five progradational parasequences that extend from the top sequence boundary at 4482.1 ftbKB (1258.55 mbsf) down to 4898 ftbKB (1385.31 mbsf). Below the MFS indicated by a change in stacking pattern from fining to coarsening up at 4898 ftbKB (1385.31 mbsf), the TST consists of two upward-fining parasequences, separated at 5000 ftbKB (1416,41 mbsf) by a flooding surface. A thin progradational section at the base of the sequence in the Berriasian (5075-5104 ftbKB; 1439.27-1448.1 m), may be a LST. I place a sequence boundary at 5104 ftbKB (1448.1 mbsf), marking the top of the MS3 sequence. Otherwise, biostratigraphy suggests that the MS2 sequence is Aptian.

In the COST G1 well (Fig. 11A), the MS3 sequence top lies at 5104 ftbKB (1448.1 mbsf), and the sequence extends down through the Mic Mac/Abenaki formation and into the Mohawk Formation, but my analysis stops at the top Mic Mac/Abenaki formation. Only the highstand systems tract of the MS3 sequence lies within the Missisauga formation. This consists of two thick retrogradational parasequences, identifiable by their low GR readings, all assigned to the lowermost Cretaceous. Below these sands lies the top of the Mic Mac / Abenaki formation, at 5296.14 ftbKB (1506.67 mbsf) with the top of the Tithonian at 5290 ftbKB (1504.80 mbsf). This analysis highlights that sequence stratigraphic units may differ significantly from lithologic

interpretation, because sequences necessarily have different depositional characteristics in the LST, TST, and HST, but a purely lithological interpretation instead divides up the sediments by mineral content instead of considering their context.

Exxon 133

My analysis of this well begins at 2527.17 ftKB (662.69 mbsf), the first low GR sand signature above Amato and Bebout's (1980) Cenomanian top (Fig. 5A). This well has a progradational package that extends down to 2632.32 ftbKB (707.84 mbsf), followed by a retrogradational package, whose base ends with the LC1 sequence boundary at 2802 ftbKB (759.56 mbsf; Fig 4A).

The HST in the LC1 sequence begins directly underneath the sequence boundary (Fig. 6A) with three coarsening upward parasequences and extends down to 3073.44 ftbKB (842.30 mbsf) where I place the MFS based on a change in stacking pattern and the highest GR values (Fig. 5A). The TST is thin, and the presence of a LST is uncertain.

The HST of the LC2 sequence (Fig. 7A) extends downward from the sequence boundary at 3103.8 ftbKB (851.55 mbsf) through three progradational parasequences, separated by a FS at 3299.25 ftbKB (911.12 mbsf), down to the top of the TST at 3384.69 ftbKB (937.17 mbsf). The retrogradational TST extends down to 3494.14 ftbKB (970.53 mbsf), where the progradational LST begins, and extends down to the next sequence boundary at 3562 ftbKB (Fig. 6A; 991.21 mbsf).

The HST of the LC3 sequence of the Exxon 133 (Fig. 8A) extends down through two progradational packages, separated by a FS at 3666.5 ftbKB (1023.06 mbsf), down to the TST at 3740.48 ftbKB (1045.61 mbsf). The retrogradational TST extends down to the

base of the Logan Canyon Formation at 4049 ftbKB (1139.64 mbsf), where the MFS signifies the start of the Naskapi Formation. The Naskapi portion of the TST has a generally higher GR signature, and has an aggradational pattern, despite some small-scale retrogradational and progradational patterns, and multiple FS throughout. The TST of the LC3 in the Exxon 133 well apparently ends at 4687.79 ftbKB (1334.35 mbsf), where the Missisauga Formation and the MS1 sequence start. Alternatively, there may be a LST below 4620 ftbKB (1313 mbsf).

The HST of the MS1 sequence at Exxon 133 (Fig. 9A) begins at the upper sequence boundary and extends down to the MFS at 5026.27 ftbKB (1437.52 mbsf) with two major FS dividing it into three parasequences. Below this flooding surface the TST continues down to 5130.43 ftbKB (1469.27 mbsf), where there is a thin transgressive surface (TS) and a LST down to 5146.27 ftbKB (1474.10 mbsf), where the MS2 sequence starts.

The HST of the MS2 sequences (Fig. 10A) shows a serrated log pattern punctuated by several flooding surfaces divided into at least 3 parasequences, though it has a generally progradational pattern down to the MFS and the top of the TST at 5413.3 ftbKB (1555.49 mbsf). The retrogradational TST continues downward through a flooding surface to the transgressive surface and top of the LST at 5531.2 ftbKB (1591.42 mbsf) where a FS marks the point where the fining upward trend of the TST reverses and the underlying parasequence coarsens upward instead. The aggradational to progradational LST ends at the MS3 sequence boundary at 5728.46 ftbKB (1651.55 mbsf).

The MS3 sequence at Exxon 133 (Fig. 11A) begins 5728.46 ftbKB (1651.55 mbsf) with the progradational HST continuing down through the Mic Mac/ Abenaki

Formation top at 5955.98 ftbKB (1720.89 mbsf) where my detailed sequence stratigraphic analysis ends. Below this formational boundary, the retrogradational TST pattern shows several sand packages separated by flooding surfaces which overly a longer aggradational section that continues down through the Berriasian top (Edson et al, 2000i).

Mobil 312

The Mobil 312 well has a progradational sand package from 2601 ftbKB (686.71 mbsf), where my analysis starts (Fig. 5A), down to the LC1 sequence boundary at 2871 ftbKB (769.01 mbsf), which sits at the first competent sand interval below the Cenomanian top at 2790 ftbKB (744.32 mbsf) (Edson et. al., 2000e). The overlying unnumbered Dawson Canyon "x" (DCx) Sequence is particularly sandy here, and would not serve as a confining bed. The Dawson Canyon Formation equivalent is too thin in the GBB to identify how many sequ3ences it might have, or which one is present in the GBB. Below the top LC1 SB, the first parasequence of the HST extends down to 2922.89 ftbKB (Fig. 5A; 784.83 mbsf), where a retrogradational parasequence lies within the HST despite its grain size trend and because of its low GR signature and implied high sand content. A second progradational parasequence extends from 2970 to 3025 ftKB (799.19 – 815.94 mbsf) where a retrogradational parasequence begins the TST at the MFS (Fig. 6A). The TST in this well is aggradational, with only slight differences between its retrogradational and progradational intervals down through a flooding surface at 3025 ftbKB, to the LST at 3149.7 ftbKB (853.96 mbsf). The progradational LST continues down to the LC2 SB at 3220 ftbKB (875.39 mbsf).

The LC2 sequence HST progrades from the overlying SB down to 3430.6 ftbKB (Fig. 7A; 939.58 mbsf), where the generally aggradational TST shows small scale retrogradational patterns down to the LST at 3567.4 ftbKB (981.27 mbsf). The LC2 LST in this well shows a relatively smooth progradational pattern down to the LC3 SB at 3657 ftbKB (1008.58 mbsf).

The HST of the LC3 sequence extends downward through the Naskapi Formation top at 4096.87 ftbKB (Fig 8A; 1142.66 mbsf) with three to four parasequences. The MFS at 4231 ftbKB (1183.54 mbsf), and a thin retrogradational parasequence down to 4296.41 ftbKB (1203.48 mbsf). At this depth the LST package begins, and very slightly progrades all the way down to the Missisauga Formation top and the MS1 SB at 4776 ftbKB (1349.65 mbsf).

The MS1 HST fines up down to 4997.29 ftbKB (Fig. 9A; 1417.10 mbsf), where the MFS and top TST begins as a retrogradational package that extends as least as far down as a flooding surface at 5030 ftbKB (1427.07 mbsf). Below this flooding surface, the TST maintains an aggradational pattern down to 5084.7 ftbKB (1443.75 mbsf), where it changes back to a clearly retrogradational pattern down to where the LST changes back to a progradational pattern at 5138.09 ftbKB (1460.02 mbsf). The LST continues down to the MS2 SB at 5184.73 ftbKB (1474.24 mbsf).

The MS2 progrades down to the thick (10 ft thick) MFS at 5404 ftbKB (Fig. 10A; 1541.07 mbsf). The TST fines upward down to 5497 ftbKB (1569.42 mbsf), where the LST package begins to coarsen upward in three parasequences down to the MS3 SB at 5784 ftbKB (1656.89 mbsf).

Only the HST of the MS3 sequence lies within the Missisauga formation. This portion of the sequence generally progrades, but with several retrogradational parasequences, down to the formation boundary at 6018.06 ftbKB (Fig. 11A; 1728.23 mbsf), which is the Mic Mac/Abenaki top.

Shell 357

My sequence stratigraphic analysis of this well begins at the first significant low GR reading overlain by a very high GR measurement, or the largest sand under the largest flooding surface, below the published Cenomanian top (Fig 5A; Edson et al., 2000f). The top of the Logan Canyon formation and the LC1 SB sit at 2915 ftbKB (Fig. 6A; 785.77 mbsf). The HST of the LC1 sequence extends down to a parasequence boundary at 2962 ftbKB (785.77 mbsf). It is aggradational then progradational downward through the MFS at 3093.5 ftbKB (840.18 mbsf). The MFS is recognized by a change from progradational above to retrogradational below. Continuing downward there are two retrogradational packages in the TST down to 3135.6 ftbKB (853.01 mbsf), and then to 3163.5 ftbKB (861.52 mbsf), followed by an aggradational section which ends at the top of the LC2 sequence at 3210 ftbKB (875.69 mbsf).

The LC2 HST extends down to 3291.5 ftbKB (Fig. 7A; 900.53 mbsf). The change to retrogradation appears at this level, though the MFS may be a zone of muds from 3291 to 3330 ftbKB (900.40 – 912.27 mbsf). The TST section of this sequence extends through this thick flooding surface, from 3291 to 3327 ftbKB (900.40 to 911.35 mbsf), to an anomalous progradational interval from 3358.3 to 3882 ftbKB (920.89 to 1080.52 mbsf)

before continuing an aggradational pattern down to the LC3 sequence boundary at 3520.2 ftbKB (970.24 mbsf). It is not clear if a LST is preserved.

The LC3 sequence HST progrades from the SB down to 4042 ftbKB (Fig. 8A; 1129.28 mbsf), despite having several retrogradational intervals (e.g.: 3582 to 3700.95 ftbKB (989.06 to 1025.33 mbsf), and 3792 to 3816.5 ftbKB (1053.08 to 1060.55 mbsf)). The MFS, the top of the TST, and the Naskapi top at 4042.28 ftbKB (1129.37 mbsf), and transitions into the progradational LST at 4221.1 ftbKB (1183.88 mbsf). The LST progrades down through the Naskapi formation to the top of the Missisauga Formation and the MS1 SB at 4729.39 ftbKB (1338.80 mbsf).

The MS1 HST progrades through several large sand packages down to the MFS and top TST at 4881 ftbKB (Fig 9A; 1385.01 mbsf). This relatively thin TST has one fining upward parasequence which extends down to the LST at 4927 ftbKB (1399.03 mbsf). The LST progrades down through two significant flooding surfaces to the MS2 sequence boundary at 5138 ftbKB (1463.34 mbsf).

The MS2 sequence HST progrades down to the MFS at 5418 ftbKB (Fig. 10A; 1548.69 mbsf), where the TST extends down to 5488.4 ftbKB (1570.15 mbsf), and the LST begins. The LST progrades down to the MS3 SB at 5714.29 ftbKB (1639 mbsf).

The MS3 HST progrades down to the TST at 5790.41 ftbKB (Fig. 11A; 1662.20 mbsf). The TST extends downward through numerous flooding surfaces to the LST at 5869 ftbKB (1686.15 mbsf), and the LST progrades at as far as the base of the Missisauga formation at 5959.57 ftbKB (1713.76 mbsf), where my analysis ends.

Exxon 975

My analysis on this well begins at the first progradational section of the GR log nearest the Cenomanian top (Edson et. al., 2000b). This section begins at 2116.4 ftbKB (Fig. 5B; 556.07 mbsf), above the Cenomanian top, and extends down to 2220.32 ftbKB (587.75 mbsf), where the GR pattern fines upward down to the top of the Logan Canyon formation and the LC1 sequence boundary at 2263 ftbKB (Fig. 6B; 600.76 mbsf). The HST of the LC1 sequence progrades down, despite a short retrogradational parasequence from 2303 to 2326 ftbKB (612.95 – 619.96 mbsf), through a second progradational parasequence to the MFS at 2372.97 ftbKB (634.28 mbsf), where the aggradational pattern of the TST continues downward to the LC2 sequence boundary at 2448 ftbKB (657.15 mbsf).

The HST of the LC2 sequence progrades down to 2491 ftbKB (Fig. 7B; 807.42 mbsf) where a thick MFS signals the beginning of the TST. This MFS extends down to 2515.3 ftbKB (677.66 mbsf), and is underlain by alternating retrogradational sections and flooding surfaces down to the LST at 2733.8 ftbKB (744.26 mbsf). The LST progrades down to the LC3 SB at 2827.44 ftbKB (772.80 mbsf).

The LC3 HST progrades down to the MFS at 3244 ftbKB (Fig. 8B; 899.77 mbsf) where the TST begins, and continues downward across the Naskapi Formation top. The Naskapi section of the LC3 TST has an aggradational pattern down to the LST at 3511.3 ftbKB (981.24 mbsf), where the GR log pattern begins to coarsen upward again. The LST ends at the top of the Missisauga formation and the MS1 SB.

The MS1 sequence HST progrades down to the MFS at 3909 ftbKB (Fig 9B; 1102.46 mbsf). The TST extends downward from this MFS, where two fining upward

parasequences extend down to a flooding surface at 4094.76 ftbKB (1159.08 mbsf), where a progradational pattern continues down to 4133.42 ftbKB (1170.86 mbsf). This progradational section extends down to 4249.35 ftbKB (1206.20 mbsf), where there's another flooding surface and the GR pattern becomes aggradational down to 4341.02 ftbKB (1234.14 mbsf), where there's a retrogradational section down to the LST at 4406 ftbKB (1253.94 mbsf). The LST section of the MS1 sequence consists of one progradational parasequence which extends down to the MS2 SB at 4531 ftbKB (1292.05 mbsf).

The MS2 HST has three parasequences and extends downward through a small flooding surface at 4689.6 ftbKB (Fig. 10B; 1340.39 mbsf) to the TST at 4941.35 ftbKB (1417.12 mbsf). The aggradational pattern of the TST extends downward to 5145.42 ftbKB (1479.32 mbsf), where the LST progrades down to the MS3 sequence boundary at 5171.16 ftbKB (1487.17 mbsf).

The MS3 HST begins at the above sequence boundary and progrades down to the MFS at 5272 ftbKB (Fig. 11B; 1517.90 mbsf). Below the MFS, the TST fines upward down to the LST at 5428.02 ftbKB (1565.46 mbsf), which progrades down to a flooding surface 5488 ftbKB (1583.74 mbsf). Below this transgressive surface the gamma log values show a retrogradational pattern down to the base of the top Mic Mac/Abenaki at 5588 ftbKB (1614.22 mbsf).

COST G2

My analysis on this well begins at the first progradational section of the GR log nearest the Cenomanian top (Fig. 5B; Amato and Simonis, 1980). The HST of the LC1

sequence begins at 2344.45 ftbKB (Fig. 6B; 607.60 mbsf) and is generally progradational though there are retrogradational parasequences from 2371.38 to 2432.79 ftbKB (615.81 to 634.52 mbsf) and progradational to the MFS at 2474 ftbKB (647.09 mbsf). The TST then fines upward down to the LST at 2515 ftbKB (654.41 mbsf), which then extends down in three parasequences to the LC2 sequence boundary at 2664.4 ftbKB (705.12mbsf).

The LC2 HST progrades from the upper SB down through two retrogradational intervals from 2732 to 2759.01 ftbKB (Fig. 7B; 725.73 – 733.96 mbsf) and 2817.08 to 2841 ftbKB (751.66 to 758.95 mbsf) to the MFS at 2881 ftbKB (771 mbsf). Below the MFS the TST fines upward down to the LST at 3022 ftbKB (814.12 mbsf) with five parasequences. The LST progrades down to the LC3 SB at 3273.83 ftbKB (890.88 mbsf), where a flooding surface marks the change from lowstand sedimentation pattern to highstand sedimentation.

The LC3 HST progrades down through the top of the Naskapi Formation to the MFS at 3407.44 ftbKB (931.60 mbsf; Fig. 8). A thin transgressive surface at 3817 ftbKB (1056.44 mbsf) overlies a progradational LST below, which terminates at the top of the Missisauga formation and the MS1 SB at 3952.2 ftbKB (1097.65 mbsf).

The MS1 HST progrades down past flooding surfaces at 4160.46, 4240.08, and 4309.73 ftbKB (Fig. 9B; 1161.12, 1185.39, 1206.62 mbsf) to the MFS 4420 ftbKB (1240.23 mbsf). Below the MFS the TST stacking pattern fines upward down to 4673 ftbKB (1317.35 mbsf), where the thick LST progrades down to a major flooding surface and the MS2 sequence boundary at 4758 ftbKB (1343.25 mbsf).

The MS2 HST progrades from the MS2 SB down to the MFS at 4910 ftbKB (Fig. 10B; 1389.58 mbsf). Below the MFS the retrogradational pattern of the TST extends downward through the MFS at 5069 ftbKB (1438.05 mbsf), to the LST at 5139 ftbKB (1459.38 mbsf). The LST progrades down to a flooding surface at 5262.57 ftbKB (1497.05 mbsf), below which there's a thick retrogradational section overlying the MS3 SB at 5391.64 ftbKB (1700.98 mbsf) similar to those seen in the Exxon 975 and Conoco 145 wells (Fig. 10B) at this same position in the sequence stacking pattern.

The MS3 HST progrades down through two parasequences, separated by a flooding surface at 5542 (Fig. 11B; 1582.21) and terminates at the MFS at 5631 ftbKB and (1609.34 mbsf). Below the MFS, the TST retrogrades through two parasequences to the LST at 5713 ftbKB (1643.34 mbsf). The LST progrades to the top of the Mic Mac/ Abenaki formation at 5818.12 ftbKB (1666.38 mbsf).

Mobil 273

My analysis of this well begins at the lowest GR reading overlain by a flooding surface between 2300 and 2600 ftbKB (Fig. 5B; 609.30 and 700.74 mbsf), as this well lacks any chronostratigraphic data above 4500 ftbKB (1279.86; Edson et. al., 2000). There is a flooding surface at 2511.3 ft ftbKB (673.70 mbsf), below which the GR log pattern fines upward down to the LC1 sequence boundary and the Logan Canyon formation top at 2544 ftbKB (Fig. 6B; 683.67 mbsf). The HST of the LC1 sequence progrades through three coarsening upward parasequences and two minor fining up intervals at 2606.32 to 2618.11 ftbKB (702.66 to 706.26 mbsf), and 2658.8 to 2681 ftbKB (718.66 to 725.42 mbsf), to a MFS at 2758 ftbKB (748.89 mbsf). Below the MFS

there is a short aggradational TST down to 2774 ftbKB (753.77 mbsf), where the LST begins and progrades down to the LC2 SB at 2840 ftbKB (773.89 mbsf).

The LC2 HST progrades down through coarsening upward parasequences to the MFS and the TST top at 3010.2 ftbKB (Fig. 7B; 825.76 mbsf). The TST fines upward down to 3042.91 ftbKB (835.73 mbsf), where the LST extends down through two progradational parasequences to the LC3 SB at 3165.89 ftbKB (873.21 mbsf).

The LC3 HST progrades down to the top of the Naskapi Formation and the TST at 3310 ftbKB (Fig. 8B; 917.14 mbsf). The TST maintains an aggregational pattern down to 3491 ftbKB (972.31 mbsf), where the fining upward pattern extends down to the LST at 3548 ftbKB (989.69 mbsf). The LST progrades down to an aggradational section from 3758 to 3932 ftbKB (1053.69 to 1106.73 mbsf) before progradational again down to the Missisauga formation top and the MS1 sequence boundary at 3999.5 ftbKB (1127.30 mbsf).

The MS1 HST generally progrades down through numerous flooding surfaces (e.g.: 4155, 4324, and 4542 ftbKB; Fig. 9B; 1174.70, 1226.21, and 1292.66 mbsf) and ~6 parasequences before reaching the MFS at the top of the TST at 4662.96 ftbKB (1329.53 mbsf). The TST fines upward down to the LST at 4711.78 ftbKB (1344.41 mbsf). The LST progrades through flooding surfaces at 4728, 4796, and 4865 ftbKB (1349.35, 1370.08, and 1391.12 mbsf) before terminating at the MS2 SB at 4900 ftbKB (1401.76 mbsf).

The MS2 HST contains two progradational parasequences from 4900 to 5039 ftbKB (Fig 10B; 1401.78 to 1463.34 mbsf), and across from 5039 to 5102 ftbKB (1444.14 to 1463.34 mbsf), to the MFS at 5138 ftbKB (1474.31 mbsf). The TST contains

two parasequences from 5138 to 5284.52to the LST at 5284.58 ftbKB (1519 mbsf). The LST consists of three progradational series from 5284.58 to 5330.92 ftbKB (1519 to 1533.12 mbsf), from 5330.92 to 5464.39 ftbKB (1533.12 to 1573.80 mbsf), and from 5464.39 to 5551.52 ftbKB (1573.80 to 1600.34 mbsf), which is also the MS3 SB.

The MS3 HST progrades down to the MFS at 5751.72 ftbKB (Fig. 11B; 1661.38 mbsf), and the TST fines upward down to 5799.63 ftbKB (1675.98 mbsf). A transgressive surface at this level overlies a prograding LST with two parasequences down to the base of the Missisauga formation at 6031 ftbKB (1746.50 mbsf).

Tenneco 187

My analysis of this well begins at the first significant low GR reading below the Cenomanian top (Fig. 5B; Edson et al., 2000). The upper sequence boundary of the LC1 is at 2234 ftbKB (Fig. 6B; 589.48 mbsf). The HST extends down from the sequence boundary to the MFS at 2371 ftbKB (631.24 mbsf). Below the MFS the TST fines upward down to 2402 ftbKB (640.69 mbsf), where the LST begins. The LST in this well has two progradational parasequences, from 2402 to 2455.75 ftbKB (640.69 to 657.07 mbsf), and from 2466 to 2560 ftbKB (660.20 to 688.85 mbsf), which both end in a flooding surface at the base. The LST ends at the LC2 SB at 2560 ftbKB (688.85 mbsf).

The LC2 HST progrades down to the MFS at 2677 ftbKB (Fig. 7B; 724.51 mbsf), below which the GR pattern has 3 retrogradational sequences from 2679 to 2711 ftbKB, 2723 to 2751 ftbKB, and 2753 – 2793 ftbKB (725.12 to 734.87 mbsf, 738.53 to 747.06 mbsf, and 747.67 to 759.87 mbsf), where the LST begins. The LST progrades down through two progradational series from 2793 to 2904 ftbKB and 2934 to 3018 ftbKB

(759.87 to 793.70 mbsf and 802.84 to 828.45 mbsf) which are separated by a flooding surface, down to the LST. The LST ends at the LC3 sequence boundary at 3018 ftbKB (828.45 mbsf).

The LC3 sequence begins with a thin retrogradational series from the upper SB down to 3081 ftbKB (Fig. 8B; 847.65 mbsf). Below this the HST begins in earnest and fines down through the Naskapi top at 3129 ftbKB (862.28 mbsf) to the TST at 3167 ftbKB (873.86 mbsf). Below this the TST is aggradational down to the LST at 3634 ftbKB (1016.20 mbsf). It is worth noting that the GR values in the TST in this well do not vary largely, and instead show multiple weak progradational and retrogradational trends at the parasequence scale. The LST has a thin progradational section down to 3553 ftbKB (991.51 mbsf), and then is aggradational down to the MS1 sequence boundary and the Missisauga formation top at 3611.29 ftbKB (1009.28 mbsf).

The MS1 HST has 3 long progradational sections separated by flooding surfaces from 3611.29 to 3683 ftbKB, 3699.5 to 3916 ftbKB, and from 3929 to 4261 ftbKB (Fig. 9B; 1009.28 to 1031.14 mbsf, 1036.17 to 1102.16 mbsf, and 1106.12 to 1207.31 mbsf). The MFS at 4261 ftbKB (1207.31 mbsf) signals the start of the retrogradational TST, which extends down to 4296 ftbKB 1217.98 mbsf), where the LST coarsen s upward down to the MS2 SB at 4400 ftbKB (1249.68 mbsf).

The MS2 HST progrades from the upper sequence boundary down through three distinct parasequences: from 4400 – 4660 ftbKB, 4664 – 4714 ftbKB, and 4721 – 4803.8 ftbKB (Fig. 10B; 1249.68 to 1328.93 mbsf, 1330.15 to 1345.39 mbsf, and 1347.52 to 1372.76 mbsf). There is no definite TST underlying the HST in this sequence in this well, but there is a lowermost progradational sequence from 4809 to 4909 ftbKB (1374.34 to

1404.82 mbsf) above the Valangian top (Edson et. al., 2000) that overlies the most notable flooding surface in this sequence at 4909 – 4914 ftbKB (1404.82 to 1406.35 mbsf). This last progradational series may be part of the HST or part of the LST. A tentative MFS at 4790 ftbKB (1368.55 mbsf) may overlie a TST down to the top of this lowermost parasequence boundary. The MS2 sequence ends at the first competent sand body below the Valangian top, at the MS3 SB at 4947 ftbKB (1416.41 mbsf).

The MS3 HST progrades down to the MFS at 5202 ftbKB (Fig. 11B; 1494.13 mbsf), which is top of the Mic Mac/Abenaki formation. Below the MFS there is one progradational section down to 5245 ftbKB (1507.24 mbsf), and then a thick gradual retrogradational TST section down to 5365 ftbKB (1559.05 mbsf) overlying a heterolithic unit, where my sequence stratigraphical analysis ends.

Conoco 145

My analysis of this well begins at 2230 ftbKB (Fig. 5B; 562.36 mbsf), which is the depth of the first competent sand body below the Cenomanian top (Edson et. al., 2000) and the LC1 sequence boundary. This sequence coarsens up down to a thin retrogradational TST at the base from 2343 (marking the MFS) to 2355 ftbKB (Fig. 6B; 596.80 – 600.46 mbsf), which directly overlays the LC2 SB at 2357.37 ftbKB (601.18 mbsf), recognized as the first sand below the Albian top (Edson et. al., 2000).

The LC2 progrades through two HST parasequences to the MFS at 2663 ftbKB (Fig. 7B; 694.33 mbsf). Below the MFS, the TST fines upward down to the LST at 2770 ftbKB (726.95 mbsf). The LST progrades down to the LC3 SB at 2862.31 ftbKB (755.084 mbsf).

The LC3 HST progrades down to the MFS at 3042 ftbKB (Fig. 8B; 809.85 mbsf), just below the Naskapi top. Below the MFS the aggradational TST extends downward with only minor variation in the GR value until the MS1 sequence boundary at 3647 ftbKB (994.26 mbsf). There may be a transgressive surface at 3550 ftbKB (964.69 mbsf) and the LST below.

The MS1 HST progrades down through two minor flooding surfaces at 3950.53 ftbKB (Fig. 9B; 1086.77 mbsf), and 4195.55 ftbKB (1161.46 mbsf) before terminating at the MFS at 4280 ftbKB (1187.20 mbsf). Below the MFS the TST fines upward down to the LST at 4340.13 ftbKB (1205.52 mbsf). The LST progrades down to the MS2 SB at 4431 ftbKB (1233.22 mbsf).

The MS2 has two long progradational series from the upper sequence boundary down to a flooding surface at 4670 ftbKB (Fig. 10B; 1306.07 mbsf), and from there down to the MFS at 4954 ftbKB (1392.63 mbsf). Below the MFS, the TST fines upward down to the MS3 sequence boundary at 5096 ftbKB (1435.91 mbsf).

The MS3 HST progrades down through the Mic Mac/Abenaki top at 5260 ftbKB (Fig. 11B; 1485.90 mbsf), and concludes at the MFS at 5544 ftbKB (1572.46 mbsf), where the sequence continues past the lithological unit change at the MFS and top of the TST.

Shell 410

My analysis of this well begins at the Cenomanian top (Edson et.al., 2000). The flooding zone nearest the Cenomanian top marks the upper boundary of a prograding parasequence at 2705 ftbKB (Fig. 5B; 686.41 mbsf), which ends at the top of the Logan

Canyon formation and the LC1 sequence boundary at 2720.8 ftbKB (691.23 mbsf). The HST of the LC1 sequence progrades down to the MFS at 2787 ftbKB (Fig. 6B; 711.40 mbsf). Below the MFS a relatively thin TST overlies the LST, which progrades down to the LC2 sequence boundary and the Albian top at 2809.73 ftbKB (718.33 mbsf).

The LC2 sequence begins with two retrogradational parasequences, from 2823 to 2866 ftbKB (Fig. 7B; 722.38 to 735.48 mbsf), and from 2866 to 2879 ftbKB (735.48 to 739.44 mbsf). The HST is more readily apparent below 2879 ftbKB (739.44 mbsf), where the low GR coarse sands can be broken up into ~5 parasequences down to the MFS at 3059 ftbKB (794.31 mbsf). Below the MFS, the TST fines upward down to the LST at 3216.88 ftbKB (842.43 mbsf). The LST in this sequence briefly progrades down to 3258.29 ftbKB (855.05 mbsf) before becoming aggradational down to the LC3 sequence boundary at 3358 ftbKB (885.44 mbsf; Fig 7B).

The LC3 sequence HST begins at the upper sequence boundary and progrades down to the MFS at 3485 ftbKB (Fig. 8B; 924.145 mbsf). Below the MFS, the TST fines upward down to 3534 ftbKB (939.09 mbsf), where the last sand body above the Naskapi Formation extends down to 3558 ftbKB (946.40 mbsf), below which the TST continues an aggradational pattern down to the LST at 3973 ftbKB (1072.90 mbsf). The LST progrades down to the top of the Missisauga formation and the MS1 sequence boundary at 4053 ftbKB (1097.28 mbsf).

The MS1 HST progrades down to the MFS and top of the TST at 4594 ftbKB (Fig. 9B; 1262.18 mbsf). The TST has 2 retrogradational parasequences from 4594 – 4665 ftbKB (1262.18 – 1283.82 mbsf), separated by a flooding surface at 4624 ftbKB (1271.32 mbsf). Below these two retrogradational series there are two progradational

parasequences from 4664 – 4747 ftbKB (1283.51 – 1308.81 mbsf), separated by a flooding surface at 4717 ftbKB (1299.67 mbsf). These are underlain by an aggradational section which extends down to 4834 ftbKB (1335.33 mbsf). That progrades down to the MS2 sequence boundary at 4890 ftbKB (1352.40 mbsf).

The MS2 HST has two clearly progradational series separated by a flooding surface from 4890 – 5030 ftbKB (Fig. 10B; 1352.40 – 1395.07 mbsf), and from 5073 – 5154 ftbKB (1408.18 mbsf). At this depth the GR pattern becomes aggradational, indicating that this is most likely the TST, despite very sandy intervals from 5194 – 5241 ftbKB (1445.06 – 1459.38 mbsf), 5332 - 5366 ftbKB (1487.12 – 1497.48 mbsf), 5394 – 5421 ftbKB (1506.02 – 1514.25 mbsf), and 5451 – 5491 ftbKB (1523.39 – 1535.58 mbsf). The LST begins to coarsen upward at 5539 ftbKB (1550.21 mbsf), and extends down to the MS3 sequence boundary at 5652 ftbKB (1584.65 mbsf).

The MS3 HST progrades down to a flooding surface at 6261 ftbKB (Fig. 11B; 1770.28 mbsf), but my sequence stratigraphical analysis ends at the Mic Mac/ Abenaki top at 6003 ftbKB (1691 mbsf).

Seismic Correlation

I identified prominent seismic reflectors for the Logan Canyon and Missisauga Formation tops after projecting the GR logs onto the nearest seismic survey data. These reflectors correlate with the MK1 and LK1 reflectors identified in the Baltimore Canyon Trough by Miller et al. (2018) and Schmeltz et al. (2018). Both the MK1 and LK1 reflectors lie at most only 1 reflector above or below the formation tops as picked on the GR cross section, but most of the formation top picks lie directly on the chosen reflectors.

This slight variability may result from the varying distances between the wells and their respective nearest seismic lines, the varying quality of the different seismic surveys, and/or the different integrated seismic well ties created within Petrel, which themselves vary depending upon the quality of the seismic survey used. These two reflectors were loop correlated across the majority of the available seismic data in the GBB (Fig. 1B).

The MK1 and LK1 reflectors are both identifiable by their high amplitude and the numerous reflectors which downlap onto them across the basin. These traits also support my interpretation that they are sequence boundaries (Miller et al., 2018).

The Naskapi Formation top was more difficult to consistently transfer from GR logs to 2D seismic surveys because this formation is defined by a change in lithology, and the change from sand to shale on GR did not consistently match up with the same seismic reflector across the basin. There is more variation in how the Naskapi Formation top correlates with seismic reflectors, as all the GR top picks for the Naskapi lie within two reflectors of the purple reflector traced in Figures 12B and 13B.

Discussion

Overview

In order to evaluate a formation's suitability for CCS, I considered the depth, thickness, porosity, permeability, and potential seals overlying the formation. The Missisauga Formation is a suitable CCS target for the GBB, but the Logan Canyon Formation not a suitable target.

The Logan Canyon Formation has two significant deficiencies: it is both too shallow to maintain pressure needed to keep sequestered CO_2 in liquid form, and it lacks a consistent seal.

The top of the Logan Canyon is characterized on gamma logs by a striking negative shift in gamma values (Fig. 5A-B and 6A-B), but this transition only moves from the sandy Dawson Canyon Formation above, to the sandier Logan Canyon Formation below. The difference in gamma readings illustrates just how sandy the Logan Canyon is, but the gamma signatures of the two sands aren't different enough to indicate that the overlying Dawson Canyon could act as a seal for the Logan Canyon. A thin trend of higher GR values directly overlies the Logan Canyon top in a few wells in the Shell 410, Conoco 145, and Shell 357 (fig 5A-B), but these wells are the farthest three wells from shore and closest to the shelf edge (Fig 1A), and the lower GR value trend seen across them above the Logan Canyon top doesn't continue further northwest into the basin.

Sequence Stratigraphic Analysis of GR Logs

In order to construct sequences from GR log patterns I used the methods of Miller et al. (2018) to identify progradational and retrogradational patterns in the log values. The HSTs stand out as low-GR sections, often with a blocky appearance. These sedimentary deposits are composed primarily of sand, and generally have more coarse sand at the top or in upper sections, and finer sand and silt at the bottom. Some of these HST deposits can be hundreds of feet thick (e.g., the LC2 HST in the Mobil 312; Fig. 7A). The HST is never limited to one continuous low to high GR pattern, but is instead broken up by

flooding surfaces identified by their abrupt changes to high GR values. Despite the interruptions by flooding surface, the HST often shows a repeat of its characteristic low GR readings, while continuing to coarsen upward through each sand package. The COST G2 LC2 sequence (Fig. 7B) is an excellent example of this pattern. This sequence has three distinct sand packages in the HST, separated by 2 relatively high GR flooding surfaces. The third parasequence from the top (2841-2880 ft KB) overlies the MFS, underneath which the deposition pattern changes. Under the MFS, the TST starts out with low GR readings at the base, and gradually increases toward the top, indicating a change from coarser grains (sands) at the bottom to more muddy and silty grains at the top, or "retrogradational." Just as the HST can at times just remain sandy over thick intervals, the TST can also be aggradational, without noticeable change in inferred grain size over thick intervals. This trend is best illustrated by the LC3 sequence in the Tenneco 187 (Fig. 8B) and the Mobil 312 (Fig. 8A) wells. In these wells, the entire Naskapi Formation is one thick aggradational section that doesn't exhibit any large-scale fining or coarsening pattern (Figs. 8A and B). It is identified as the TST instead by comparing its contextually high GR readings to the low-GR (inferred sand-rich) HST and LST deposits above and below.

LSTs show similar trends as the HSTs. They also coarsen upward and have more sandy deposits at the top, with less sandy, or more silty/muddy/shaley deposits at the base. The difference is that while LSTs have the same shape on GR logs, they characteristically have a higher GR baseline value indicating they are less sandy than HSTs. The LST in the Shell 357 MS2 sequence (Fig. 10A) shows this difference best. While both the HST and LST in this sequence show consistent progradational GR

patterns, the HST has much lower GR measurements at the top than the LST does at its own top. However, these GR log patterns are not always sufficient by themselves to identify depositional sequences.

In order to correlate the sequences across all ten wells consistently I had to consider the age of the sediments in addition to the trends in GR values identified. The LC1 sequence in each well must be the same age in order for them to be the same sequence (Miller et al., 2018). Published biostratigraphic data (Amato and Bebout, 1980; Edson et.al, 2000a-i) often forced me to cut sequences short where I would otherwise have interpreted them differently. Further evaluation of biostratigraphic data is warranted with further iterations on the precise placement of the sequence boundaries. Despite this limitation, I can confidently correlate 3 LC and 3 MS sequences.

LC1 sequence

The upper sequence boundary (SB) of the LC1 sequence is placed at the first strong low GR signature below a higher GR reading, or flooding zone, below the published Cenomanian top (Fig. 6A and B). A flooding "zone" is a longer period of flooding indicated on the GR log by a thicker high GR section, indicating a longer period of flooding persisted during the time these sediments were deposited. The Mobil 273 well lacks biostratigraphic data at this depth (Edson et al, 2000d), so for this well I identified the LC1 top through both the sequence stratigraphic analysis methods and seismic integration. Projecting the GR logs of all ten wells onto seismic data allowed me to identify and trace the reflector that coincided with the LC1 tops of the other nine wells

across the Mobil 273 (Fig. 13B) and match that reflector to a sand package at 2544 ft KB (Fig. 6B).

The LST in the LC1 sequence is generally thinner (roughly 1/3rd the thickness) than the HST, has higher GR values, and ends at the first major decrease in the GR log below the Albian top. This last criterion suggests the absence of the LST in the Conoco 145 and the Shell 410 wells. The biostratigraphic data in these wells shows the Albian top at a much shallower depth from the upper SB than the other eight wells in the basin, but these two wells are also the closest wells to the edge of the continental shelf, which may have affected sedimentation rate or erosion of sediments differently than the other eight wells. The Albian top in both of these wells should be confirmed.

LC2 Sequence

This sequence generally begins at the most dramatic shift to low GR values nearest the Albian top though there are many exceptions. The LC2 sequence is generally Albian, though correlation at Shell 357 suggests it possibly reaches into the lowermost Cenomanian (Fig. 7A; Edson et al, 2000f). The COST G1 Albian top occurs in the center of a substantial sand body (Amato and Bebout, 1980) and I've placed the sequence boundary at the next underlying GR low (Fig. 7A). In the Mobil 312, Shell 357, and the Tenneco 187, I've placed the LC2 SB (Figs. 6A and B, 7A and B) at the top of the sand where the Albian top is placed in the well (Edson et al, 2000e, f, and h). The LC2 sequence is generally Albian, but it commonly also contains the Aptian top in wells nearest the shelf edge.

LC3 Sequence

The HST of the LC3 sequence is part of the Logan Canyon Formation lithologically, but the TST and LST are included in the Naskapi formation due to their high GR readings and high shale content. On the western side of the basin, the LC3 HST is fairly thick (Fig. 8A), but it thins into the center of the GBB and toward the shelf edge (Fig. 8B). The LC3 is generally Aptian in age, but Barremian-Hauterivian markers were found in the TST in both the COST G1 (Amato and Bebout, 1980) and the Mobil 312 (Edson et al, 2000e) wells (Fig. 8A).

MS1 Sequence

The MS1 sequence top is based on lithologic criteria. Its easily identified by finding the first strong low GR spike below the Naskapi Shale (Figs. 9A and B). It is generally Barremian-Hauterivian in age, although biostratigraphic markers don't occur until near the base of the sequence in the Shell 357. The Mobil 273 also has anomalous Albian and Aptian biostratigraphic markers in this sequence (Fig. 9B), most likely because there was no biostratigraphic analysis performed above 4500 ftbKB (Edson et al, 2000d).

MS2 Sequence

I identified the MS2 sequence top primarily through GR pattern matching, but also confirmed with sequence stratigraphical analysis. The COST G2 well GR log has a very clearly defined MS2 sequence with a clear sandy HST, a TST with a retrogradational parasequence overlying an aggradational section, and strong LST that ends in a very prominent flooding surface (Fig. 10B). I matched the pattern of highs and lows in the

COST G2 LST GR log across to the Exxon 975, Shell 357, Exxon 133, Mobil 273, and the Shell 410 wells (Figs. 10A and B). The LST of the MS2 sequence at Shell 357 contains a Hauterivian age marker, which I was able to correlate to the same marker in the Tenneco 187 (Edson et al, 2000f and h). The COST G1, Exxon 975, and COST G2 MS2 sequences contain a Berriasian biostratigraphic marker in the TST (Amato and Bebout, 1980; Amato and Simonis, 1980; Edson et al, 2000b) which is recorded in the TST of the MS3 sequence in both the Exxon 133 and the Mobil 312 wells (Figs. 10A and B; Edson et al, 2000i and e).

MS3 sequence

The scope of my project extends from the top of the Logan Canyon Formation to the base of the Missisauga Formation, but the MS3 sequence extends below the base of the Missisauga and into the Jurassic, just as the LC3 extends beyond the Logan Canyon Formation and into the Naskapi Formation. Consequently, I didn't extend my sequence stratigraphical evaluation below the HST after I determined that the Missisauga Formation doesn't extend beyond the MS3 HST in the COST G1 well (Fig 10A; Amato and Bebout, 1980; Pogue, 1982). In the COST G1 well, there are two clear blocky sand deposits at the top of the MS3 sequence, followed by a thick slightly retrogradational pattern that extends down to the Mohawk Formation (Fig. 11 A). I projected this Missisauga Formation base onto seismic data, and correlated it across the basin in order to identify the base of the Missisauga on well logs where it was unclear (Figs 12 B and 13 B). The COST G1 HST is easily identifiable in the Conoco 145 GR log data, and the Shell 357 logs (Figs 11 B and A respectively). I correlated the patterns of spikes in the

GR curves from these two wells to the Exxon 133 well and identified the Missisauga base in that well. The Missisauga base in the Exxon 975 comes from seismic correlation, and the base in the COST G2 is from Amato and Simonis (1980). I used the Berriasian top in the HST of the MS3 sequence at the COST G2 well as a guide to identify the base of the Missisauga in the Mobil 273 and Tenneco 187 wells, where the Berriasian top overlies a strong flooding surface at the base of the Missisauga Formation (Fig. 10 B; Edson et al, 2000d and h).

Sediment Distribution and Source Regions

The first-order observation that can be made from examining the zone top maps is that there's a persistent "nose" or topographic high in the northeast portion of the GBB (Figs 14-17). This area of higher elevation corresponds with relatively thinner sediment thickness in the Logan Canyon Formation (Figs. 14 and 18), and relatively thicker sediments in the Missisauga Formation (Figs. 15 and 19). The Naskapi Formation thickness (Fig. 19) does not show a similar trend to either the Logan Canyon or the Missisauga formations.

The area of higher elevation has more relief in the older formations (Fig. 17) and the transition from high areas to low spots becomes smoother as more sediment fills the basin (Figs. 16, 15, and 14). This trend probably indicates that there was a primary sediment source to the northeast of the basin, and the varying unit thicknesses may indicate the changing strength of that source over time. The nose was created some time prior to the deposition of the Missisauga, Naskapi, and Logan Canyon Formations (Figs. 2 and 17). The Missisauga Formation is thicker on the nose and thins into the basin to the

west (Fig. 20), showing that sediment coming into the basin from the Berriasian to the Barremian deposited more heavily onto that nose than out into the basin. This may indicate a continued trend from the Late Jurassic, if the nose was created by sedimentation patterns, or it could indicate the nose was a young feature at that time and sediment was filling in around a newly created rift structure. In either case, the Missisauga Formation is thickest to either side of the nose (Figs. 16 and 20), and thinnest out in the southwest part of the basin, farthest from the nose and sediment source. By the end of the Barremian all the sharp relief seen during the Late Jurassic is gone, smoothed over by the deposition of the Missisauga Formation (Fig. 16).

The nose is much less pronounced in the Logan Canyon Formation (Fig. 14). The sharp relief seen at the end of the Jurassic is completely absent, and the contour line spacing has become more regular. The only evidence of the nose is a bump that pushes out into the basin overlying the space where the nose previously dominated the topography. The Logan Canyon sediment thickness on top of the nose has the reverse trend of the Missisauga: its now thinnest over the nose (and directly to the east and southeast), and thickest to the southwest toward the center of the basin (Figs. 18 and 14).

The Naskapi Formation top contributes to the pattern of sediment gradually filling in the areas to either side of the Jurassic nose because its contour lines are more regular than in the older Missisauga top. The thickness of the Naskapi Formation is thinnest on either side of the nose, and thickest out into the basin (Fig. 19), similar to the Logan Canyon Formation, but the Logan Canyon Formation shows that the thickest part of the formation has started to migrate south of the nose. This may indicate a shift in sediment source.

There is a second probable sediment source in the northwest area of the basin near the COST G-1 well. The structural contour on top of the Jurassic (Fig. 17) shows the second source of sediments best. At this time, the sediment on the northwest of the basin would have been approaching the same elevation (water depth) as the sediment on the nose in the east, and it is unlikely that the sediment coming off the nose would have traveled approximately 17 km across the basin to deposit only ~150' lower on the opposite side. This same height difference between the two sides of the basin persists through the top of the Logan Canyon Formation (Fig. 14). The isopach maps of the three units don't illustrate this sediment source as well as the source in the northeast. The Missisauga Formation shows only a slight spreading of contour lines toward the northwest (Fig. 20), and the Naskapi Formation shows no real change in thickness to support a second sediment source in the northwest (Fig. 19). The Logan Canyon Formation thins toward this second proposed sediment source the same way it thins on the Eastern part of the Basin (Fig. 18). It is worth noting that this is the direction to the nearest land, where the sediment could be coming from.

Future Work

My work focuses on the two Cretaceous sand units within the GBB because my project is an extension of previous work performed in the Baltimore Canyon Trough. Preliminary evaluations indicate a loss of porosity below 10,000 ft (3084 mbsl; Edson et al., 1980) so I focused on the Cretaceous sands. While the shallower depths of these formations negatively affect the suitability of the Logan Canyon Formation, it also brings

the deeper Mohawk Formation up to a sufficiently shallow depth that it also should be evaluated for CCS.

The initial paleontology reports of the ten exploratory wells within the GBB are currently being reevaluated by L. Jordan (Rutgers, Dept. of Earth + Planetary Sciences) to establish consistent age controls across the wells. Future work by A. Adams (Rutgers, Dept. of Earth + Planetary Sciences) will extend the seismic studies throughout the basin into the Jurassic, and in more detail searching for reflector terminations and interpreting seismic facies.

Conclusions

I constructed well log sequences in the GBB and correlated them to major seismic reflectors in the BCT. The Cretaceous sands examined by Miller et al. (2018) lie shallower in the GBB. This makes the Logan Canyon Formation unsuitable for CCS in the GBB, but the Missisauga remains a viable target. The Logan Canyon and Missisauga Formation tops correlate with the MK1 and LK1 seismic reflectors identified in Miller et al. (2018) and are correlateable on both seismic and well log data. Both target formations contain three depositional sequences each. The Naskapi Formation is comprised of the TST and LST of the LC3 sequence. Similarly, the TST and LST of the MS3 sequence are contained in the stratigraphic unit below the Missisauga Formation, the Mic Mac/Abenaki Formation. The Naskapi Formation provides an adequate seal for the Missisauga formation across the basin.

Figure Captions

Figure 1

A: Location map of the Eastern portion of the Georges Bank Basin (GBB). Map, scale 1:100000, shows location of GBB relative to Cape Cod, MA. Ten exploratory wells, shown by well head location, are labeled according to Drilling company and lease block number. Red diagonal line near upper right of the map is the international maritime border with Canada. Map is overlain onto a map image of the sea floor of the area taken from GeoMapApp (http://www.geomapapp.org). All available 2-D seismic survey data locations are displayed by color according to survey. The five dark blue survey lines are USGS lines 1, 12, 19, 20, and 33. The fusia (bright pink) set of lines are survey B-02-79-AT, available at https://walrus.wr.usgs.gov/namss/survey/b-02-79-at/. The teal set of lines are survey B-06-76-AT, available at https://walrus.wr.usgs.gov/namss/survey/b-06-76-at/. The mustard yellow grid of lines is survey B-01-83-AT, available at https://walrus.wr.usgs.gov/namss/survey/b-01-83-at/. The violet grid of lines is survey B-01-03-AT, available at https://walrus.wr.usgs.gov/namss/survey/b-01-83-at/. The salmon (light pink) grid of lines shows the location of survey W-2-77-GK, available at https://walrus.wr.usgs.gov/namss/survey/w-2-77-gk/. The light blue set of lines show the location of survey B-08-75-AT, available at https://walrus.wr.usgs.gov/namss/survey/b-08-75-at/

B: Closeup of the well locations and 2-D seismic survey locations within the Eastern GBB. Scale is 1:327680. Other features depicted are as described in A above.
C. Map of the composite seismic sections (Figs. 11 and 12) used to project well tops from Gr logs onto seismic data. Green line shows the Western composite 2-D seismic line, while the blue shows the Eastern composite 2-D composite seismic line. Specific seismic lines used to build composites listed in captions for Figure 4 A and C.

Figure 2

A: Geologic timeline from Late Jurassic to Late Cretaceous; Tithonian to Cenomanian stages and 140 Ma – 94 Ma. Includes nannofossil assemblage in the center column, and shows how the sequence boundaries from the six sequences in the Logan Canyon and Missisauga Formations in the Baltimore Canyon Trough and the Eastern Georges Bank Basin correspond with geologic ages. The LC1 is Cenomanian, the LC2 is Albian, the LC3 is Aptian, the MS1 is Aptian to Barremian, and the MS2 is Barremian to Berriasian, and MS3 is Hauterivian to Berriasian. The Missisauga sequences' ages are poorly defined in the GBB due to inconsistent biostratigraphic data from the ten well bores. This inconsistent bio-data is reflected by the diagonal dashed lines in the stratigraphy column that cross several age lines. The yellow shaded areas of the stratigraphy column indicate

lithology dominated by sands, while the purple shaded areas denote lithology dominated by shales.

B: Generalized stratigraphic column from Post et al. (2013) showing geologic time scale, and eustatic curve for the central Atlantic coast of the United States. Red rectangle encloses and highlights the time periods and lithologic units examined by this study.

Figure 3

Close up of the COST G1 LC2 sequence, including GR shading key. Depicts idealized sequence structure of a depositional sequence on a GR log. HST overlies MFS, which is the transition point from HST to TST. The retrogradational TST overlies LST, which terminates at the lower SB with a flooding surface.

Figure 4

A: Gamma Log cross section of the western 4 wells in the Eastern GBB (Fig. 1C); from left to right (northwest to southeast) the COST-G1, the Exxon 133, the Mobil 312, and the Shell 357. Measured Depth (MD), in feet, and two-way-time (TWT), in milliseconds, scales are shown for each log. Logs are hung from the top of the youngest sequence in the Logan Canyon formation, the LC I. Sequence boundaries drawn in red denote sequence boundaries identified by examining grain size stacking patterns. Gamma logs are shaded yellow (low values) to brown (high values.). This shading style simulates sand-colored layers at low gamma readings, to correlate with sand lithologic units, and mud-colored layers at high gamma readings, to correlate with mud or shale. The space between Gr curves is constant, not reflective of actual distance between wells, and is colored according to lithologic units: the Logan Canyon formation is yellow, the Naskapi formation is purple, and the Missisauga formation is orange. Available biostratigraphic data is labelled on both sides of the cross section. Each gamma log is bordered on each side by a discrete log depicting my grain size analysis, from which I extracted stacking patterns and identified sequence boundaries. In this grain-size-trend log yellow intervals indicate progradational grain size, blue intervals indicate retrogradational intervals, green intervals represent major flooding surfaces, and red intervals indicate sequence boundaries.

B: Gamma Log cross section of the eastern 6 wells in the Eastern Georges Bank Basin (GBB); from left to right (northeast to southwest) the Exxon 975, the COST-G2, the Mobil 273, the Tenneco 187, the Conoco 145, and the Shell 410. Other display elements are as described in 2-A above. See caption for Figure 4A, and 3C respectively for exact description of 2-D survey lines used.

Figure 5
A: Lithology and gamma ray logs of the Dawson Canyon and top of the LC1 sequence in 4 wells in the western cross section of the EGBB shown in Fig 1C .

B: Lithology and gamma ray logs of the Dawson Canyon and top of the LC1 sequence in 6 wells in the eastern cross section of the EGBB shown in Fig 1C. All wells are hung from the LC1 upper sequence boundary. Colors and labels are the same as described in Fig. 3.

Figure 6
A: Lithology and gamma ray logs of the entire LC1 sequence in 4 wells in the western cross section of the EGBB shown in Fig 1C.

B: Lithology and gamma ray logs of the entire LC1 sequence in 6 wells in the eastern cross section of the EGBB shown in Fig 1C. All wells are hung from the LC1 upper sequence boundary. Colors and labels are the same as described in Fig. 3.

Figure 7
A: Lithology and gamma ray logs of the entire LC2 sequence in 4 wells in the western cross section of the EGBB shown in Fig 1C.

B: Lithology and gamma ray logs of the entire LC2 sequence in 6 wells in the eastern cross section of the EGBB shown in Fig 1C. All wells are hung from the LC2 upper sequence boundary. Colors and labels are the same as described in Fig. 3.

Figure 8
A: Lithology and gamma ray logs of the entire LC3 sequence in 4 wells in the western cross section of the EGBB shown in Fig 1C.

B: Lithology and gamma ray logs of the entire LC3 sequence in 6 wells in the eastern cross section of the EGBB shown in Fig 1C. All wells are hung from the LC3 upper sequence boundary. Colors and labels are the same as described in Fig. 3.

Figure 9
A: Lithology and gamma ray logs of the entire MS1 sequence in 4 wells in the western cross section of the EGBB shown in Fig 1C.

B: Lithology and gamma ray logs of the entire MS1 sequence in 6 wells in the eastern cross section of the EGBB shown in Fig 1C. All wells are hung from the MS1 upper sequence boundary. Colors and labels are the same as described in Fig. 3.

Figure 10
A: Lithology and gamma ray logs of the entire MS2 sequence in 4 wells in the western cross section of the EGBB shown in Fig 1C.

B: Lithology and gamma ray logs of the entire MS2 sequence in 6 wells in the eastern cross section of the EGBB shown in Fig 1C. All wells are hung from the MS2 upper sequence boundary. Colors and labels are the same as described in Fig. 3.

Figure 11
A: Lithology and gamma ray logs of the entire MS3 sequence in 4 wells in the western cross section of the EGBB shown in Fig 1C.

B: Lithology and gamma ray logs of the entire MS3 sequence in 6 wells in the eastern cross section of the EGBB shown in Fig 1C. All wells are hung from the MS3 upper sequence boundary. Colors and labels are the same as described in Fig. 3.

Figure 12
A: Uninterpreted 2-D composite seismic section of the four western wells in the Eastern Georges Bank Basin. Cross section is oriented left to right from shore-ward to sea-ward (see Fig. 1C), in a general dip line style. XY scale is 1:300000m, and vertical exaggeration is 28. CDP numbers within each respective 2D seismic line are listed above the seismic image, and left axis shows two-way-time from 400 to 2000 milliseconds. Seismic lines in this cross section were chosen in an effort to create a dip-oriented section that also most closely intersected the geographic locations of the four exploratory well bores and the available correllatable data from those wells. Seismic lines displayed from left to right are line D-133_migr_Amplitudes, from survey B-02-79-AT, available at (https://walrus.wr.usgs.gov/namss/survey/b-02-79-at/), line D-162-2_migr_Amplitudes, from survey B-02-79-AT, available at (https://walrus.wr.usgs.gov/namss/survey/b-02-79-at/), line LMG-81_migr, from survey B-06-76-AT, available at (https://walrus.wr.usgs.gov/namss/survey/b-06-76-at/), D-135_migr_Amplitudes, from survey B-02-76-AT, available at (https://walrus.wr.usgs.gov/namss/survey/b-02-79-at/), line D-176A-2_migr_Amplitudes from survey B-02-79-AT, available at (https://walrus.wr.usgs.gov/namss/survey/b-02-79-at/), D-137R2_migr_Amplitudes, from survey B-02-79-AT, available at (https://walrus.wr.usgs.gov/namss/survey/b-02-79-at/), line 83MG-12_migr from survey B-01-83-AT, available at (https://walrus.wr.usgs.gov/namss/survey/b-01-83-at/), line 83MG-05_migr from survey B-01-83-AT, available at (https://walrus.wr.usgs.gov/namss/survey/b-01-83-at/), line D-184B_migr_Amplitudes from survey B-02-79-AT, available at (https://walrus.wr.usgs.gov/namss/survey/b-02-79-at/), Line USGS 33_fpstm, and Line USGS 1_fpstm. Vertical black lines are tie points between the seismic lines listed above.

2D seismic lines were aligned vertically with one another using Petrel's "mistie analysis tool."

B: Shaded gamma ray logs are projected onto the same seismic lines as in 11A, and interpreted zone tops of the Logan Canyon Formation (yellow), Naskapi Formation, (purple), Missisauga Formation (orange), and Mic Mac Formation (blue), have been traced across the nearest seismic reflector to the depths where they overlay the seismic data displayed. The gamma ray logs are shaded yellow (low gamma values, generally indicating sand-rich sediment) to brown (high gamma values generally indicating clay-rich sediment).

Figure 13

A: Uninterpreted 2-D composite seismic section of the six eastern wells in the Eastern Georges Bank Basin. Cross section is oriented left to right from shore-ward to sea-ward, in a general dip line style (see Fig. 1C). XY scale is 1:300000m, and vertical exaggeration is 28. CDP numbers within each respective 2D seismic line are listed above the seismic image, and left axis shows two-way-time from 400 to 2000 milliseconds. Seismic lines in this cross section were chosen in an effort to create a dip-oriented section that also most closely intersected the geographic locations of the six exploratory well bores and the available correllatable data from those wells. Seismic lines displayed from left to right are line USGS 19_fpstm, USGS 12_fpstm, D-129_migr_Amplitudes, from survey B-02-79-AT, available at (https://walrus.wr.usgs.gov/namss/survey/b-02-79-at/), line D-182-2_migr_Amplitudes, from survey B-02-79-AT, available at (https://walrus.wr.usgs.gov/namss/survey/b-02-79-at/), line TP79-118_migr, from survey B-02-79-AT, available at (https://walrus.wr.usgs.gov/namss/survey/b-02-79-at/), D-135_migr_Amplitudes, from survey B-02-76-AT, available at (https://walrus.wr.usgs.gov/namss/survey/b-02-79-at/), line D-186A_migr_Amplitudes from survey B-03-75-AT, available at (https://walrus.wr.usgs.gov/namss/survey/b-03-75-at/), D-137R2_migr_Amplitudes, from survey B-02-79-AT, available at (https://walrus.wr.usgs.gov/namss/survey/b-02-79-at/), line USGS 33_fpstm, line PR-177B_31357.1, from survey W-2-77-GK, available at https://walrus.wr.usgs.gov/namss/survey/w-2-77-gk/, USGS line 19_fpstm, available at (add link?), line 83MG-12_migr from survey B-01-83-AT, available at (https://walrus.wr.usgs.gov/namss/survey/b-01-83-at/), line 83MG-05_migr from survey B-01-83-AT, available at (https://walrus.wr.usgs.gov/namss/survey/b-01-83-at/), line D-196A_migr_Amplitudes from survey B-02-79-AT, available at (https://walrus.wr.usgs.gov/namss/survey/b-02-79-at/), line D-137B_migr_Amplitudes from survey B-02-79-AT, available at (https://walrus.wr.usgs.gov/namss/survey/b-02-79-at/), line PR-181A_31357.1, from survey W-2-77-GK, available at https://walrus.wr.usgs.gov/namss/survey/w-2-77-gk/, line PR-126_31091.1, from survey W-2-77-GK, available at https://walrus.wr.usgs.gov/namss/survey/w-2-77-gk/, line D-137B_migr_Amplitudes from survey B-02-79-AT, available at (https://walrus.wr.usgs.gov/namss/survey/b-02-79-at/), line USGS 19_fpstm. Vertical

black lines are tie points between the seismic lines listed above. 2D seismic lines were aligned vertically with one another using Petrel's "mistie analysis tool."

B: Shaded gamma ray logs are projected onto the same seismic lines as in Fig. 12A, and names and color schemes of formation tops and gamma ray log data are also the same as in Fig. 11B.

Figure 14
Structural isopach map showing the top of the Logan Canyon Formation. Scale is 1:327650m. Depths are in feet to correspond with well log depth measurements. Depths range from 1811 to 3236 milliseconds. Shallower depths shown in reds, and deeper depths shown in blue hues. Color table is scaled to the data displayed. Contour interval is 50 ms. All 2D seismic lines used to trace this zone top are displayed as grey-colored lines. Longitude and latitude data displayed outside all four sides of map. Thin black contour lines outside the colored area at the lower right corner of map denote location of the edge of the continental shelf.

Figure 15
Structural isopach map of the Naskapi Formation top. Depths range from 2635 to 4603ms. Other display elements are as described in 13 above.

Figure 16
Structural isopach map of the Missisauga Formation top. Depths range from 3198 to 5289ms. Other display elements are as described in 13 above.

Figure 17
Structural isopach map of the Mic Mac/ Abenaki Formation top. Depths range from 4885 to 6211 ms. Other display elements are as described in 13 above.

Figure 18
Thickness map (isochore) of the Logan Canyon Formation. Thickness calculated in Petrel using Naskapi top as the base of the Logan Canyon. Contour interval is 50 milliseconds. Maximum thickness is displayed as purple, decreasing from blues to greens to yellows, and ending with minimum thickness displayed in red. Color table is scaled to the data displayed. Thicknesses range from 650' to 1400', with an average thickness of 1036'.

Figure 19
Thickness map (isochore) of the Naskapi Formation. Thickness calculated in Petrel using Missisauga top as the base of the Naskapi. Thickness varies from 350 to 900 milliseconds with an average thickness of 575 ms. All other display elements are the same as described in Figure 18 above.

Figure 20
Thickness map (isochore) of the Missisauga Formation. Thickness calculated in Petrel using the Mic Mac/Abenaki top as the base of the Missisauga. Thickness varies from 850 to 2150 milliseconds, with an average thickness of 1531 ms. All other display elements are the same as described in Figure 18 above.

References

Amato, R. V., & Bebout, J. W. (1980). *Geologic and Operational Summary, COST NO. G-1 Well, Georges Bank Area, North Atlantic OCS.* United States Departmnt of the Interior, Geological Survey. Atlantic OCS Region.

Amato, R. V., & Simonis, E. K. (1980). *Geologic and Operational Summary, COST NO. G-2 Well, Georges Bank Area, North Atlantic OCS.* Open File Report 80-269, United States Department of the Interior, Geological Survey.

Bachu, S. (2002). Sequestration of CO2 in Geological Media in Response to Climate CHange: Road Map for Site Selection Using the Transform of the Geological Space into the CO2 Phase Space. *Energy Conversion and Management, 43*, 87-102.

Edson, G. M., Olson, D. L., & Petty, A. J. (2000a). *Conoco Lydonia Canyon BLock 145 No. 1 Well - Geological and Operational Summary.* U.S. Department of the Interior, Minerals Management Services. New Orleans: Gulf of Mexico OCS region, Office of Resource Evaluation. Retrieved from https://www.boem.gov/uploadedFiles/BOEM/Oil_and_Gas_Energy_Program/Resource_Evaluation/Geological_and_Geophysical_Data_Acquisition/AtlanticCOST2000-034.pdf

Edson, G. M., Olson, D. L., & Petty, A. J. (2000b). *Exxon Corsair Canyon Block 975 No. 1 Well - Geological and Operational Summary.* U.S. Department of the Interior, Minerals Management Service. New Orleans: Gulf of Mexico OCS Region, Office of Resource Eavluation. Retrieved from https://www.boem.gov/uploadedFiles/BOEM/Oil_and_Gas_Energy_Program/Resource_Evaluation/Geological_and_Geophysical_Data_Acquisition/AtlanticCOST2000-032.pdf

Edson, G. M., Olson, D. L., & Petty, A. J. (2000c). *Georges Bank Petroleum Exploration, Atlantic Outer Continental Shelf.* U.S. Department of the Interior, Minerals Management Service. New Orleans: Gulf Of Mexico OCS Region, Office of Resource Evaluation. Retrieved from https://www.boem.gov/OCS-Report-MMS-2000-031/

Edson, G. M., Olson, D. L., & Petty, A. J. (2000d). *Mobil Lydonia Canyon Block 273 No. 1 Well - Geological and Operational Summary.* U.S. Department of the Interior, Minerals Management Service. New Orleans: Gulf of Mexico OCS REgion, Office of resource Evaluation. Retrieved from https://www.boem.gov/uploadedFiles/BOEM/Oil_and_Gas_Energy_Program/Resource_Evaluation/Geological_and_Geophysical_Data_Acquisition/AtlanticCOST2000-036.pdf

Edson, G. M., Olson, D. L., & Petty, A. J. (2000e). *Mobil Lydonia Canyon Block 312 No. 1 Well - Geological and Operational Summary.* U.S. Department of the Interior, Minerals Management Service. New Orleans: Gulf of Mexico OCS Region, Office of Resource Evaluation. Retrieved from https://www.boem.gov/uploadedFiles/BOEM/Oil_and_Gas_Energy_Program/Resource_Evaluation/Geological_and_Geophysical_Data_Acquisition/AtlanticCOST2000-037.pdf

Edson, G. M., Olson, D. L., & Petty, A. J. (2000f). *Shell Lydonia Canyon Block 357 No. 1 Well - Geological and Operational Summary.* U.S. Department of the Interior, Mineral Management Service. New Orleans: Gulf of Mexico OCS Region, Office of Resource Evaluation. Retrieved from https://www.boem.gov/uploadedFiles/BOEM/Oil_and_Gas_Energy_Program/Resource_Evaluation/Geological_and_Geophysical_Data_Acquisition/AtlanticCOST2000-038.pdf

Edson, G. M., Olson, D. L., & Petty, A. J. (2000g). *Shell Lydonia Canyon Block 410 No. 1R Well - Geological and Operational Summary.* U. S. Department of the Interior, Mineral Management Service. New Orleans: Gulf of Mexico OCS Region, Office of Resource Evaluation. Retrieved from https://www.boem.gov/uploadedFiles/BOEM/Oil_and_Gas_Energy_Program/Resource_Evaluation/Geological_and_Geophysical_Data_Acquisition/AtlanticCOST2000-039.pdf

Edson, G. M., Olson, D. L., & Petty, A. J. (2000h). *Tenneco Lydonia Canyon Block 187 No. 1 Well - Geological and Operational Summary.* U.S. Department of the Interior, Minerals Management Service. New Orleans: Gulf of Mexico OCS Region, Office of Resource Evaluation. Retrieved from https://www.boem.gov/uploadedFiles/BOEM/Oil_and_Gas_Energy_Program/Resource_Evaluation/Geological_and_Geophysical_Data_Acquisition/AtlanticCOST2000-035.pdf

Edson, G. M., Olson, D. L., & Petty, A. J. (2000i). *Exxon Lydonia Canyon Block 133 No. 1 Well - Geological and Operational Summary.* U.S> Department of the Interior, Minerals Management Service. New Orleans: Gulf of Mexico OCS REgion, Office of Resource Evaluation. Retrieved from https://www.boem.gov/uploadedFiles/BOEM/Oil_and_Gas_Energy_Program/Resource_Evaluation/Geological_and_Geophysical_Data_Acquisition/AtlanticCOST2000-033.pdf

Gradstein, F., Ogg, J., Schmitz, M., & Ogg, G. (2012). *The Geologic Time Scale 2012 2-Volume Set* (Vols. 1-2). Oxford, UK: Elsevier BV.

Jansa, L. F., & Wade, J. A. (1975). Geology of the Continental Margin off Nova Scotia and Newfoundland. In W. J. Van Der Linden, & J. A. Wade, *Offshore Geology of*

eastern Canada, Volume 2- Regional Geology (pp. 51-105). GEological Survey of Canada.

Libbey-French, J. (1981). Lithostratigraphy of Shell 272-1 and 273-1 Wells: Implications as to Depositional History of the Baltimore Canyon Trough, Mid- Atlantic OCS. *American Association of Petroleum Geologists Bulletin, 65*(8), 1476-1484.

Libby-French, J. (1984). Stratigraphic Framework and Petreleum Potential of Northeastern Baltimore Canyon Trough, Mid-Atlantic outer Continental Shelf. *American Association of Petroleum Geologists Bulletin, 68*(1), 50-73.

McIver, N. L. (1972). Cenozoic and Mesozoic Stratigraphy of the Nova Scotia Shelf. *Canadian Journal of Earth Sciences, 9*, 54-70.

Metz, V., Amram, K., & Ganor, J. (2005, April 1). Stoichiometry of Smectite Dissolution Reaction. *Geochemica et Cosmochimica Acta, 69*(7), 1755-1772. Retrieved from https://doi.org/10.1016/j.gca.2004.09.027

Miller, K. G., Lombardi, C. J., Browning, J. V., Schmelz, W. J., Gallegos, G., Mountain, G. S., & Baldwin, K. E. (2018). Back To Basics of Sequence Stratigraphy: Early Miocene and Mid-Cretaceous Examples from teh New Jersey Paleoshelf. *Journal of Sedimentary Research, 88*(1), 148-176. Retrieved from https://doi.org/10.2110/jsr.2017.73

Monteverde, D. H., Sugarman, P. J., Miller, K. G., Browning, J. V., Mountain, G. S., Romero, P., & Seker, Z. (2011). *Characterization of the carbon dioxide storage potential beneath the continental shelf and slope offshore New Jersey, in New Jersey Geological Survey, Preliminary Characterization of CO2 Sequestration Potential in New Jersey and the Offshore Coastal Regio.* U.S. Department of Energy, National Energy Technology Laboratory. Midwest Regional Carbon Sequestration Partnership.

Poag, C. W. (1978). Stratigraphy of the Atlantic Continental Shelf and Slope of the United States. *Annual Review of Earth and Planetary Sciences, 6*, 251-280.

Poag, C. W. (1982). Stratigraphic Reference Section for Georges Bank Basin - Depositional Model for New England Passive Margin. *American Association of Petroleum Geologists Bulletin, 66*(8), 1021-1041.

Post, P. J., Elliott, E. T., Klazynski, R. J., Kloeck, E. S., Decort, T. M., Riches, T. J., and Kun Li. (2013). US central Atlantic: New Plays and Petroleum Prospectivity. *Geological Society of London Special Publications, 369*(1), 323-336. doi:10.1144/SP369.2

Schlee, J. S., & Klitgord, K. D. (1982). Geologic Setting of the Georges Bank Basin. In P. A. Scholle, & C. R. Wenkham (Eds.), *Geological Studies of the COST Nos. G-1 and G-2 Wells, United States North Atlantic Outer Continental Shelf* (861 ed., pp. 4-10). U.S. Department of the Interior.

Schlee, J., & Fritsch, J. (1983). Seismic Stratigraphy of the Georges Bank Basin Complex. In J. Watkins, & C. Drake (Eds.), *Studies in Continental Margin Geology* (pp. 223-251). American Association of Petroleum Geologists. doi:https://doi.org/10.1306/M34430

Schmelz, W. J., Miller, K. G., Mountain, G. S., Browning, J. V., & Baldwin, K. E. (in press). Onshore-offshore correlations of fluvial-deltaic sequences from the mid-Cretaceous of the southern Baltimore Canyon Trough. *American Association of Petroleum Geologists Bulletin*.

Scholle, P. A., & Wenkham, C. R. (1982). *Geological Studies of the COST Nos. G-1 and G-2 Wells, United States North Atlantic Outer Continental Shelf*. U.S Department of the Interior, Geological Survey.

Triezenberg, P. J.; Hart, P. E.; Childs, J. R. (2018). *The National Archive of Marine Seismic Surveys*. (USGS, Producer) doi:https:/doi.org/10.5066/F7930R7P

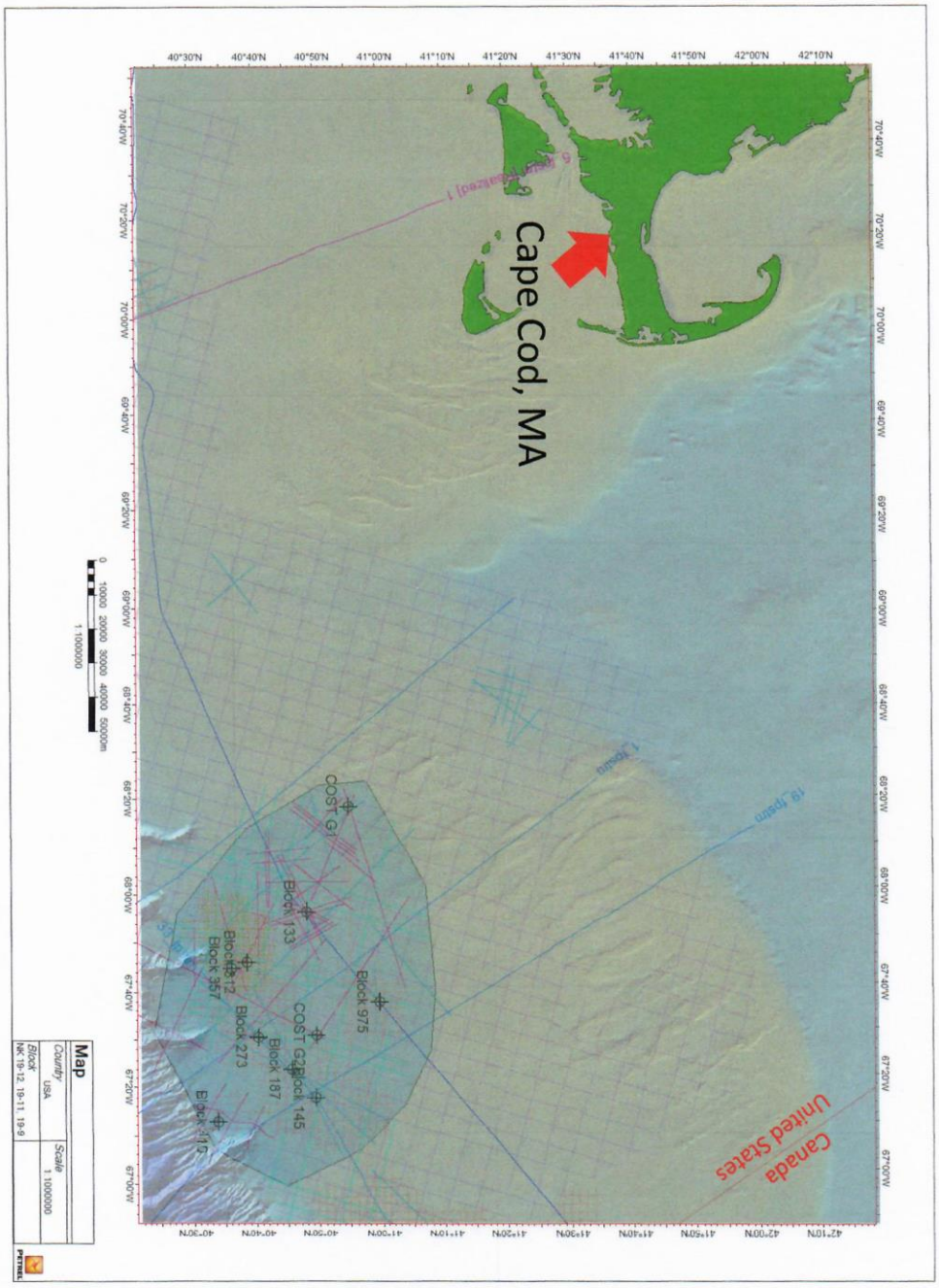

Figure 1A: East Georges Bank Basin Location

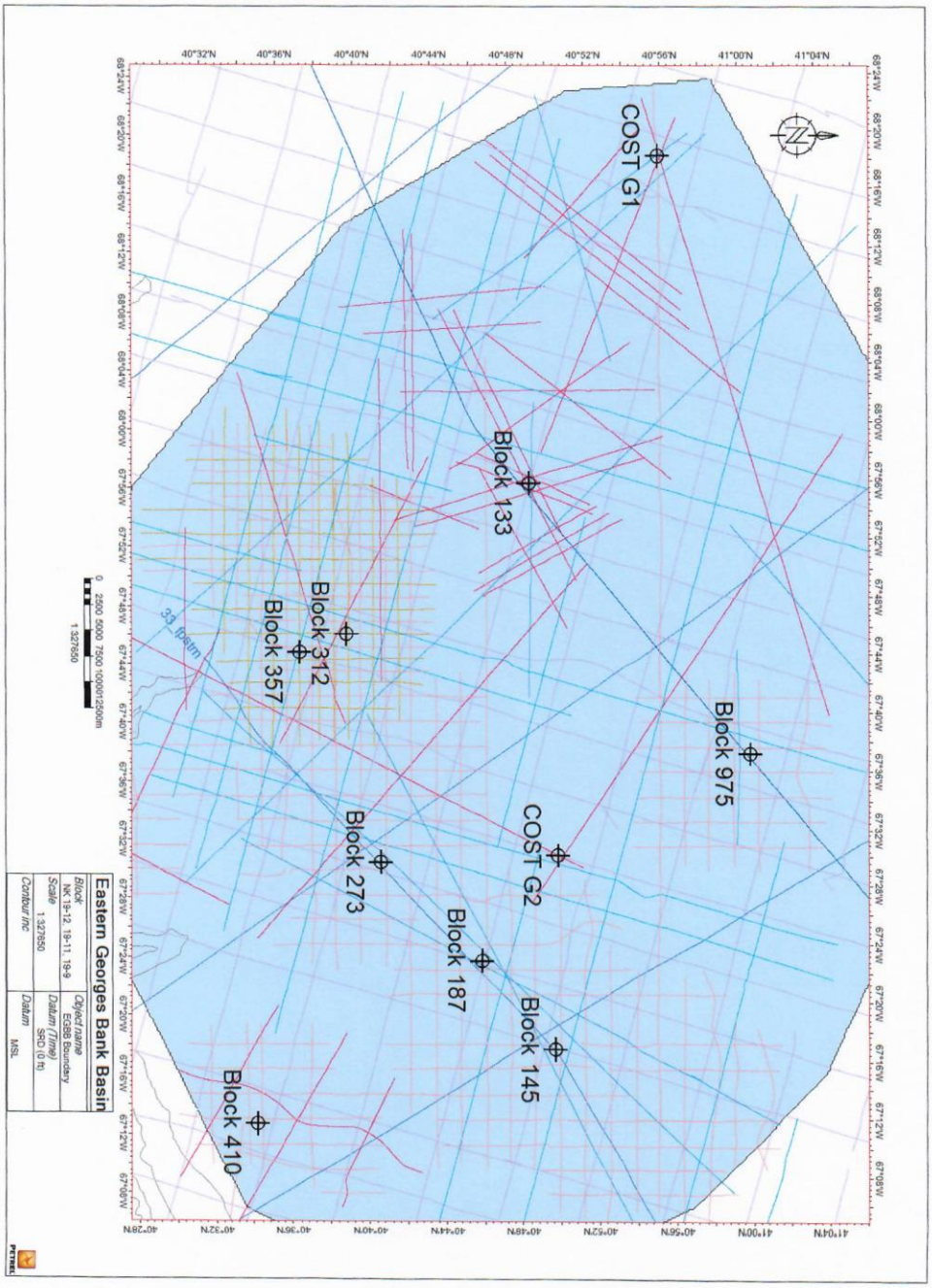

Figure 1B: All Seismic Data Within EGBB

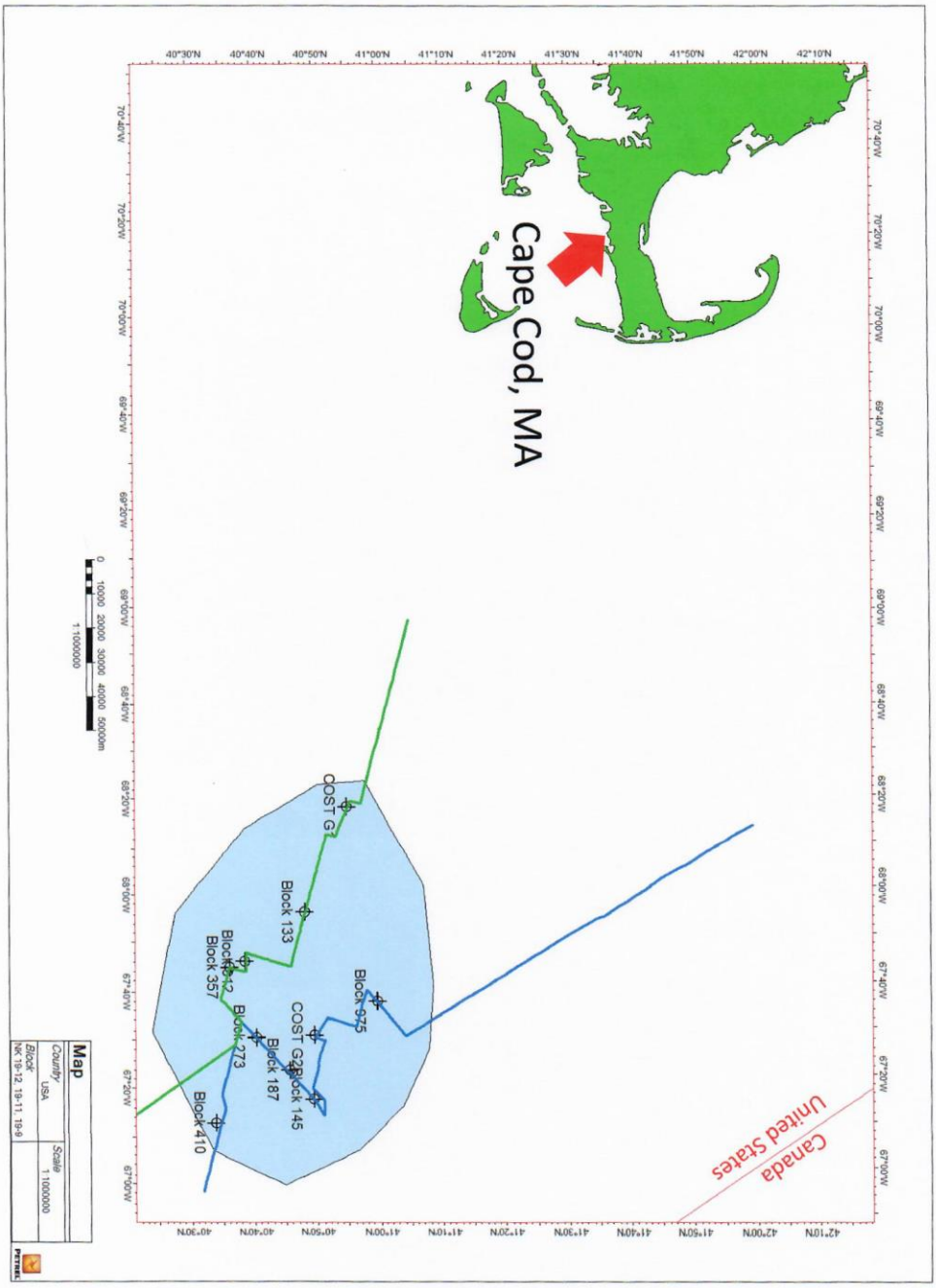

Figure 1C: Composite Seismic Line Construction

Figure 2A: Geologic Timeline and Stratigraphic Column of Units Studied

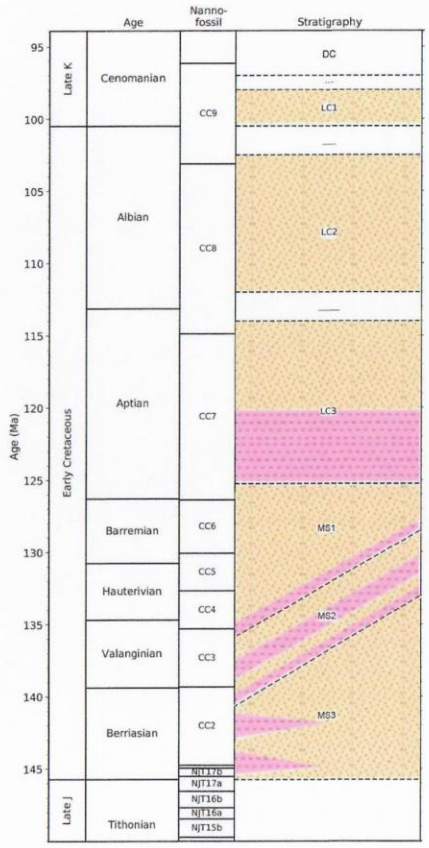

Figure 2B: Geologic Timeline and Stratigraphic Column

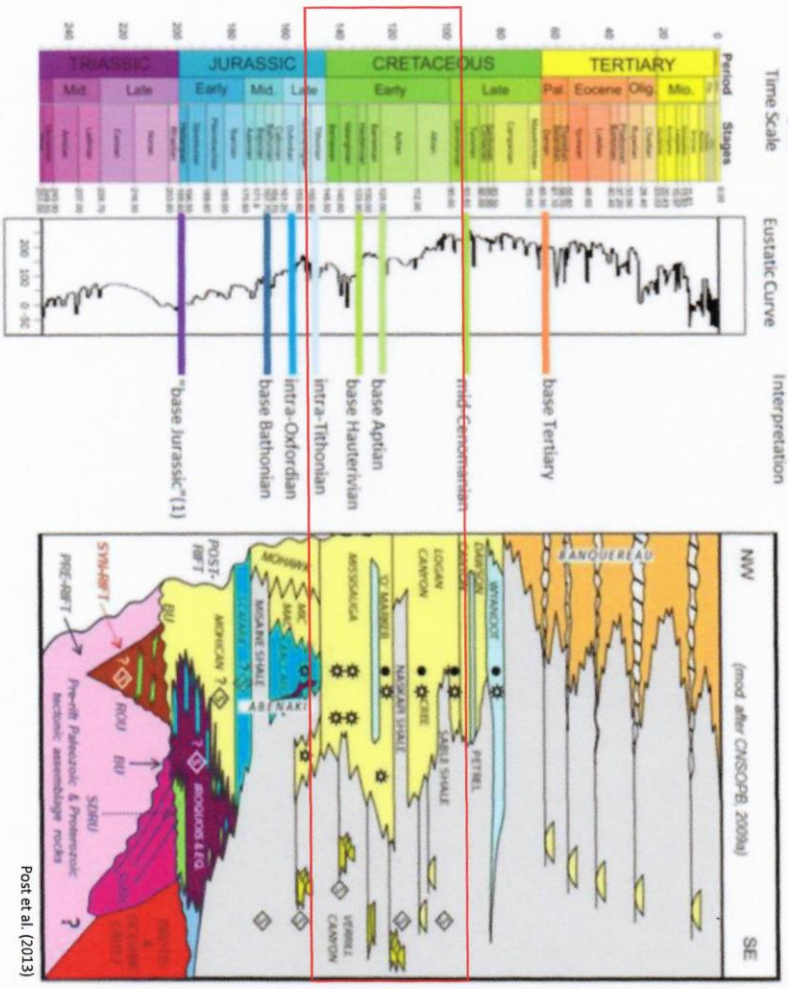

Post et al. (2013)

Figure 3: Sequence Stratigraphic Analysis

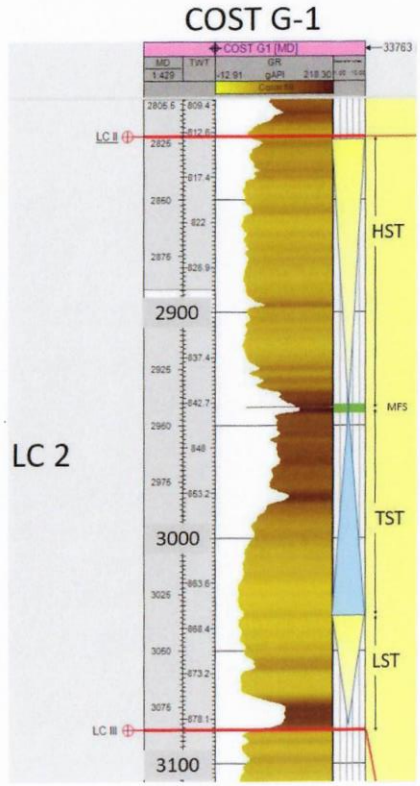

Figure 4A: Western Gamma Log Cross-section

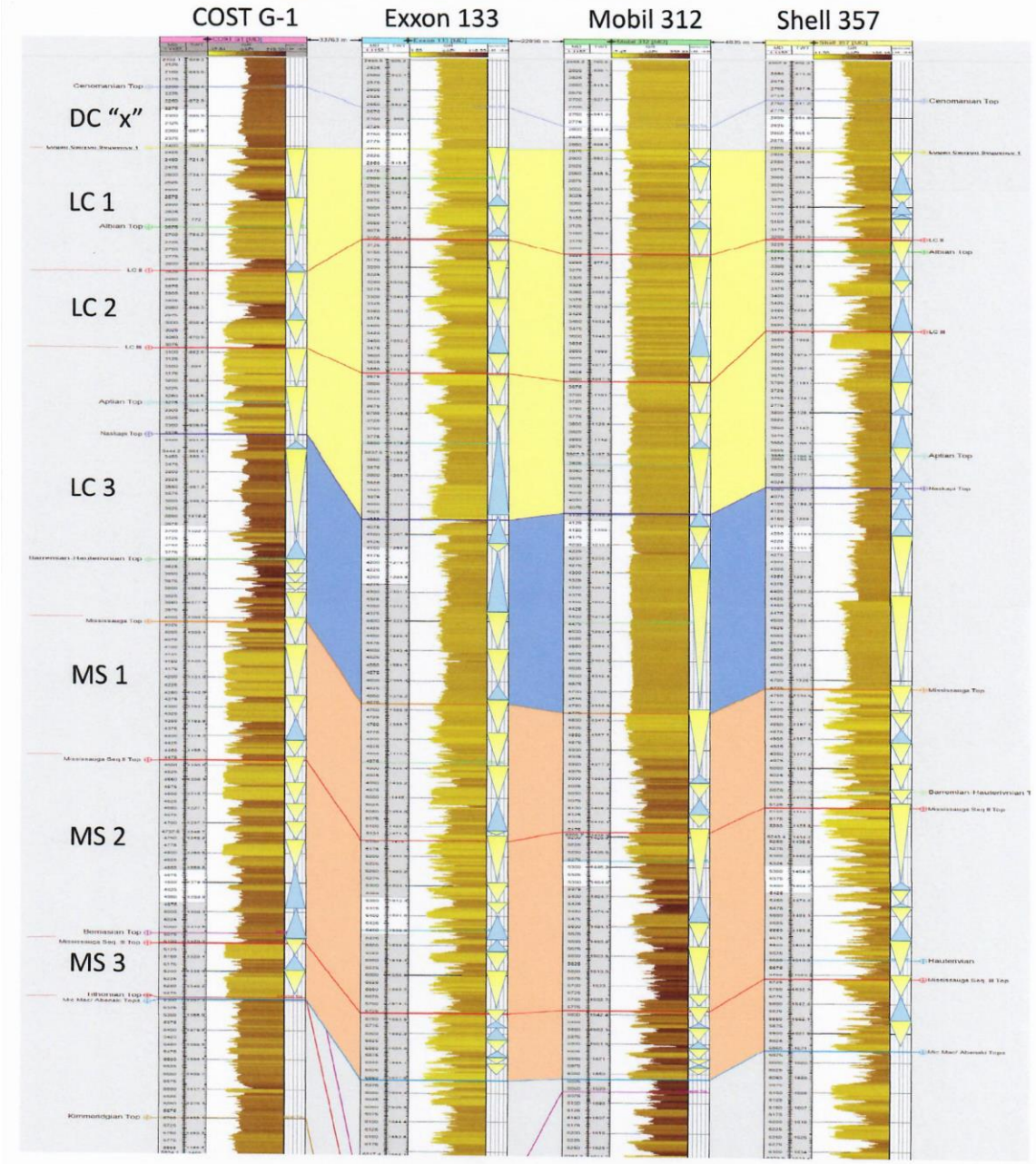

Figure 4B: Eastern Gamma Log Cross -section

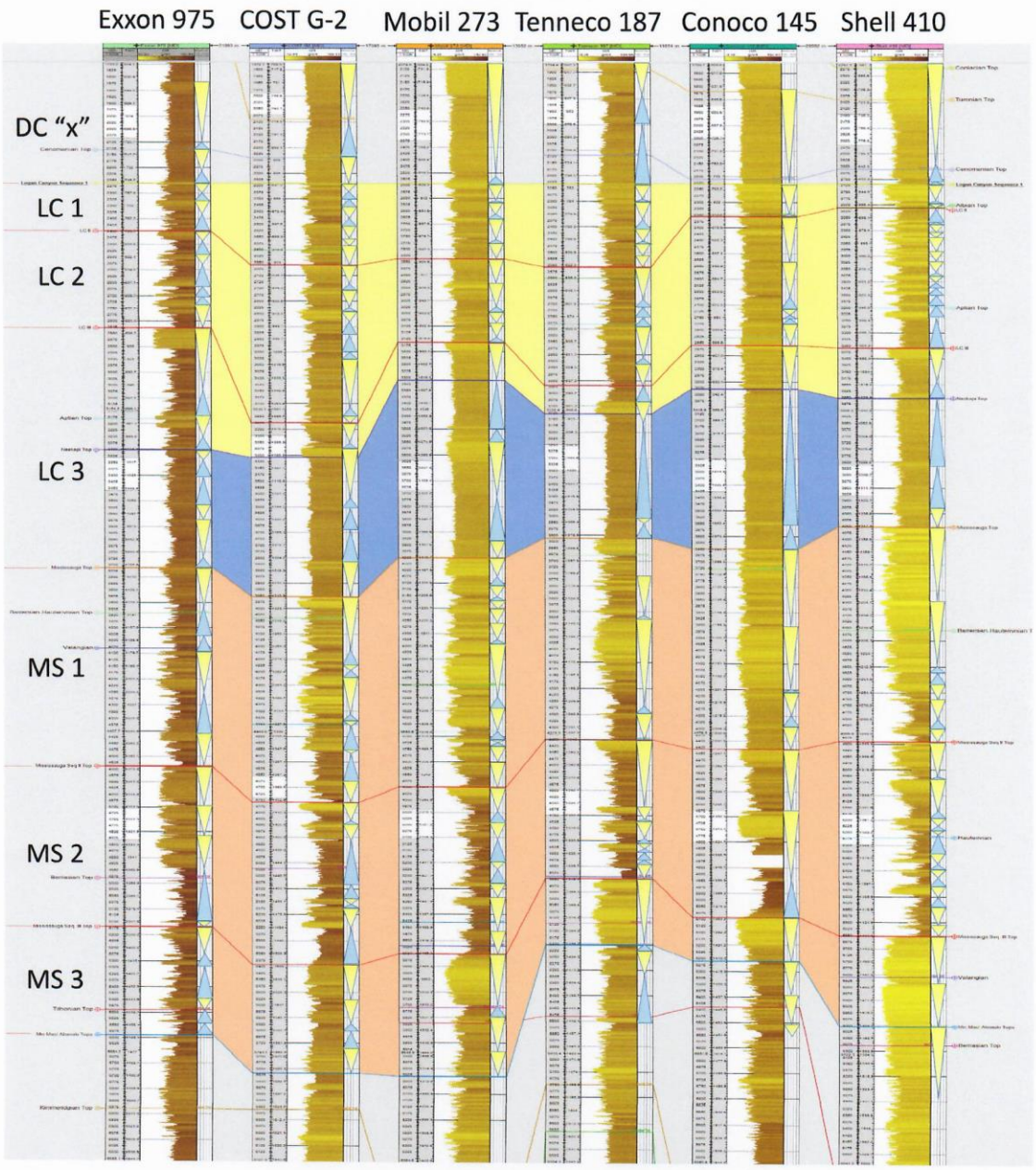

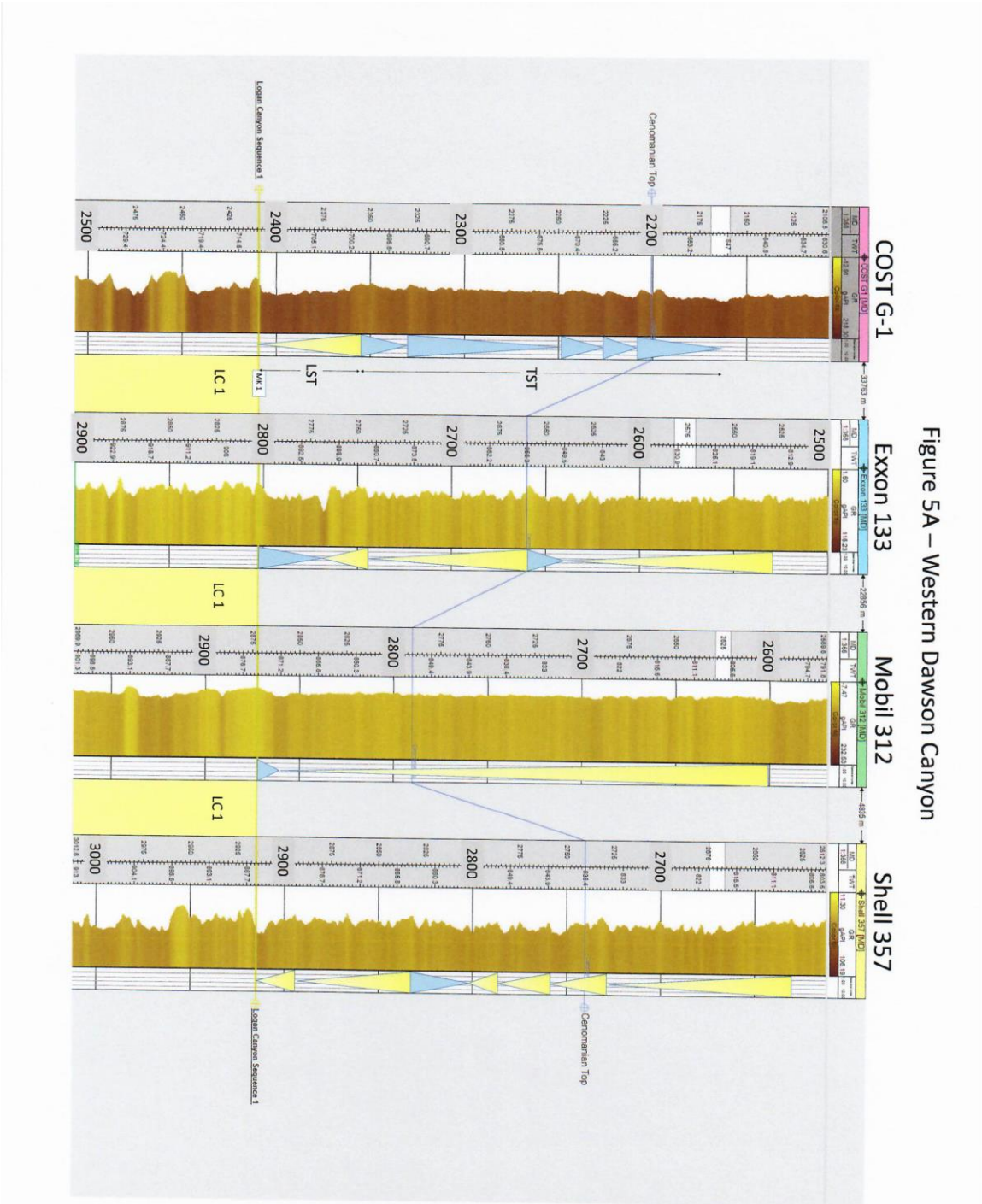

Figure 5A – Western Dawson Canyon

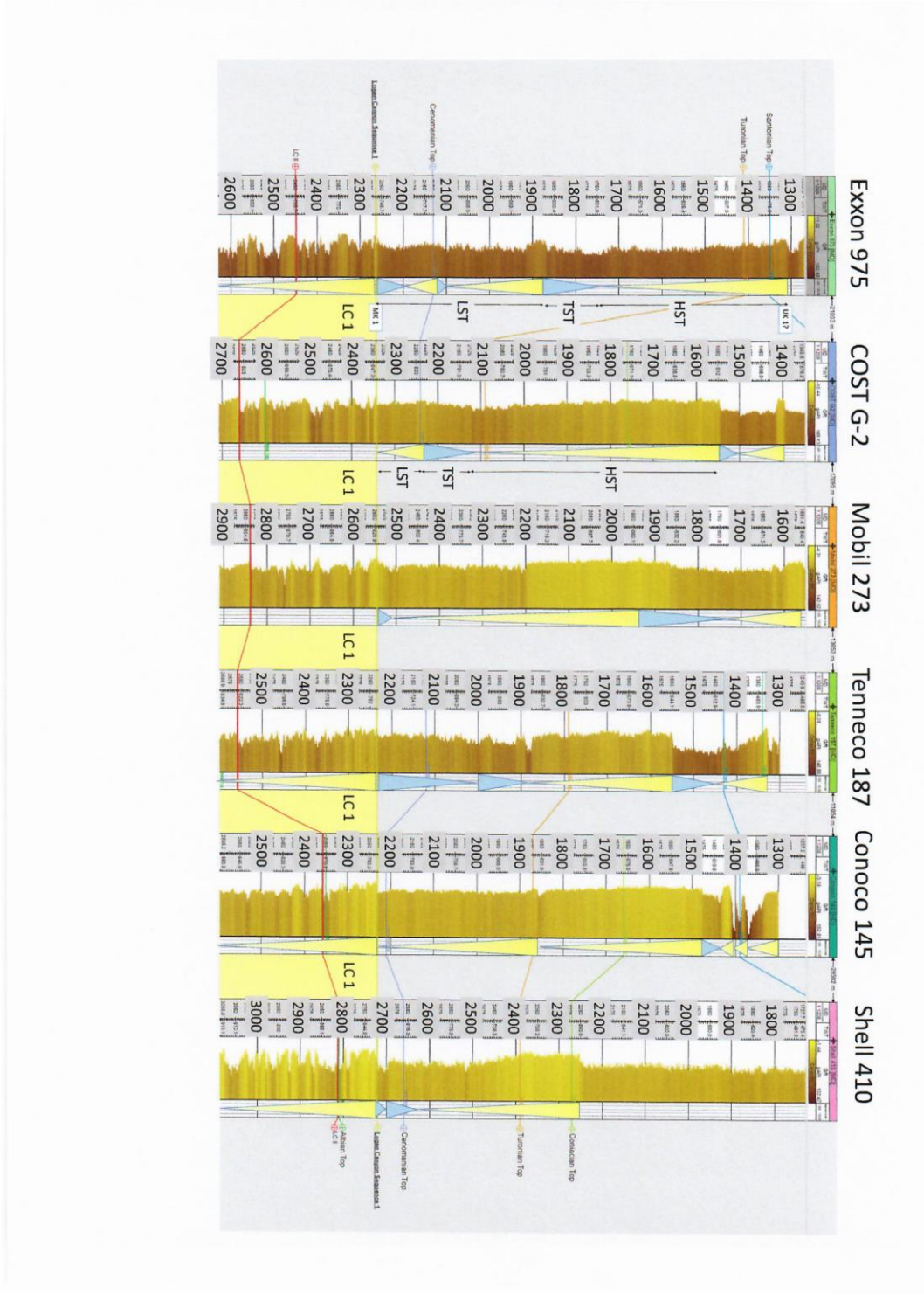

Figure 5B – Eastern Dawson Canyon

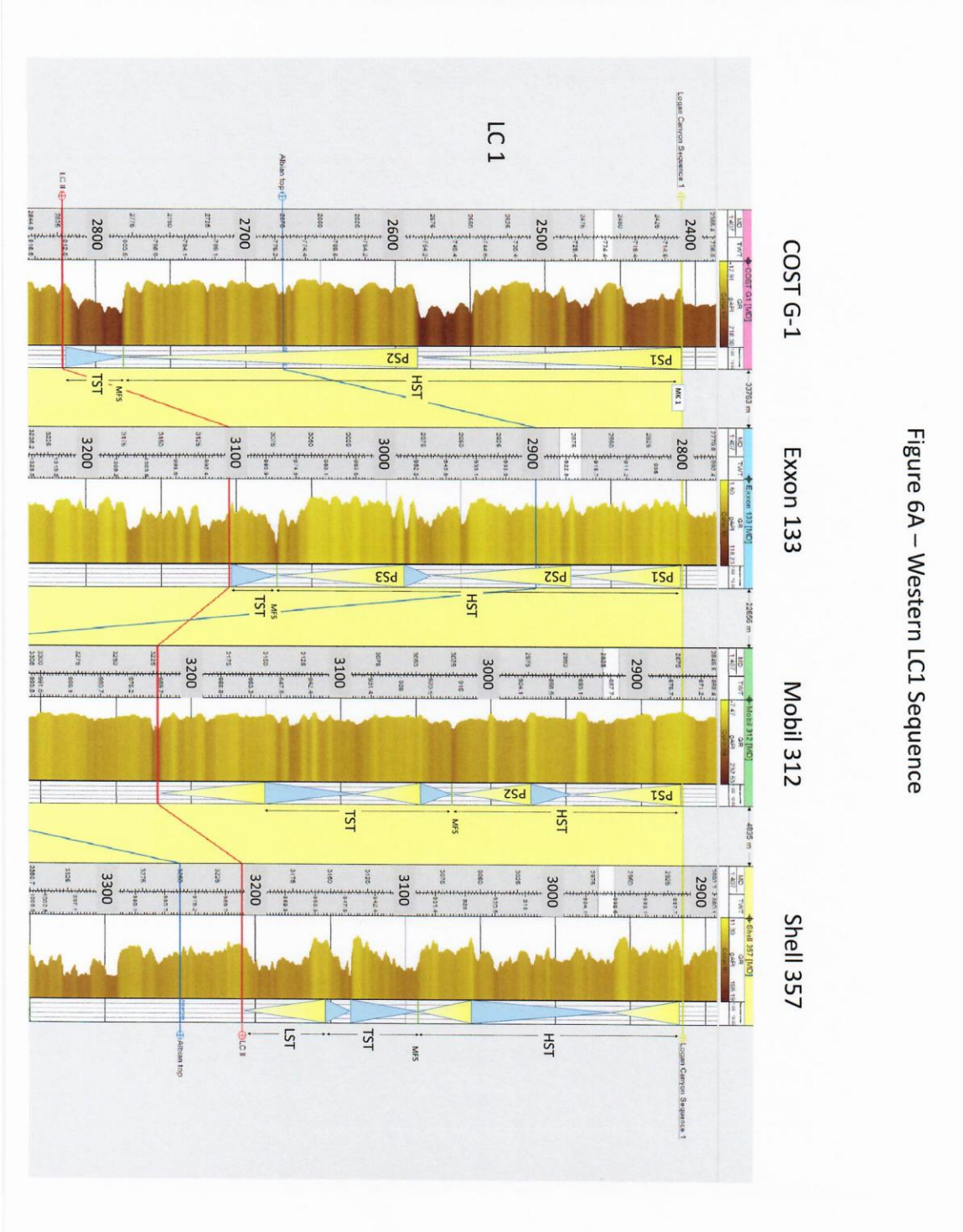

Figure 6A – Western LC1 Sequence

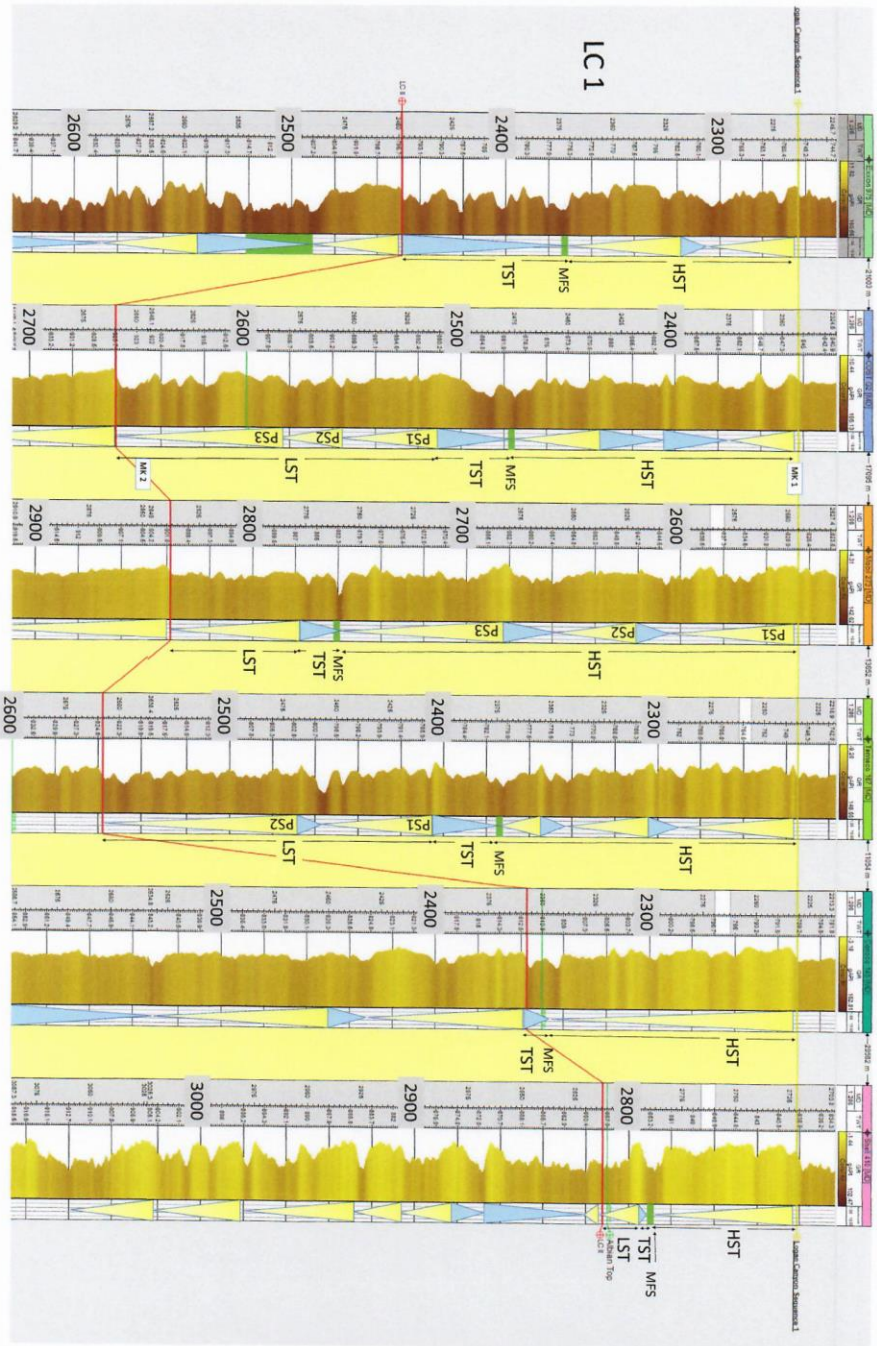

Figure 6B – Eastern LC1 Sequence

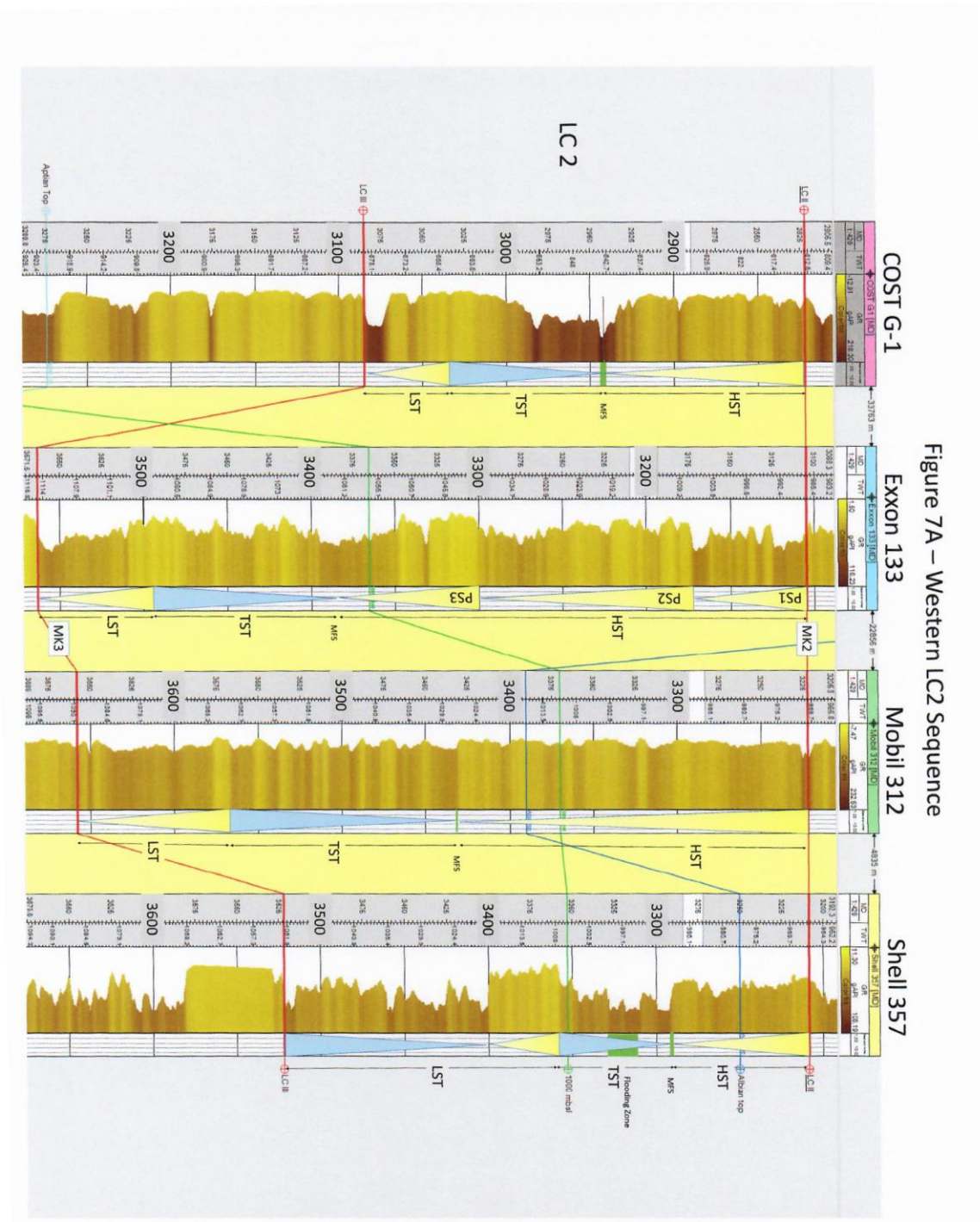

Figure 7A – Western LC2 Sequence

Figure 7B – Eastern LC2 Sequence

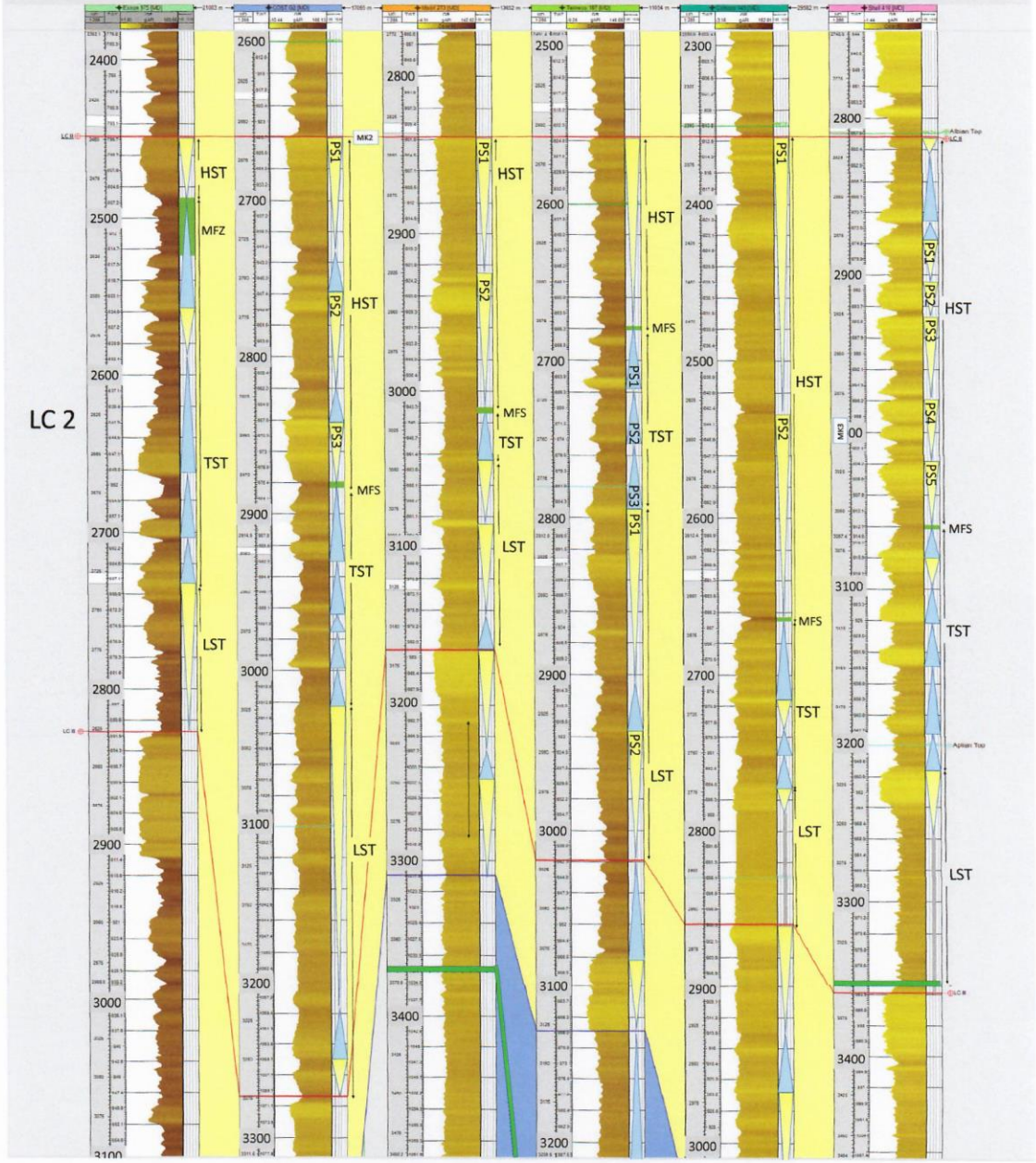

Figure 8A – Western LC3 Sequence

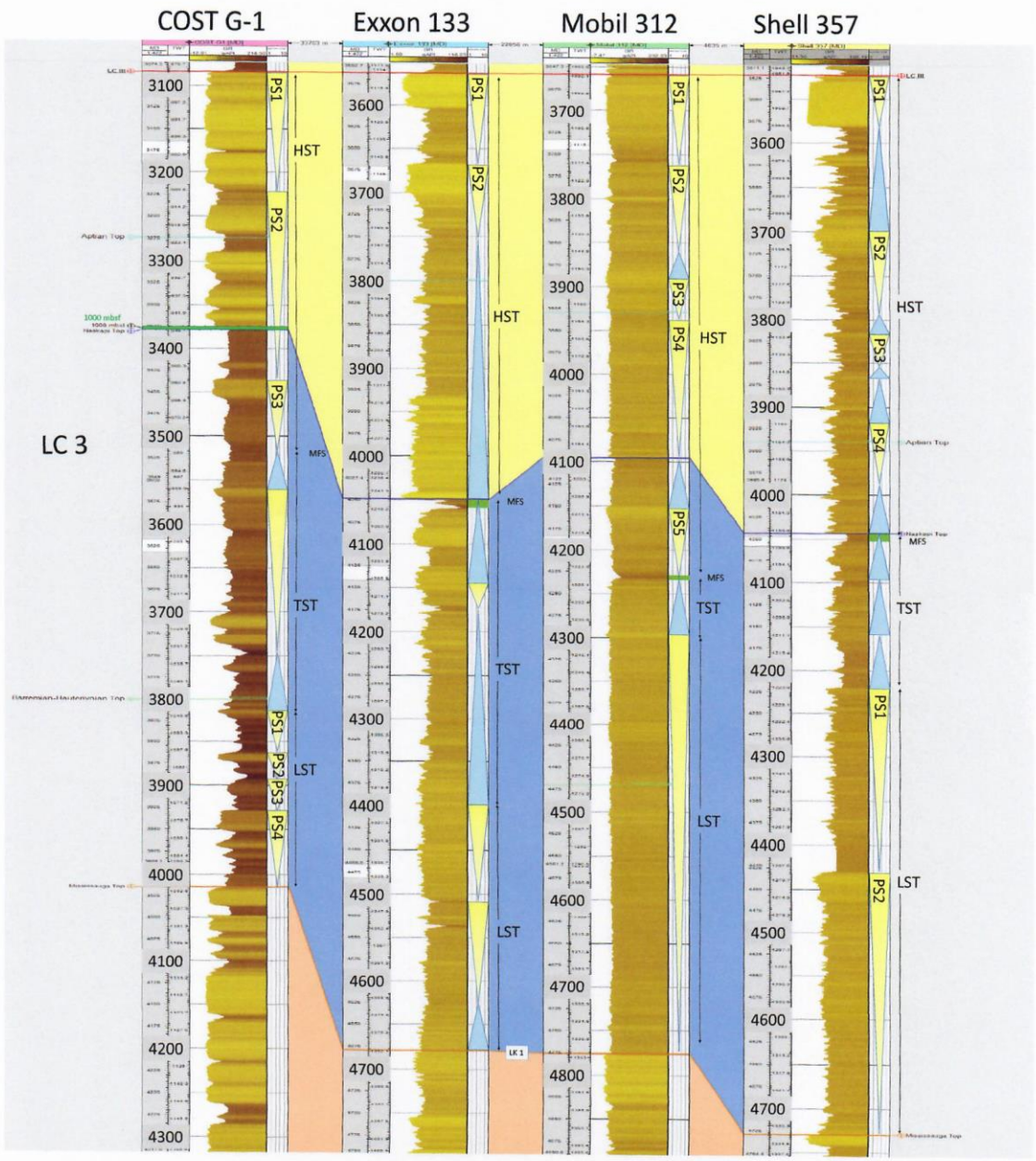

Figure 8B – Eastern LC3 Sequence

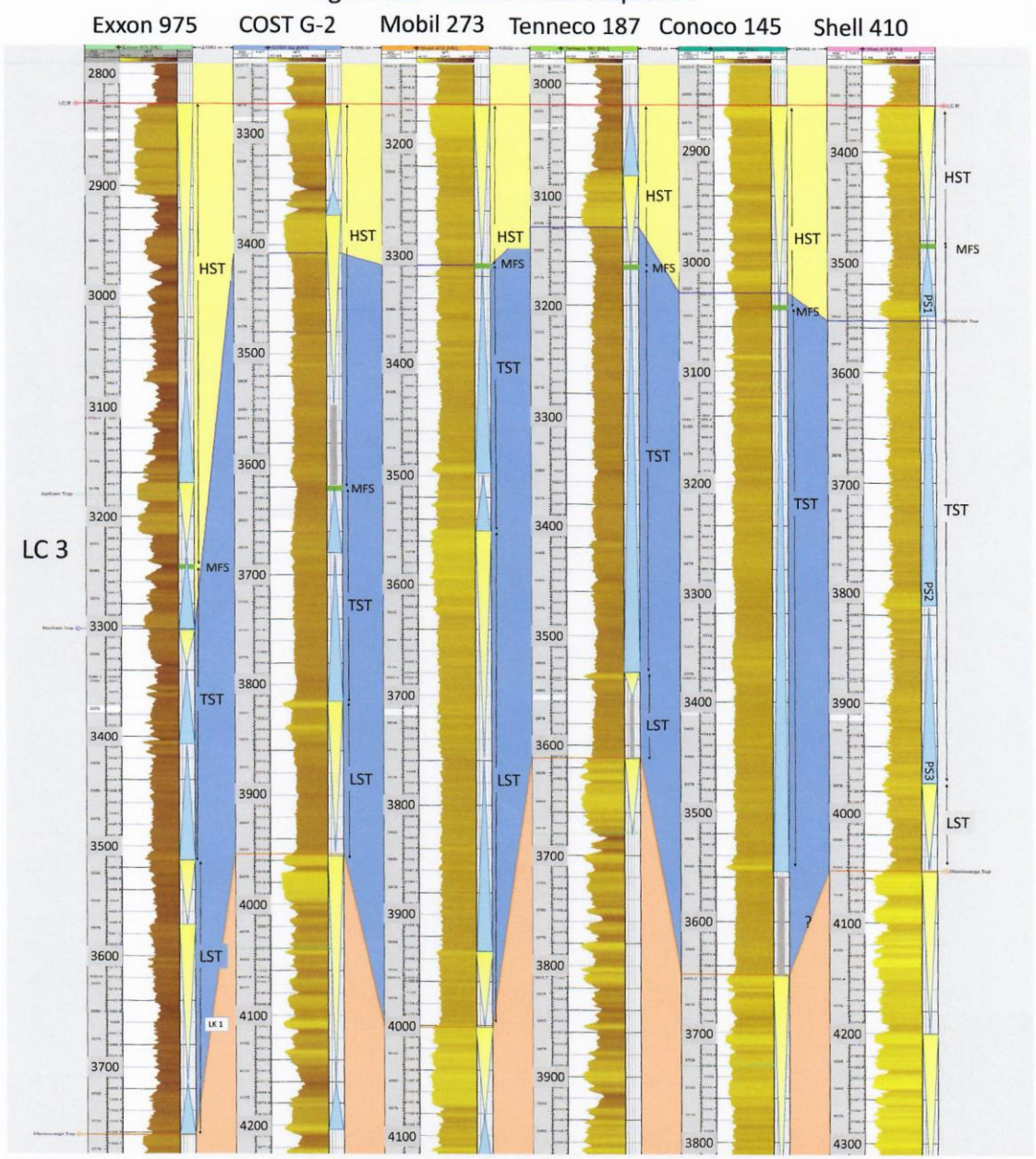

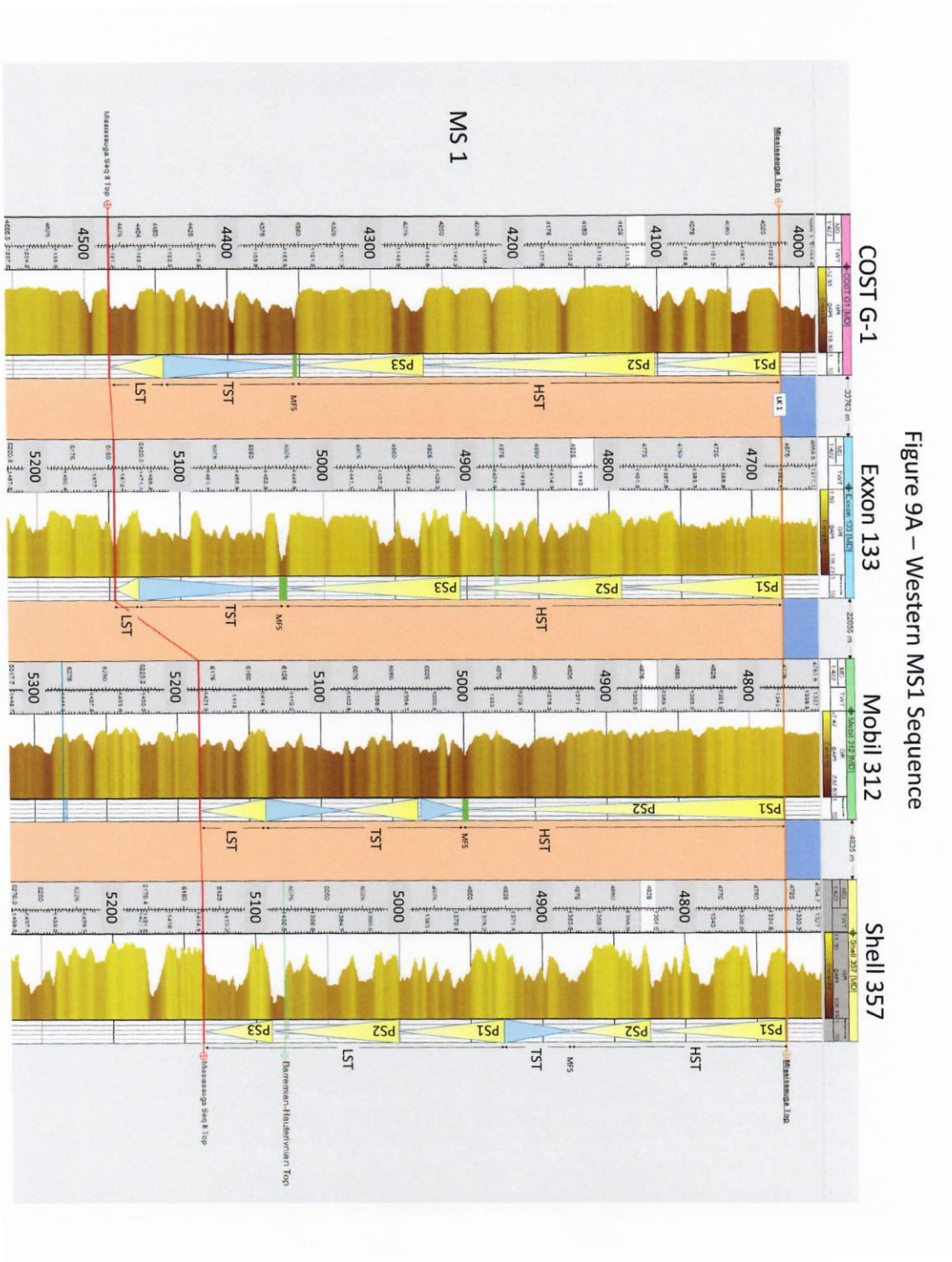

Figure 9A – Western MS1 Sequence

Figure 9B – Eastern MS1 Sequence

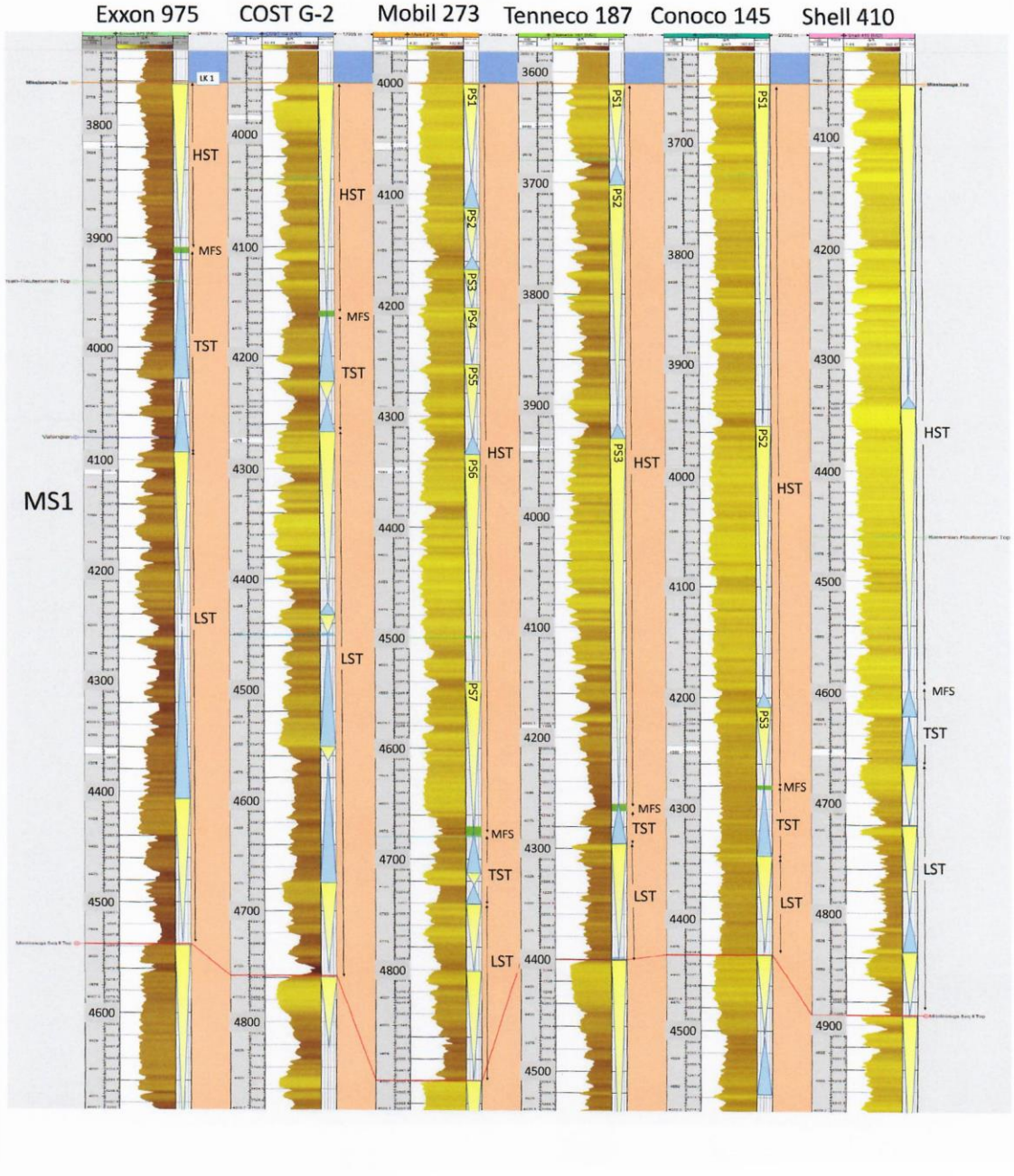

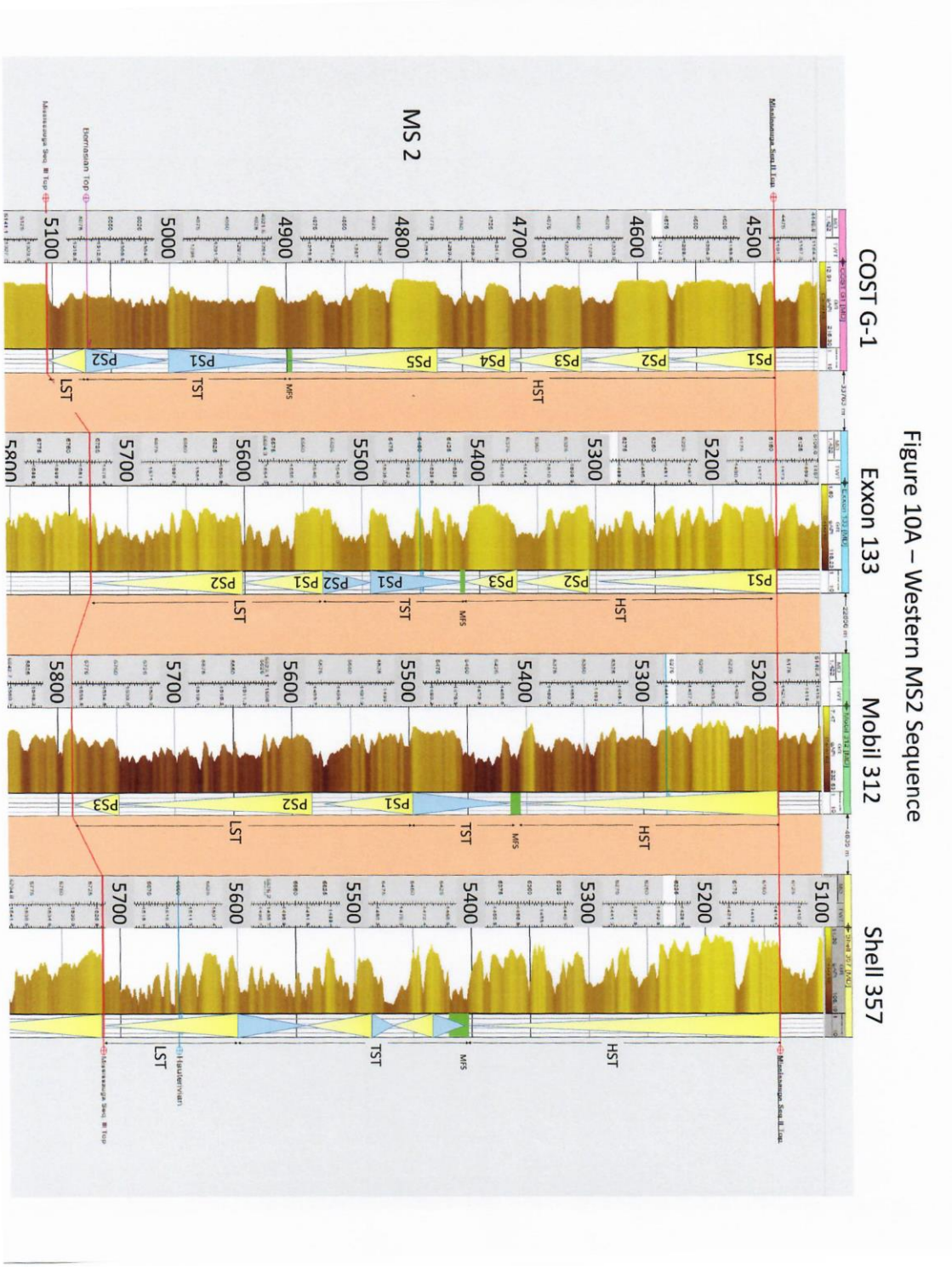

Figure 10A – Western MS2 Sequence

Figure 10B – Eastern MS2 Sequence

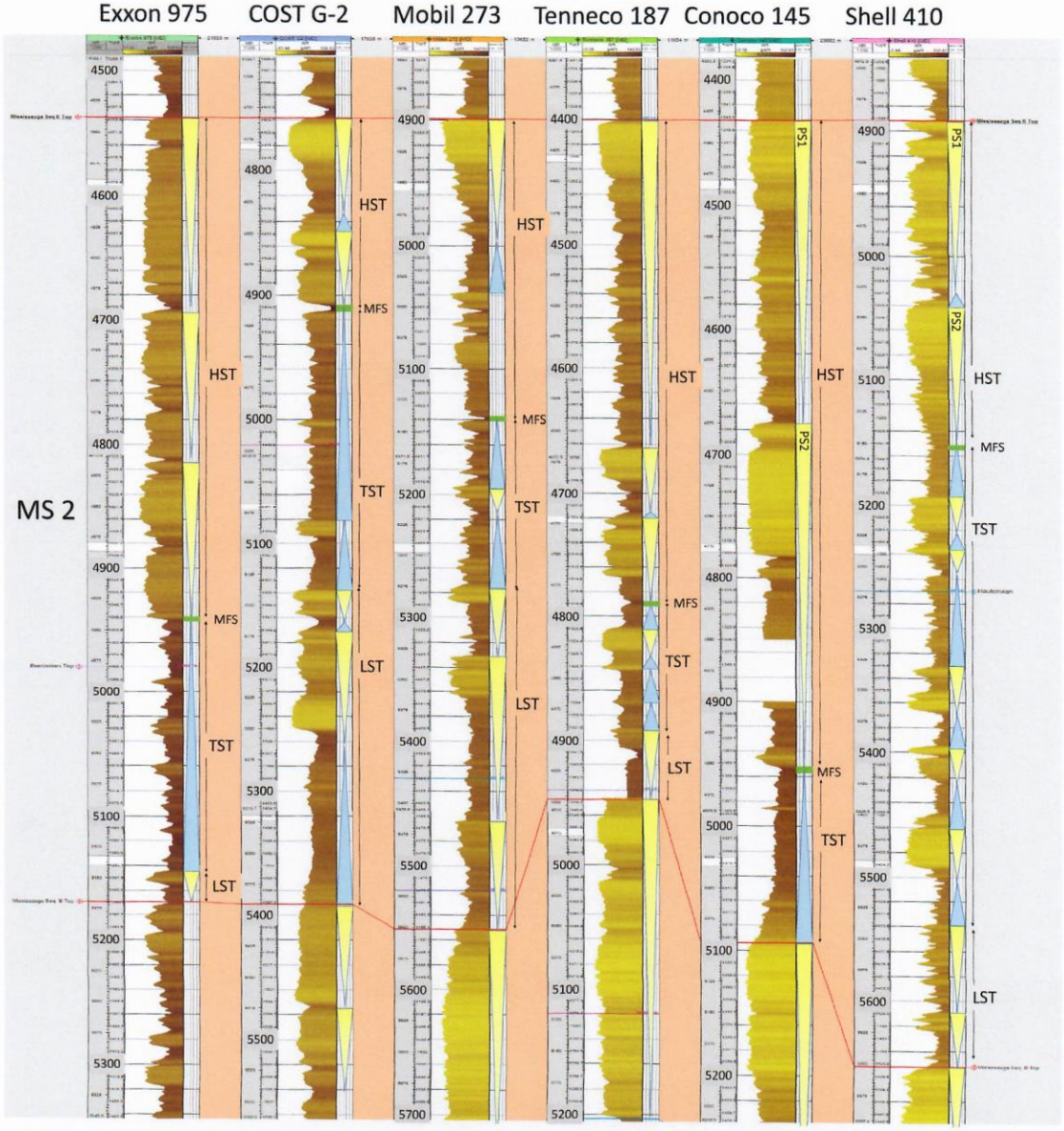

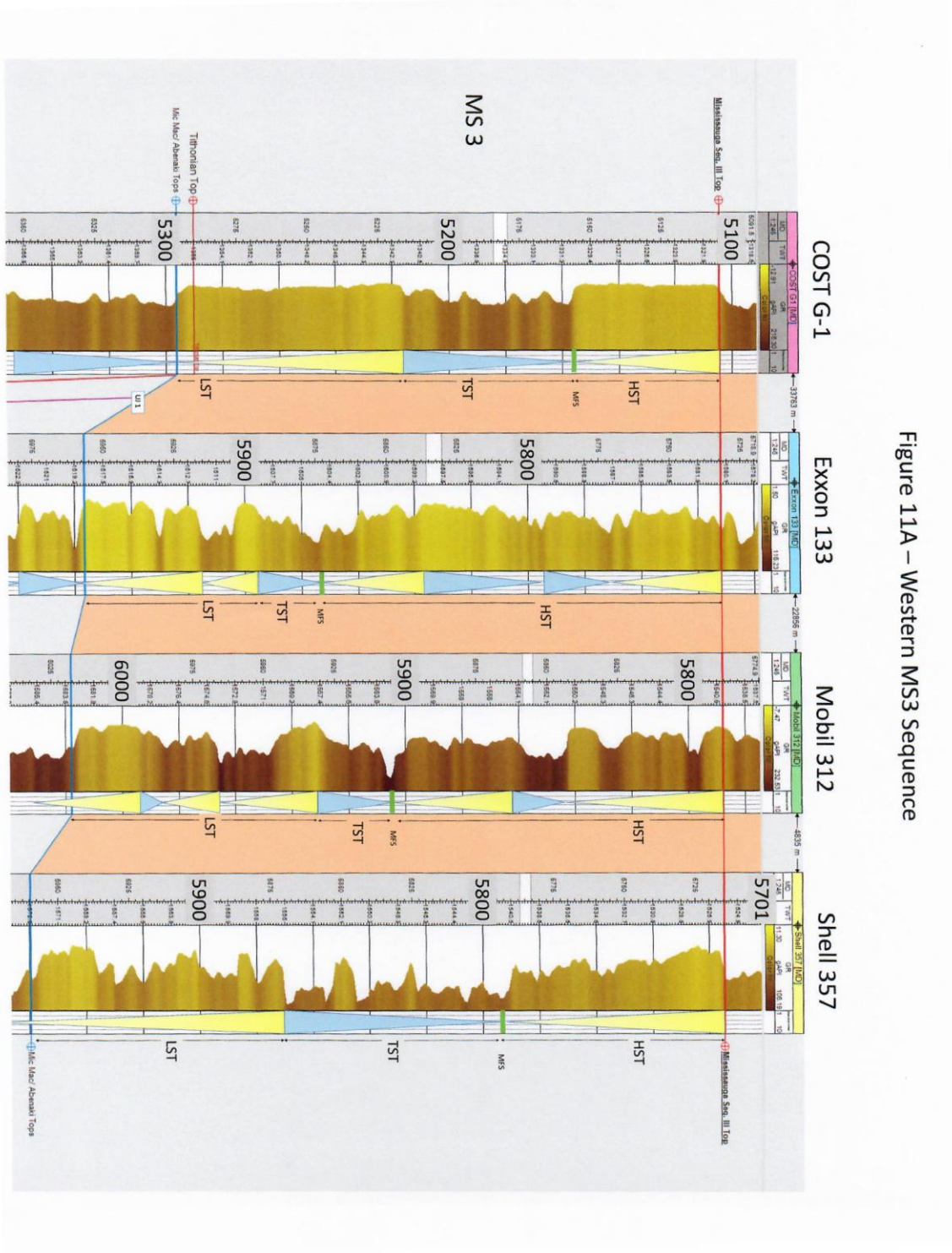

Figure 11A – Western MS3 Sequence

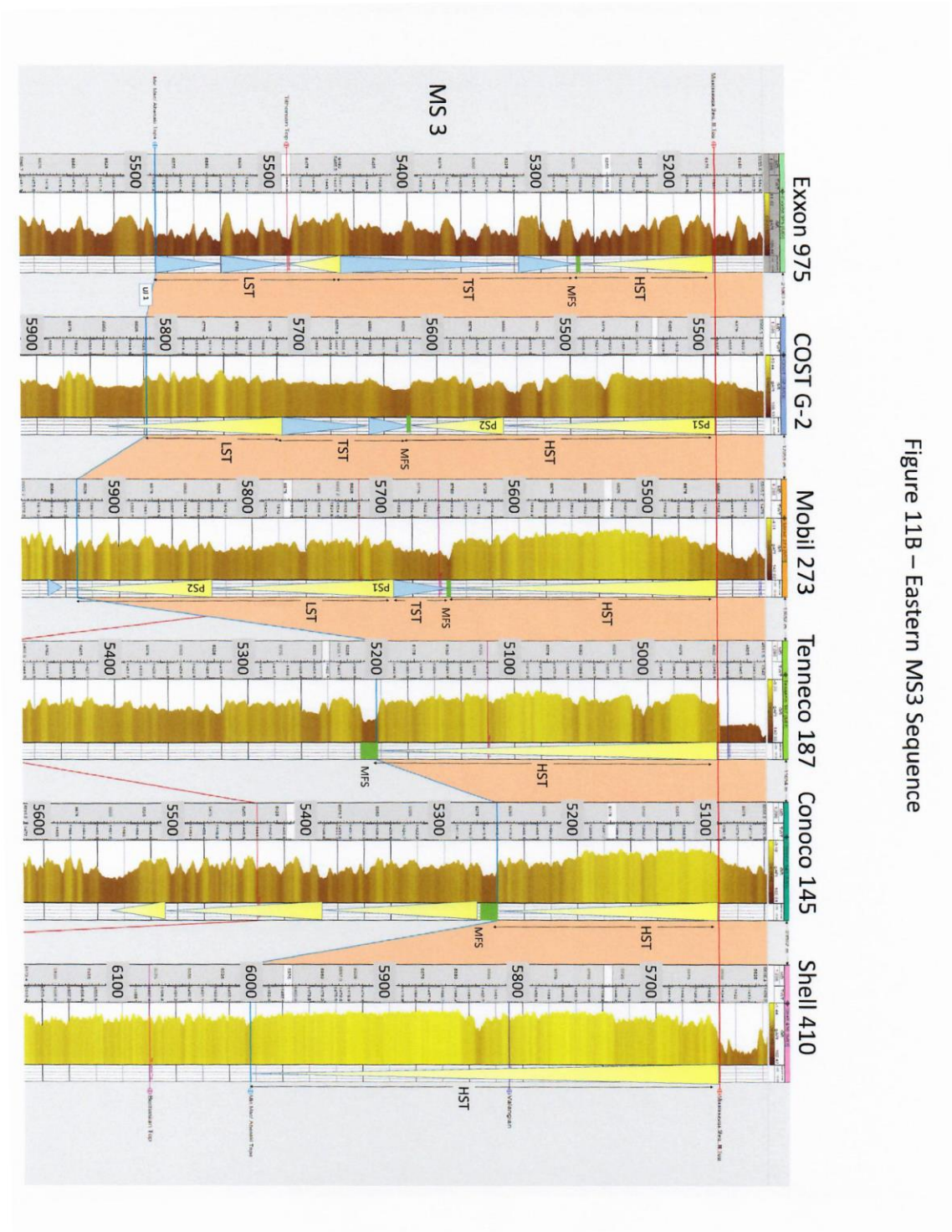

Figure 11B – Eastern MS3 Sequence

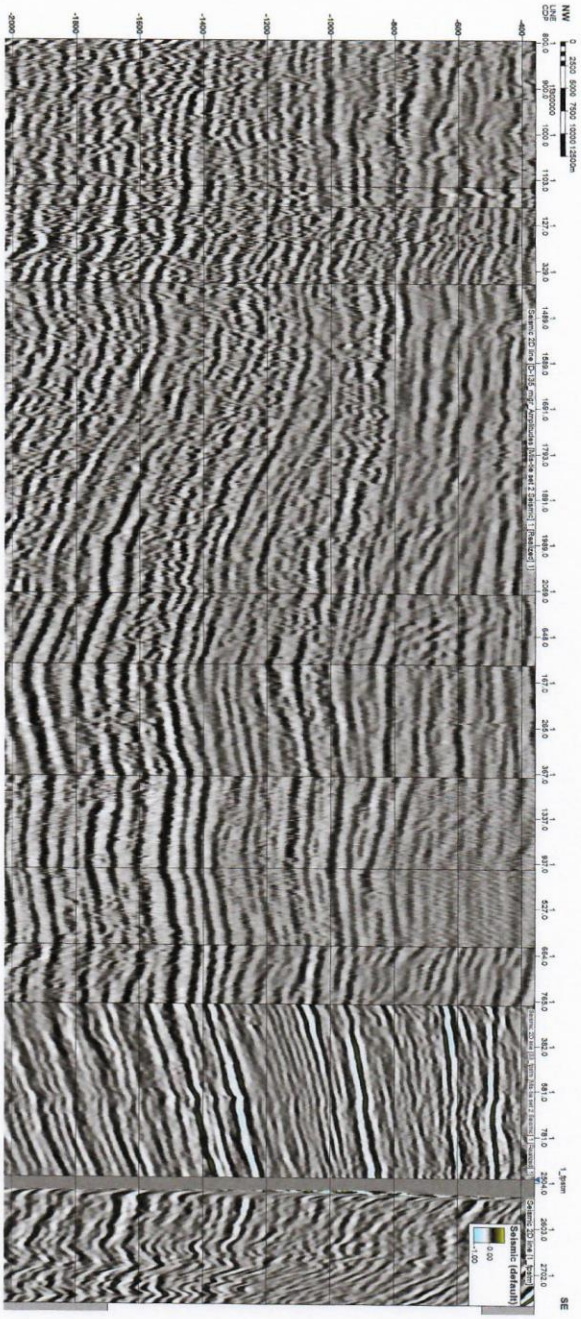

Figure 12A: Uninterpreted Western Composite 2-D Seismic Line

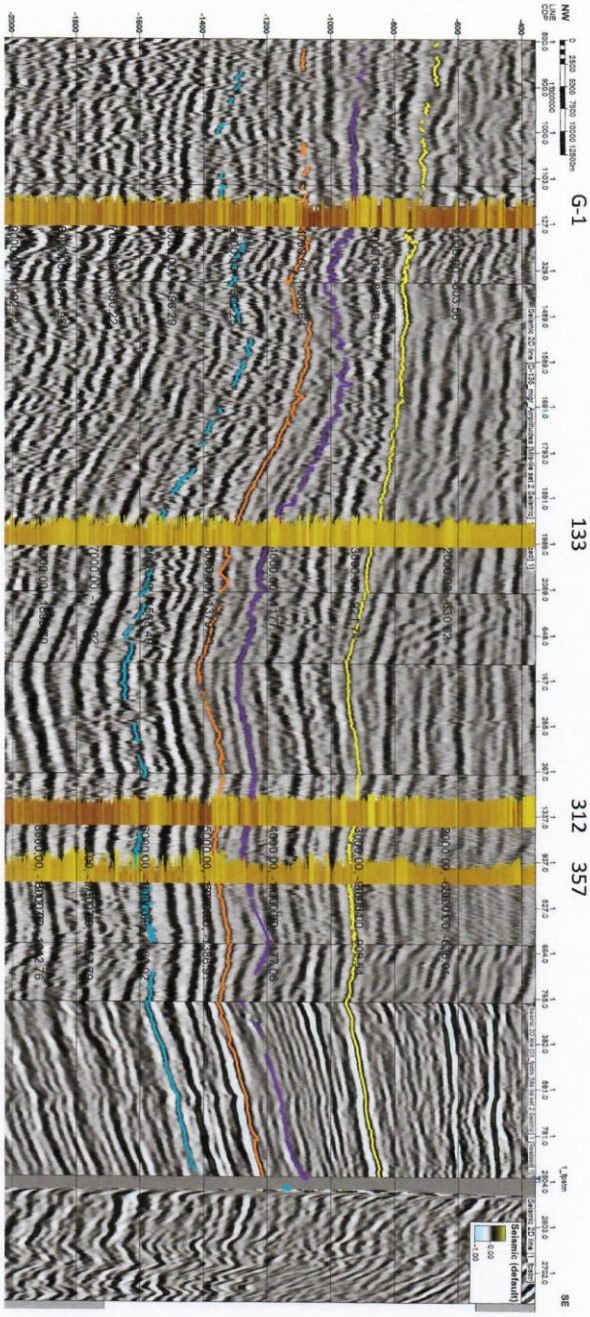

Figure 12B: Interpreted Western Composite 2-D Seismic Line

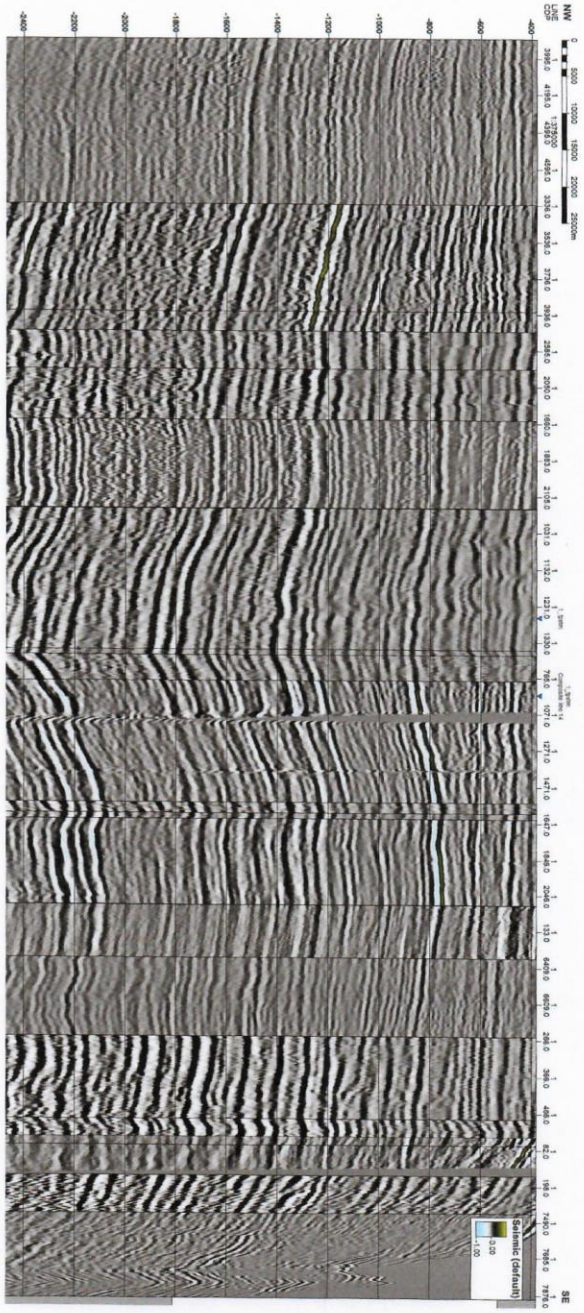

Figure 13A: Uninterpreted Eastern Composite 2-D Seismic Line

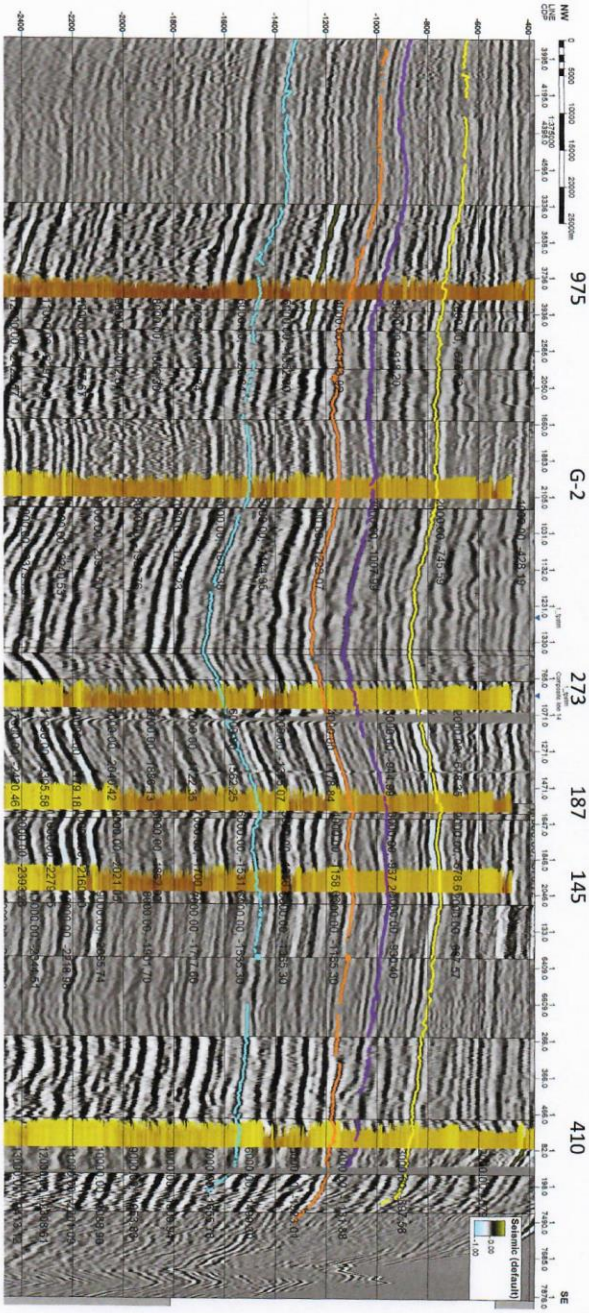

Figure 13B: Interpreted Eastern Composite 2-D Seismic Line

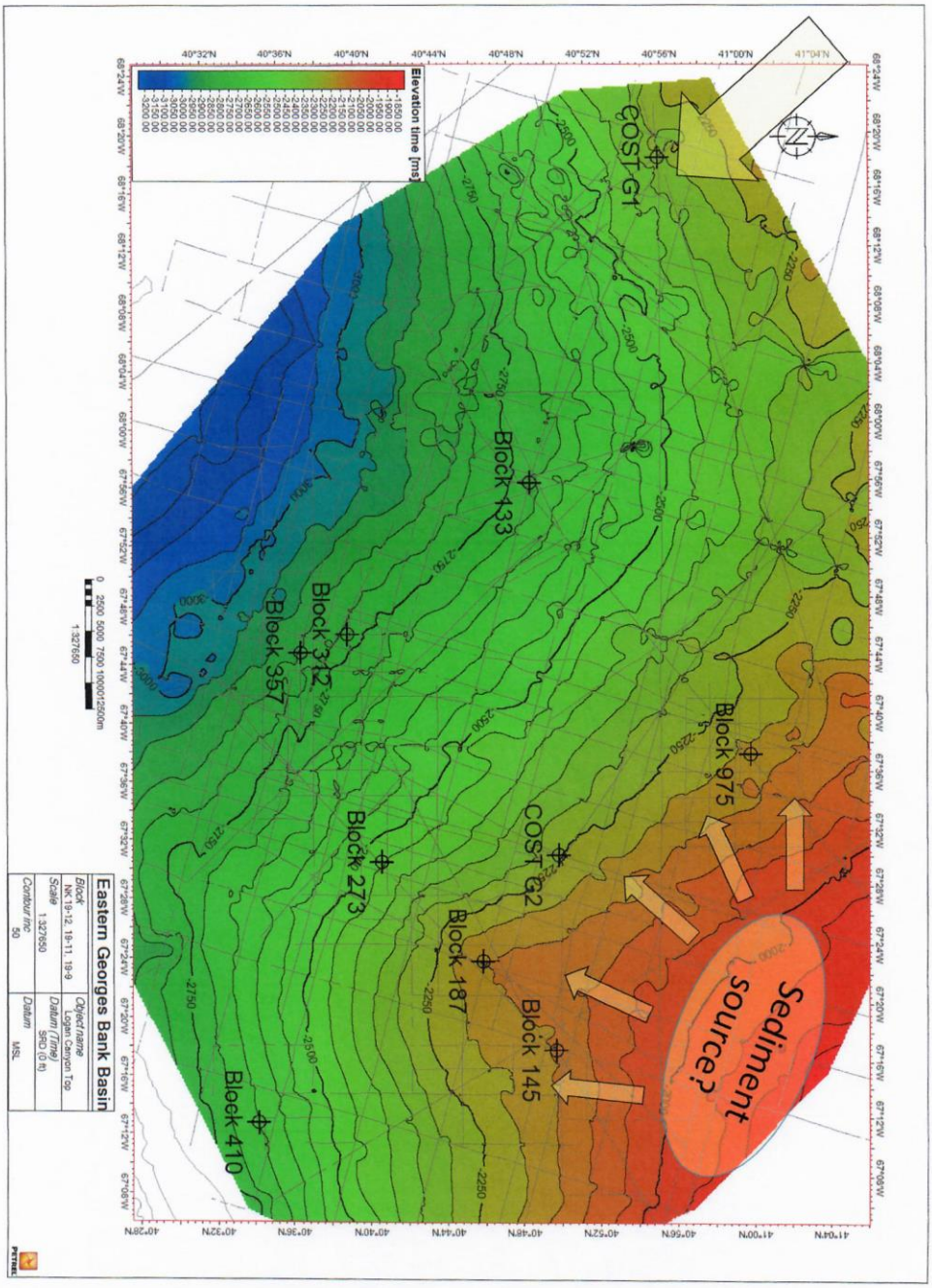

Figure 14: Logan Canyon Top Depth

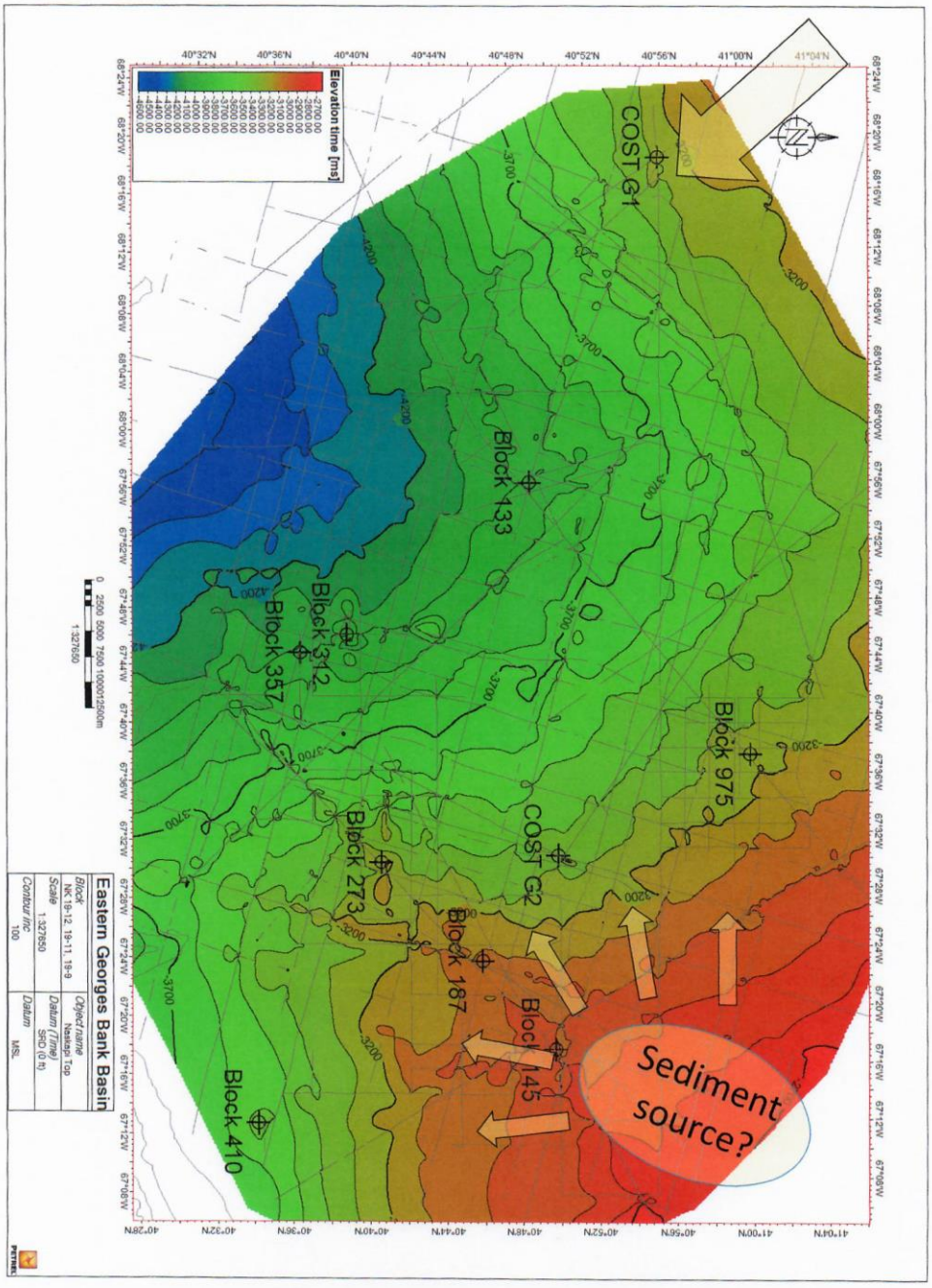

Figure 15: Naskapi Top Depth

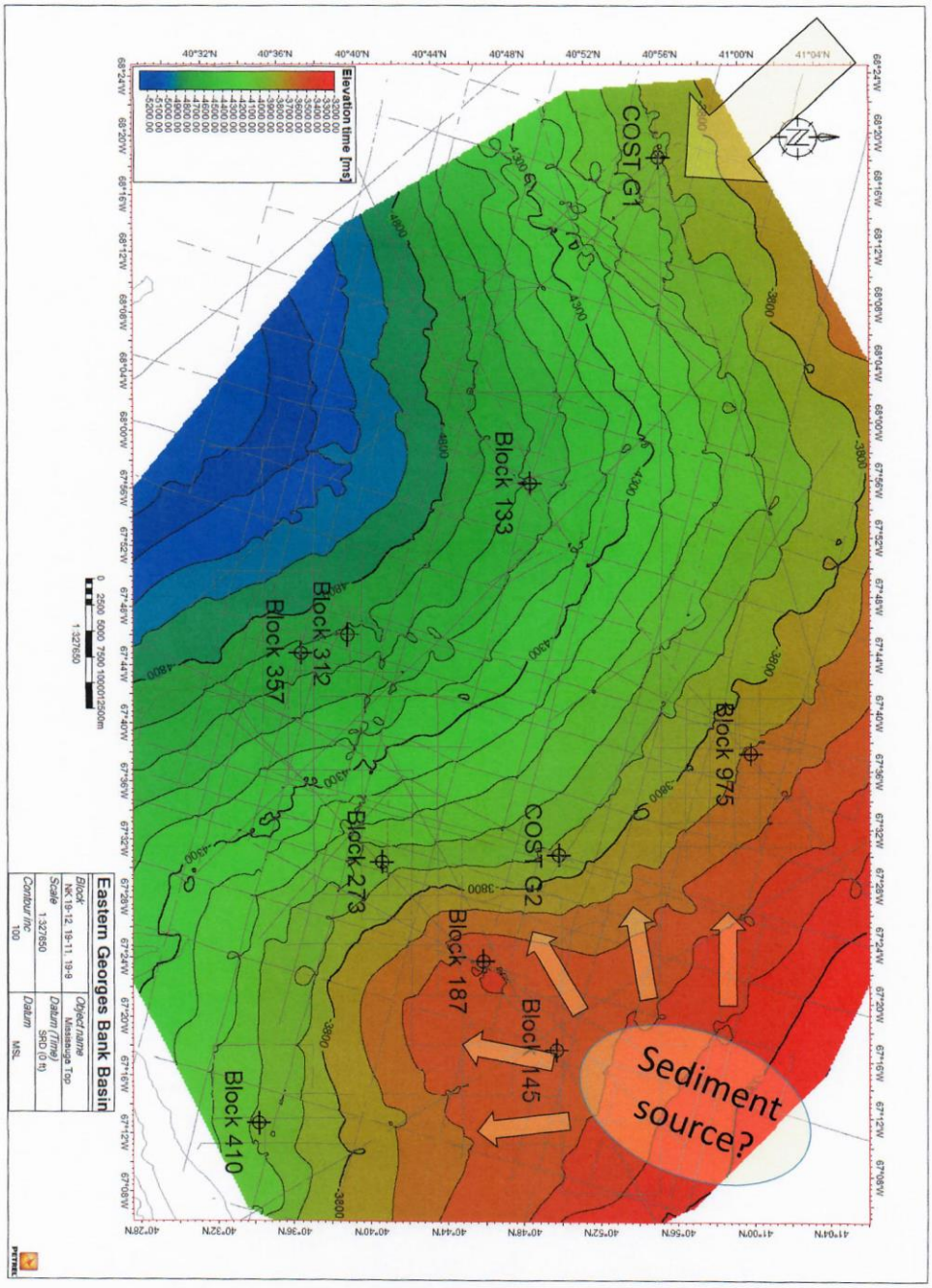

Figure 16: Missisauga Top Depth

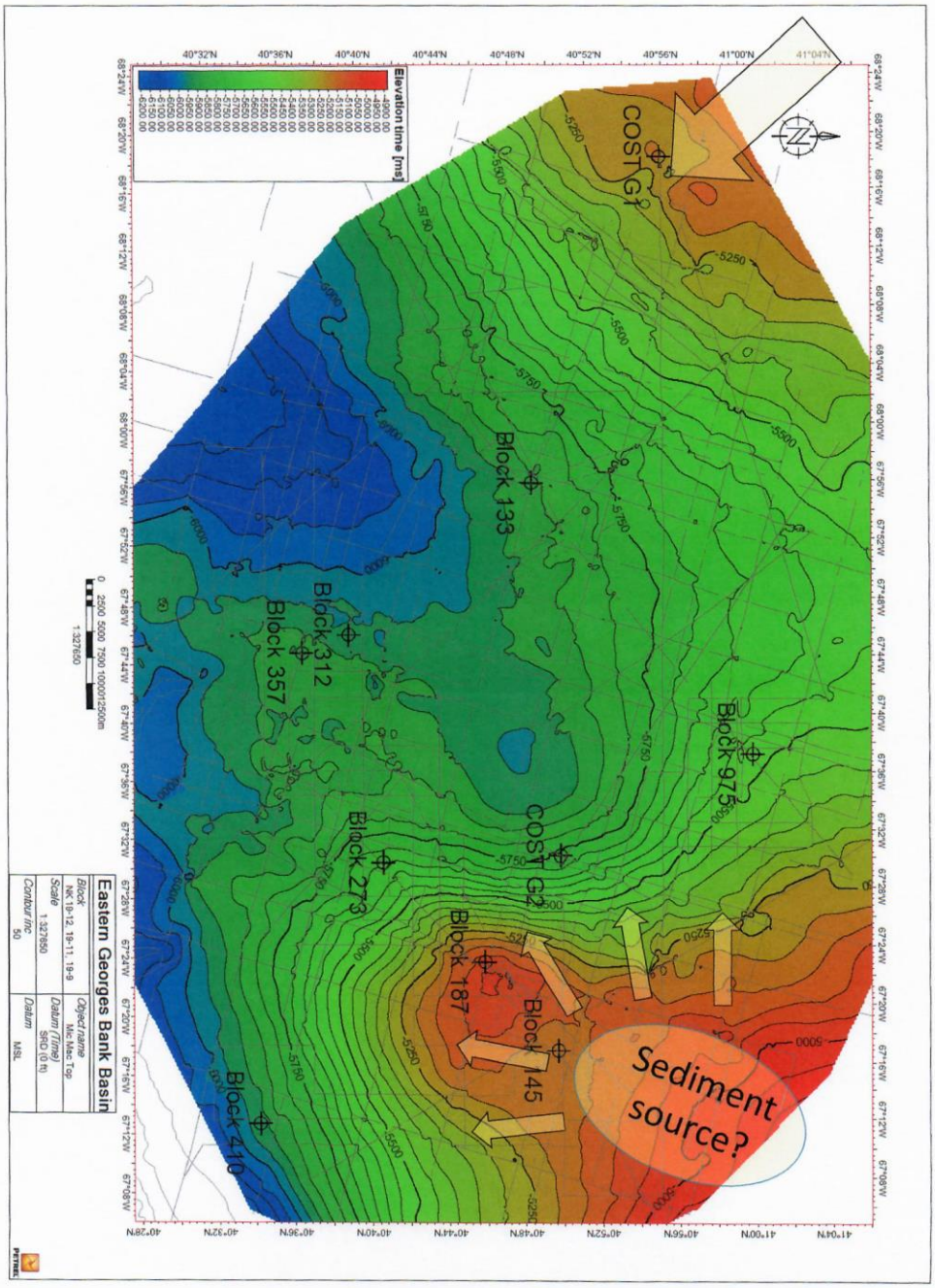

Figure 17: Mic Mac / Abenaki Top Depth

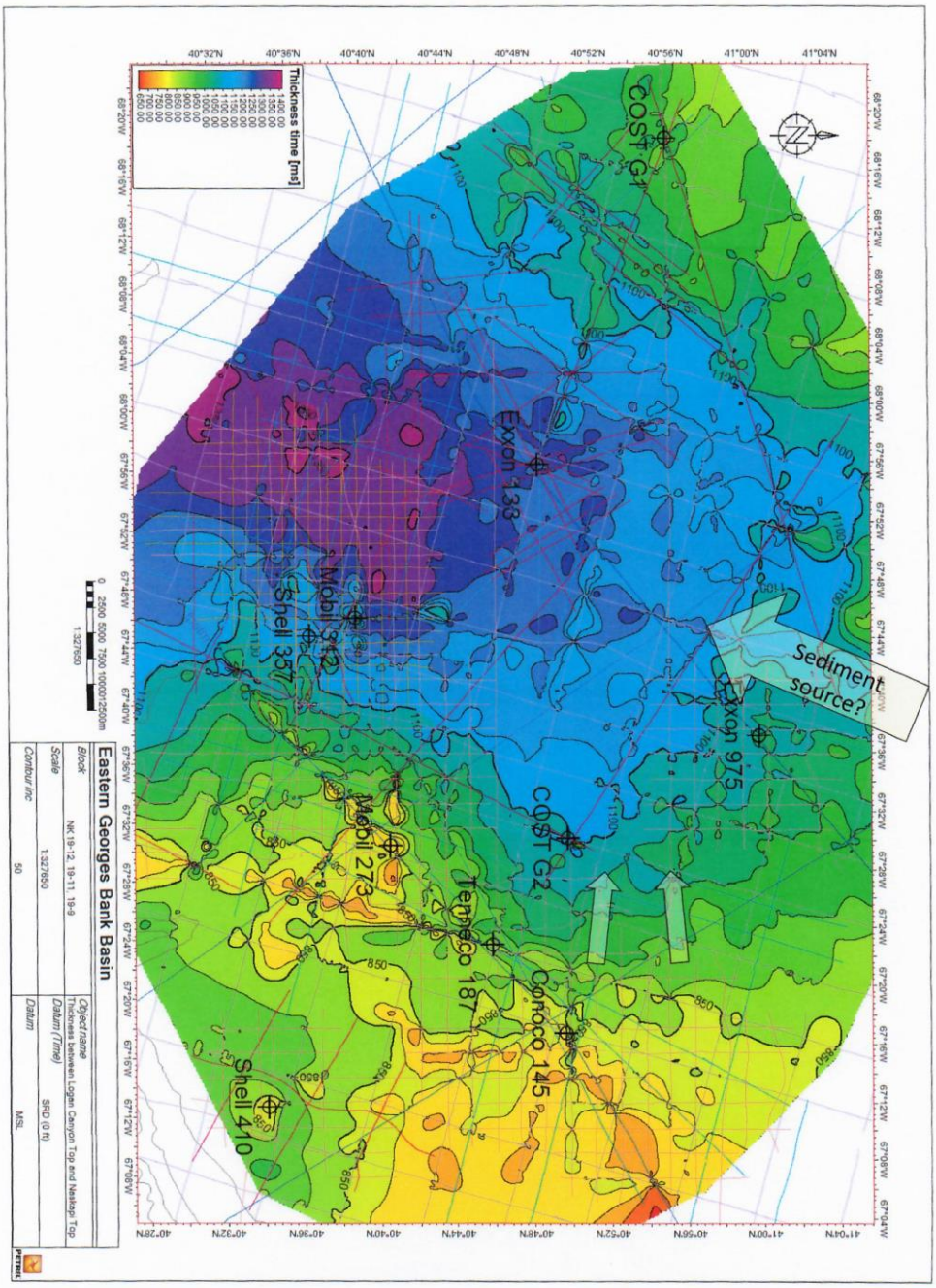

Figure 18: Logan Canyon Thickness

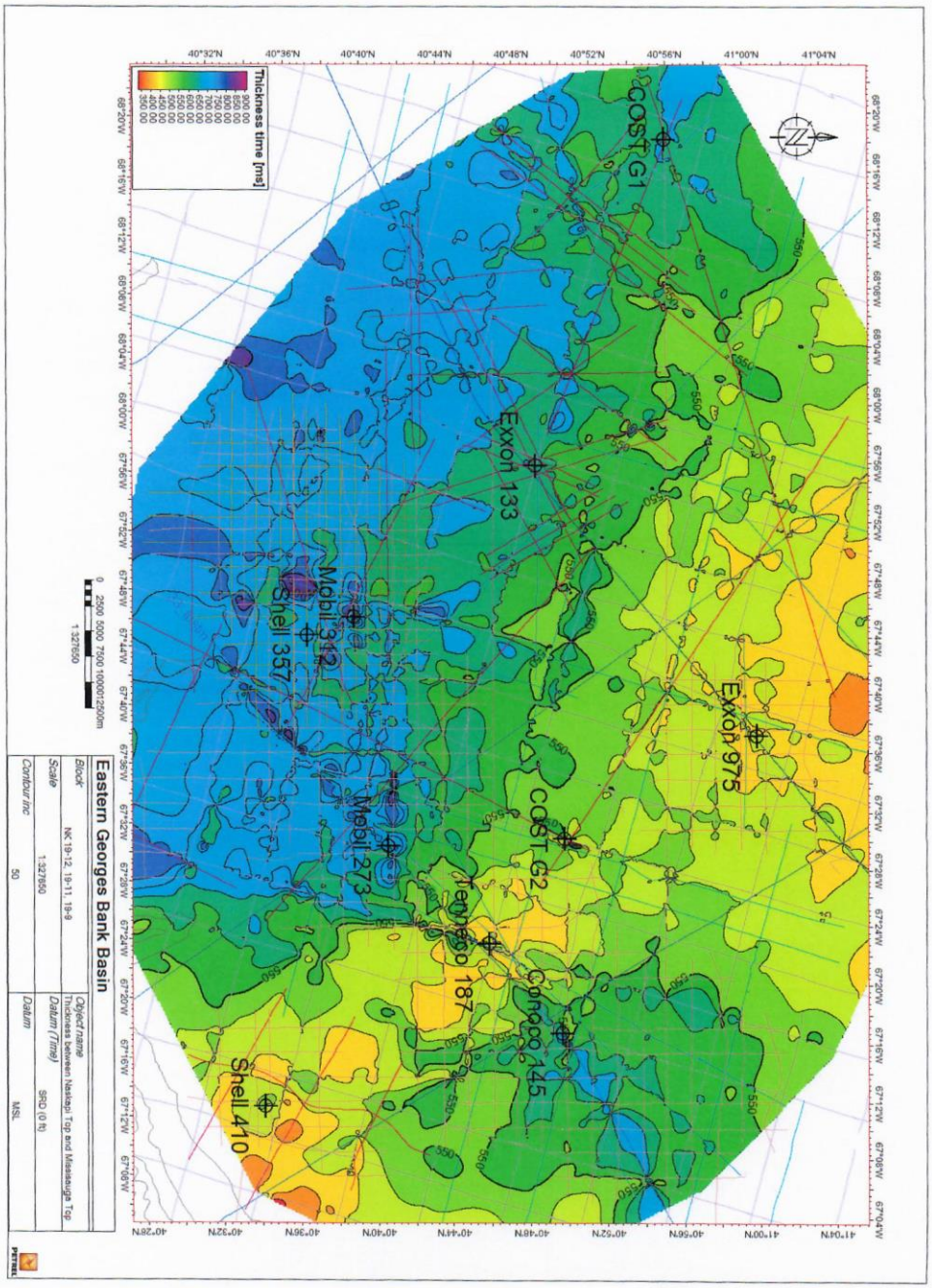

Figure 19: Naskapi Thickness

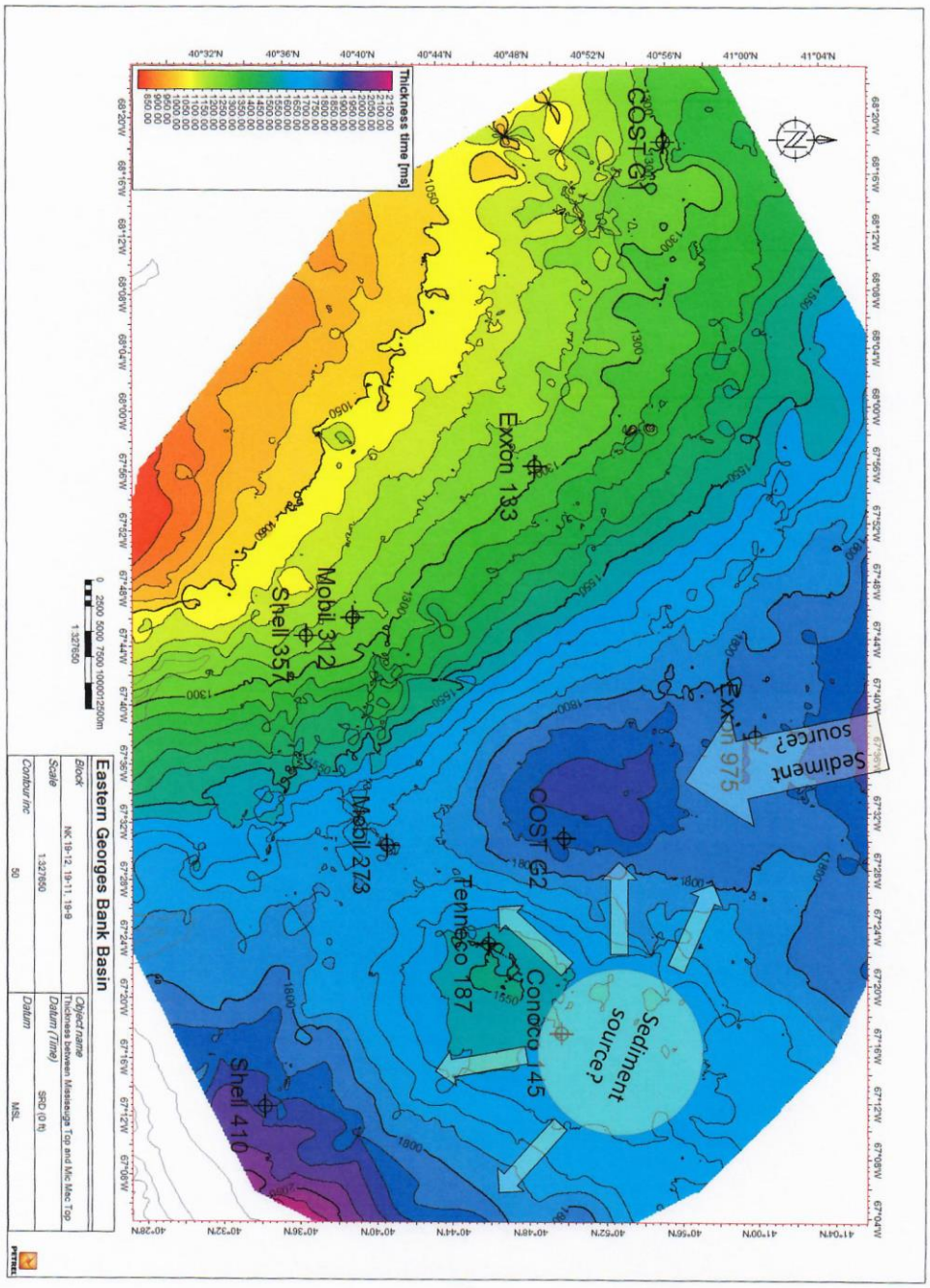

Figure 20: Missisauga Thickness

Table 1

Well Name	Units	LC1 SB	LC2 SB	LC3 SB	Naskapi Top	MS1 SB	MS2 SB	MS3 SB
Cost G1	ft KB	2409.22	2821.76	3084.87	3378.13	4013.76	4482.98	5104.53
	ftbSF	2056.22	2468.76	2731.87	3025.13	3660.76	4129.98	4751.53
	MBFS	626.74	752.48	832.67	922.06	1115.80	1258.82	1448.27
Exxon 133	ft KB	2802.56	3104.54	3563.24	4048.87	4679.06	5145.81	5731.80
	FBSF	2492.56	2794.54	3253.24	3738.87	4369.06	4835.81	5421.80
	MBFS	759.73	851.78	991.59	1139.61	1331.69	1473.95	1652.56
Mobil 312	ft KB	2871.58	3222.05	3657.82	4095.77	4775.93	5184.58	5787.77
	FBSF	2523.58	2874.05	3309.82	3747.77	4427.93	4836.58	5439.77
	MBFS	769.19	876.01	1008.83	1142.32	1349.63	1474.19	1658.04
Shell 357	ft KB	2915.00	3208.57	3521.64	4043.07	4729.19	5136.69	5714.66
	FBSF	2578.00	2871.57	3184.64	3706.07	4392.19	4799.69	5377.66
	MBFS	785.77	875.25	970.68	1129.61	1338.74	1462.95	1639.11
Exxon 975	ft KB	2263.27	2448.30	2827.16	3302.34	3761.87	4538.18	5169.48
	FBSF	1971.27	2156.30	2535.16	3010.34	3469.87	4246.18	4877.48
	MBSF	600.84	657.24	772.72	917.55	1057.62	1294.24	1486.66
COST G2	ft KB	2342.16	2659.65	3273.83	3407.55	3953.91	4758.12	5391.14
	FBSF	1991.16	2308.65	2922.83	3056.55	3602.91	4407.12	5040.14
	MBSF	606.91	703.68	890.88	931.64	1098.17	1343.29	1536.23
Mobil 273	ft KB	2544.99	2838.27	3164.97	3309.41	4001.31	4899.03	5551.54
	FBSF	2243.99	2537.27	2863.97	3008.41	3700.31	4598.03	5250.54
	MBSF	683.97	773.36	872.94	916.96	1127.85	1401.48	1600.36
Conoco 145	ft KB	2230.80	2357.16	2859.64	3028.84	3647.72	4432.32	5094.00
	FBSF	1845.80	1972.16	2474.64	2643.84	3262.72	4047.32	4709.00
	MBSF	562.60	601.11	754.27	805.84	994.48	1233.62	1435.30
Tenneco 187	ft KB	2234.47	2557.62	3019.12	3128.91	3611.29	4400.44	4947.45
	FBSF	1934.47	2257.62	2719.12	2828.91	3311.29	4100.44	4647.45
	MBSF	589.63	688.12	828.79	862.25	1009.28	1249.81	1416.54
Shell 410	ft KB	2721.37	2812.12	3358.82	3553.70	4053.37	4891.92	5652.23
	FBSF	2268.37	2359.12	2905.82	3100.70	3600.37	4438.92	5199.23
	MBSF	691.40	719.06	885.69	945.09	1097.39	1352.98	1584.73

Table 2

Survey Name	Tracklines	Distance shot (KM)
B-01-83	26	685
B-02-79	40	1287
B-03-75	326	28511
B-08-75	52	2009
B-25-76	175	4332
W-2-77	180	4460
Totals:	799	41284

Table 3

Log Description	simultaneous compensated neutron formation density	compensated formation density log gamma-gamma	compensated neutron gamma ray	simultaneous compensated neutron formation density	5in simltaneous compensated neutron formation density
Priority Index #	1	1	1	1	1
LAS file	lc000187.las	lc000198.las	lc000265.las	lc000238.las	Lc000179.las
Log Code	NPHI DPHI **GR**	RHOB/GR	**NPHI/GR**	NPHI **DPHI** GR	**NPHI DPHI GR**
Log Scale(s) (inc)	5	5	5	5	5
% of Total well	94.80%	94.80%	94.00%	70.90%	96.04%
Total depth covered	20737	20737	13271	10009	14951
Top of Log (ft.)	1057	1057	367	4101	610
Bottom Log (ft.)	21794	21794	13638	14110	15561
log Run Date	8/9/1977	8/9/1977	11/3/1981	10/19/1981	3/19/1982
Block	141	141	133	133	410
Area	LC	LC	LC	LC	LC
File Size(in bytes)	9243213	9671347	4012514	5818191	6022978
Log Image File Name	lc000187.tif	lc000198.tif	lc000265.tif	lc000238.tif	lc000179.tif
Well Name	G002	G002	1	1	1
Lease	COST	COST	A00170	A00170	A00218
Well Color Code					